VELOCITY, ATTENUATION, AND NATURAL FRACTURES IN SHALLOW BOREHOLES

A DISSERTATION
SUBMITTED TO THE DEPARTMENT OF GEOPHYSICS
AND THE COMMITTEE ON GRADUATE STUDIES
OF STANFORD UNIVERSITY
IN PARTIAL FULFILLMENT OF THE REQUIREMENTS
FOR THE DEGREE OF
DOCTOR OF PHILOSOPHY

By
Daniel Moos
February 1983

TABLE OF CONTENTS

Title page i

Table of contents ii

List of tables iii

List of illustrations iv

Introduction 1

Chapter 1

The effect of fractures on *in situ* velocities 8

Chapter 2

Pressure dependence of P- and S-wave velocities 39

Chapter 3

Measurements of velocity and attenuation

from vertical seismic profiles 58

Conclusions 85

Appendix 87

Bibliography 94

LIST OF TABLES

Table 1.1 2

Table 2.1 4

Table 2.2 5

Table 3.1 8

LIST OF ILLUSTRATIONS

Figure 1.1 10
Figure 1.2 11
Figure 1.3 13
Figure 1.4 16
Figure 1.5 17
Figure 1.6 18
Figure 1.7 19
Figure 1.8 23
Figure 1.9 27
Figure 1.10 28
Figure 1.11 32
Figure 1.12 36
Figure 2.1 42
Figure 2.2 43
Figure 2.3 47
Figure 2.4 48
Figure 2.5 50
Figure 2.6 55
Figure 3.1 61
Figure 3.2 61
Figure 3.3 63
Figure 3.4 64
Figure 3.5 66
Figure 3.6 67
Figure 3.7 68
Figure 3.8 70
Figure 3.9 75

Figure 3.10 76
Figure 3.11 78
Figure 3.12 79
Figure 3.13 81
Figure A.1 89

INTRODUCTION

Surface and borehole seismic surveys have been used traditionally to infer interesting rock properties (such as mineralogy, porosity, permeability, temperature, fracture density, or pore fluid constituents) from measurements of the velocity and attenuation of elastic waves. The inference of these properties from the measurements has been facilitated by laboratory measurements on "similar" rocks under conditions which are assumed to duplicate those prevailing *in situ*. It has been recognized for some time that laboratory results cannot always be applied directly to field problems for a variety of reasons. First, it is unlikely that a single sample removed from a large volume of heterogeneous rock would be adequately representative of the intrinsic properties of the entire volume. Assuming that the sample is in fact representative of the intrinsic properties of the rock mass from which it was removed, the presence of *in situ* fractures, which cannot by their very nature be removed to the laboratory for study, causes changes in the bulk properties of the material. Also, duplicating *in situ* conditions in the laboratory can be quite difficult. Further complications involve changes in the properties of the sample due to its removal. These include the development of microscopic cracks due to the release of confining pressure (Wang and Simmons, 1978), and the loss or change of pore fluid constituents.

A second problem is the possible scale dependence of rock properties. At very long wavelengths, fractures and other inhomogeneities affect the bulk properties of the rock volume. The aggregate material with inclusions is assumed to be a continuum with effective properties determined by the interaction of the relatively small scale inhomogeneities. Above some finite frequency the propagation of the elastic wave can no longer be described with reference to these effective properties. By studying the difference between the elastic properties at different frequencies of rocks with fractures and other inhomogeneities, the limitations of the continuum assumption can be determined.

A third problem is the frequency dependence of rock properties. In a purely elastic material body waves travel at a constant velocity which is independent of frequency. However, in a medium characterized by anelastic attenuation the conversion of wave energy to heat is accompanied by frequency-dependence of the elastic moduli, and hence of the velocities. When measurements of velocity are made

with sufficient accuracy, this frequency-dependence can affect the results. The larger the range of frequencies, and the greater the intrinsic attenuation, the more important the effect becomes.

This thesis is concerned with various aspects of the problem of the measurement of the elastic properties of the earth's crust. All of the field measurements were made in or near shallow boreholes which are less than 1 km deep. Each of the problems mentioned above is addressed briefly at various points. Where the affects are significant the problem is addressed in greater detail. The broader implications of the work presented here regarding these problems are addressed in the Conclusions.

In order to simplify this discussion, several useful terms will be defined. First, the various measurements of elastic parameters will be separated by frequency. The term "seismic" will be used to describe measurements made below 1 KHz (seismic refraction, reflection, and vertical seismic profiles, (VSP's)), "sonic" will be used to describe the results of the well logs (at frequencies from 1-30 KHz), and "ultrasonic" will be used to describe the results of the laboratory measurements, which were made at frequencies above 1 MHz. Sonic logging tools have been called "acoustic", but I will reserve that term to mean propagation through either a real or an assumed fluid, where the shear modulus is equal to zero. The term "elastic" will be reserved for propagation through materials which are able to support shear stresses. Also under this classification, the borehole televiewer (BHTV), which is described below, is an ultrasonic device. The televiewer has also been called an "Acoustic Borehole Televiewer", or ATV (Paillet and White, 1982).

The first chapter of this thesis deals primarily with the interaction between *in situ* macroscopic fractures and the sonic velocity of shear and compressional waves. The macroscopic fractures were detected using an ultrasonic borehole televiewer (BHTV), which detects fractures intersecting the wellbore by the change in reflectivity of the borehole wall. The distribution, orientation, and formation of the fractures has been discussed previously (Seeburger and Zoback 1982). In order to differentiate between these macroscopic fractures, which generally cannot be studied in the laboratory, and microcracks, whose effects have been discussed extensively in the literature, I will use the term "macrofracture" to refer to the macroscopic fractures, and "microcrack" to refer to features smaller than a few millimeters, which are not seen in BHTV records. Sonic velocities were measured using a borehole sonic logging tool, which is described at length in the appendix. Laboratory ultrasonic velocity measurements were made in saturated core samples from each of the wells, and the laboratory-determined velocities are compared

to the *in situ* sonic velocity.

The relationship between the pressure dependence of P- and S-wave velocities of intact laboratory samples and of fractured rock *in situ* is addressed in the second chapter. The sonic well logs presented in the first chapter are fitted to velocity-pressure curves, and these curves are compared to similar curves fitted to the laboratory data. Using these theoretical curves, quantitative comparisons are made between the pressure dependence of the elastic properties of crystalline rock in the field and in the laboratory. Measurements of *in situ* stresses in the wells are compared to the calculated pressure sensitivities, to determine if high shear stress causes an increase in pressure sensitivity.

The technique of vertical seismic profiling (VSP) is applied in the third chapter to the measurement of the velocity and attenuation constant (1/Q) of vertically travelling compressional waves. The measurements were carried out in one well drilled into fractured crystalline rock (XTLR) and in a second well drilled into sedimentary rocks at the East Mesa KGRA (Known Geothermal Resource Anomaly) in the Imperial Valley of southern California. Synthetic VSP's generated from borehole sonic logs at the two sites are used to constrain the attenuation models. The velocity obtained from the sonic logs is compared to that obtained from the VSP's, to determine the importance of dispersion and scale factors on the measurements at the two sites.

HISTORY OF THE TECHNIQUES

The measurement of elastic wave velocities in boreholes has primarily been accomplished in two ways. Sonic logging tools containing one or more sources and receivers are used to measure the velocity of P- and S- waves in boreholes at frequencies above 1 KHz. As a sonic tool is pulled up the borehole, the arrival-time of the energy refracted along the borehole wall is measured as a function of depth. Typical source-receiver offsets are a few tens of cm to a few m. Check-shot surveys or vertical seismic profiles (VSPs) are run with a source at or near the surface and a series of receivers at fixed points in the borehole. Alternatively, the receiver can be placed at the surface and the sources can be placed at depth. The receivers are either hydrophones, which detect the pressure pulse generated by the interaction of the elastic wave with the cyllindrical borehole, or side-wall clamped geophones, which measure directly

the response of the borehole wall to the incident wave. VSP's are typically run with explosive sources, air guns, or mechanical vibrators at frequencies from a few tens of Hz to about 1 KHz. Rice *et al.*, (1982) discuss some of the most recent developments of geophysical logging methods. Details of the methods and equipment employed here are discussed in the individual chapters, and the overall system is described in the appendix.

Vertical Seismic Profiles

The earliest use of check-shot surveys was to tie down the results of seismic reflection surveys run adjacent to the wells. At first, only the arrival-time of the compressional wave was recorded. Before the advent of digital computers, the data obtained from check-shots were corrected by hand to remove the effects of finite offsets (Dix, 1945). Kokesh (1952) suggested using small sources such as perforator guns at depth in the well, and recording the response at the surface. A later paper (Kokesh, 1956) suggested using hydrophones suspended in the well above these sources, to compensate for their finite size.

As researchers began to record the entire seismic signal from check-shot surveys, the analysis of check-shot data became increasingly sophisticated. Riggs (1955) recognized the presence of a guided wave traveling along the fluid- filled borehole, and found fairly close correspondence between the measured velocity of this tube wave and the velocity predicted by Biot (1952). Levin and Lynn (1958) recognized multiple reflections on the full waveform records of seismic surveys in several wells. The reflections were correlated with those observed in surface seismograms. Van Zandt and Levin (1963) showed that at low frequencies the presence of well-cemented casing has no effect on the character of either ambient noise or the seismic signal.

The additional information obtained from the full waveforms in VSP's provides the opportunity for a wide variety of measurements to be obtained from downhole surveys. Recently, VSP's have been used to calculate intrinsic attenuation (1/Q). One of the first of these studies is that of McDonal *et al.* (1958). However, attenuation is difficult to separate from other effects, such as multiple reflections between thin beds, which cause an apparent loss of high frequency energy as the wave travels (Schoenberger and Levin, 1974; 1978). This effect is impossible to separate from the effect of intrinsic attenuation using

spectral amplitudes alone. Recent studies of attenuation using VSP data have been reported by Ganley and Kanasewich (1980) and Kan *et al.* (1981), in which forward modeling has been applied to correct for the effects of intrabed multiples. A second problem in the analysis of full waveform data in boreholes is the generation of borehole tube waves by the incident energy. The elimination of tube wave noise has become increasingly important as analysis of VSP data has become more sophisticated. Hardage (1981) discusses possible methods for the reduction of tube wave noise by optimizing experimental geometry, or by applying appropriate velocity filters to the data. DiSienna *et al.* (1981) also discusses the application of filters to improve VSP imaging, and uses signals recorded on three-component geophones to discriminate between radial and transverse partical motions.

Recently, techniques have been developed to calculate VSP synthetics. Ganley (1981) presents a frequency-domain technique utilizing propagator matrices to calculate synthetic VSP's in layered acoustic media which includes the effects of intrinsic attenuation for vertically incident waves. Kennett (1981) applies a similar approach to solving the full elastic problem for non-vertical incidence. This method can model a complete VSP including the effects of mode conversions and spherical divergence. By solving for the Green's function response of a layered half-space, Bouchon (1981) includes mode conversions, spherical divergence and the effects of attenuation in synthetic VSP's. Mencke and Richards (in press) discuss the effect of several classes of periodic media on the wavefield. Hron and Mikhailenko (1981) suggest that non-geometrical effects may dominate the near-field response of a layered elastic medium with an explosive source near the free surface; this may be particularly important in VSP modelling. The synthetic VSP's presented in Chapter 3 were generated by Ganley's (1981) method. None of these methods, however, can account for the tube waves generated at inhomogeneities in the borehole wall.

Sonic Logging

Although I have been able to find no historical treatment of the development of sonic logs as a viable oil-field technique, these logs apparently did not come into common use until after check-shot surveying had become standard practice. At that time there was considerable interest in the comparison

of sonic logs ("continuous" well velocity surveys) and check-shots ("conventional" surveys). Gretener (1961) discusses possible explanations for some systematic variations he observed between the two measurements. He mentions the possibility of velocity dispersion to explain the slightly lower velocities observed in check-shot surveys.

In the late 1950's and early 1960's a series of papers was published addressing some of the problems inherent in the measurement of sonic travel-time in boreholes. Among the problems discussed was the effect of thin beds (Thurber, 1957), changes in borehole diameter, and alteration of rock properties near boreholes due to the drilling process (Kokesh and Blizzard, 1959; Hicks, 1959). Sonic tools in use at the time either employed several receivers, or used empirical relationships to correct single-receiver measurements for changes in hole size. Tuman (1961) discussed the effects of temperature and stress gradients adjacent to the borehole on the energy propagated along the borehole wall. Other researchers have suggested that the amplitude of the refracted arrivals could contain significant information about formation permeability and the density of natural fractures (Morris *et al.*, 1961; Walker, 1962; Pickett, 1963). Laboratory experiments reported by Crawford *et al.* (1972) demonstrated that propagation along boreholes is accompanied by filtering of the transmitted signals. They suggested that the effect is dependent on formation velocity and borehole size. Aron *et al.* (1978) described experimental techniques for the measurement of both shear and compressional interval transit times, and Arditty *et al.* (1981) presented methods for the computation of formation velocities over an array of 12 receivers, using digitally recorded waveforms. There are at present several multi-receiver multi-source sonic logging tools on the market. By digitally recording the sonic signal an extremely large amount of high quality data can be produced.

The theoretical problem of wave propagation in fluid-filled boreholes has received considerable attention in the last 30 years. Biot's (1952) paper discussed one form of guided wave (the tube wave), later recognized in VSP data (Riggs, 1955), which is commonly seen in full waveform logs. White and Zechman (1968) presented theoretical waveforms calculated for a fluid-filled borehole in a viscoelastic medium. Viscoelasticity had been introduced to remove singularities in the Fourier inversion integral. Rosenbaum (1966) presented theoretical microseismograms calculated for purely elastic media, and later (1974) generalized his results to include both intrinsic attenuation due to the viscoelasticity of the material surrounding the borehole and the effect of the finite permeability of the borehole wall on the

fluid-born energy. Peterson (1974) also developed a method for computing wave propagation along a fluid-filled cyllinder. Tsang and Rader (1979) was the first theoretical work that included the effects of the tool in the borehole. Recently Cheng and Toksöz (1981) and Paillet and White (1982) have derived exact forms for the dispersion curves of the different borehole modes. They have analyzed the effect of variations in tool size, hole size, and the properties of the formation and of the borehole fluid. Using these theoretical results, experimental waveforms can be analyzed by separating the arriving energy into specific time windows. Cheng and Toksöz, (1981) used this technique to separate shear arrivals from the possible interference of normal modes. Effects such as the generation or attenuation of tube wave energy at permeable fractures can also be studied if the arrival-time and characteristics of the fluid-borne energy are known (Cheng and Toksöz, 1982). Experimental techniques can therefore be designed to aid in the detection of these features (Paillet, 1980; 1981; Paillet and White, 1982). Cheng *et al.* (1982) have also used these results to aid in the measurement of intrinsic attenuation.

The analysis of the data presented here was carried out at the same time as most of the more recent theoretical developments mentioned above. Some of the analytical methods were suggested by previously published work, and some of the methods were developed independently. I will not present here any quantitative analysis of the sonic-log waveforms. However, the increased understanding of such waveforms provided by the above theoretical work has been important in explaining some of their observed features. Where parallels exist between my work and that of other researchers, I have included a more detailed discussion of the published papers.

CHAPTER 1

The effect of fractures on *in situ* velocities

The manner in which microcracks affect the velocity of crystalline rock is well known from laboratory measurements. Birch (1960, 1961) showed that in dry crystalline rock, increased confining pressure causes a marked increase in compressional velocity due to the closure of microcracks. Nur and Simmons (1969) later showed that in saturated granitic rock the seismic velocity is markedly higher than in dry rocks and the degree to which confining pressure increases velocity is somewhat diminished.

Although it is well known that the presence of macroscopic fractures in an otherwise homogeneous rock can profoundly affect its seismic velocity, few attempts have been made to systematically relate fracture occurrence and seismic velocities *in situ*. There are two primary reasons for understanding the relationship between seismic velocity and fractures in the crust. Interpretation of geologic units from seismic velocities depends critically on the degree to which fractures affect velocity. Furthermore, because fractures in the crust are of interest for a variety of reasons, seismic velocity can be used as a tool for the study of those fractures.

Comparisons of field data with laboratory measurements demonstrate the importance of understanding the role of *in situ* fractures in controlling seismic velocity. Simmons and Nur (1968) measured the P wave velocity of granites in a 3-km-deep hole in the Wind River Range of Wyoming and a 3.8-km-deep hole near Troy, Alabama. They found that *in situ* velocities were uniformly higher than laboratory measurements on dry samples and increased more slowly with pressure. They attributed this difference to the presence of water in the microcracks *in situ*. In a similar case, Wang and Simmons (1978) found that *in situ* velocities for gabbroic rock at 5.3 km depth in the Michigan Basin are equal to or slightly higher than the velocity of saturated laboratory samples at the appropriate pressure. This discrepancy was attributed to the introduction of stress relief microcracks when the core was removed.

The results are much different when numerous macroscopic fractures are present *in situ*. Stierman and Kovach (1979) observed little systematic increase of velocity with depth in a 700-m-deep well drilled

in highly fractured quarts diorite 1.2 km from the San Andreas fault. Furthermore, a sample from the well had a measured P wave velocity of more than 6 km/s in the laboratory, while *in situ* P wave velocities were less than 4 km/s. This marked difference was attributed to the numerous macroscopic fractures in the well which were not present in the laboratory specimen. Keys (1979) reported lower sonic compressional velocities associated with fracture zones in the Lac du Bonnet batholith in central Canada at depths up to 350 m. In another study, Sjogren *et al.* (1979) showed that in very shallow (<25 m) boreholes, macroscopic fractures reduced *in situ* compressional wave velocity and that in igneous and metamorphic rocks there was a good correlation between compressional wave velocities and the number of macroscopic fractures.

In order to understand the factors controlling seismic wave velocities in fractured rock we examine here the relationship between macroscopic fracture (macrofracture) density and P and S wave velocities in four wells drilled in fractured granitic rocks. By studying in detail the effect of isolated fractures and fracture zones on seismic velocity we have attempted to understand the mechanisms by which fractures affect velocity *in situ*. By comparing *in situ* velocities with measurements made on laboratory samples we have attempted to determine the conditions under which the change of ultrasonic velocity of laboratory samples with pressure adequately explains the change in sonic velocity with depth. Finally, by applying a few simple modeling techniques we examine the conditions under which subsurface fracture zones might be detected by conventional seismic reflection profiling.

SITE CHARACTERISTICS

Data from four wells are presented in this study. Two wells were drilled near the Monticello Reservoir in South Carolina (Figure 1.1) and two were drilled in the western Mojave Desert in southern California (Figure 1.2). The total depth of the wells varies between 580 and 1200 m.

Fractures intersecting the borehole wall were detected using a borehole televiewer (BHTV). A detailed description of the BHTV operation is given by Zemanek *et al.* (1970). Seeburger and Zoback (1982) present a detailed analysis of the macrocracks observed in these wells, and the results of their study will only be summarized here. The fractures observed on the BHTV logs probably do not represent the entire fracture population. Because the BHTV detects variations of well bore reflectivity, only those fractures which are held open to some degree, or which are filled with alteration minerals, will be

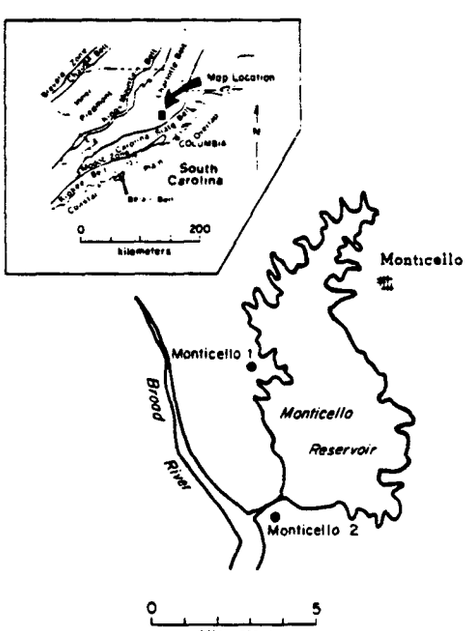

Fig. 1.1: Map showing the location of the Monticello wells (after Seeburger and Zoback, 1982). The wells were drilled into late Paleozoic granodiorite bodies in the Charlotte Belt.

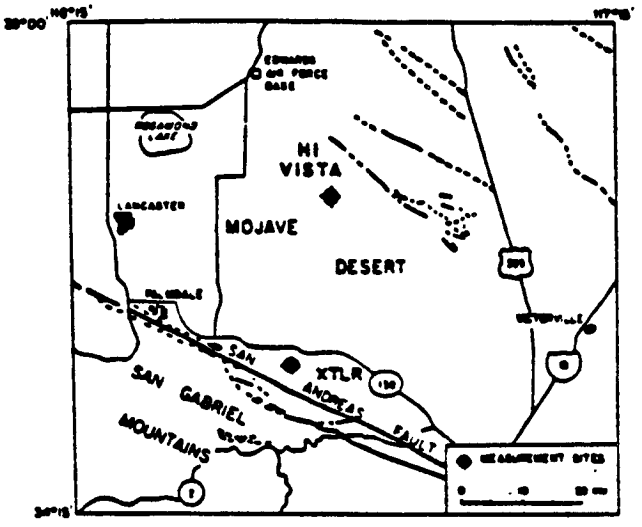

Fig. 1.2: Map showing the location of the Crystallaire and Hi Vista wells, which were drilled 4 and 34 km, respectively, northeast of the San Andreas fault in the western Mojave Desert (after Seeburger and Zoback, 1982).

detectable by the BHTV. Fractures that are partly or completely mineralized can be seen because the drilling process causes spalling of the rock near the fracture at the borehole. We use the term "apparent aperture" when discussing measurements of fracture width because the aperture of the fractures measured from the BHTV log may not be directly related to conditions in the fracture away from the borehole wall. The televiewer can resolve features at the borehole wall with apparent apertures as small as 0.5 mm. The BHTV log provides no information about the distribution of microcracks.

In South Carolina, wells MONT-1 and MONT-2 were drilled to depths of 1100 m and 1203 m, respectively, in small plutons of granitic to granodioritic composition which were intruded into the Charlotte Belt metamorphic rocks of the Piedmont Province (Figure 1.1). The Charlotte Belt is a complicated sequence of folded interlayered gneiss, amphibolite and schist which was intruded at the end of the late Paleozoic by granitic to granodioritic plutons similar to those into which the Monticello wells were drilled. The region has undergone several episodes of uplift and erosion, but there has been no major tectonic activity since the Jurassic. Monticello Reservoir is the site of considerable reservoir-induced seismicity (see Talwani *et al.*, 1980). Most of the earthquakes in the vicinity of the reservoir are small ($M < 2$) events at extremely shallow depth (<1-2 km). *In situ* stress measurements in MONT-1 and MONT-2, the orientation of fractures in the wells, composite focal plane mechanisms, and the magnitudes of the events all suggest that thrust-type motion on fractures similar to many of those observed in the wells is responsible for this seismicity (Zoback and Hickman, 1982).

Examination of cores and cuttings from the two wells (Secor *et al.*, 1982) reveals that the rock at MONT-1 is a relatively homogeneous coarse-grained granodiorite, but that at MONT-2 the granodiorite contains several amphibolite inclusions, mostly concentrated in the upper 830 m. From this Secor *et al.* (1982) suggest that the MONT-2 well was drilled close to the margin of one of the plutons, where inclusions of country rock are more common. Cored fractures in the MONT-2 well contain retrograde chlorite which was later altered to a green mixed-layer clay, some carbonate and small amounts of pink zeolite. Only one small chloritized shear was found in the core samples from MONT-1 (D. C. Prowell, written com.). Apart from the amphibolite inclusions in MONT-2, there is little change in mineralogy or composition with depth in the Monticello wells.

Figure 1.3 shows the density of macrofracturing as observed by the BHTV for the wells in this study. The depth to which casing extends in each well is indicated in the figure, and no information

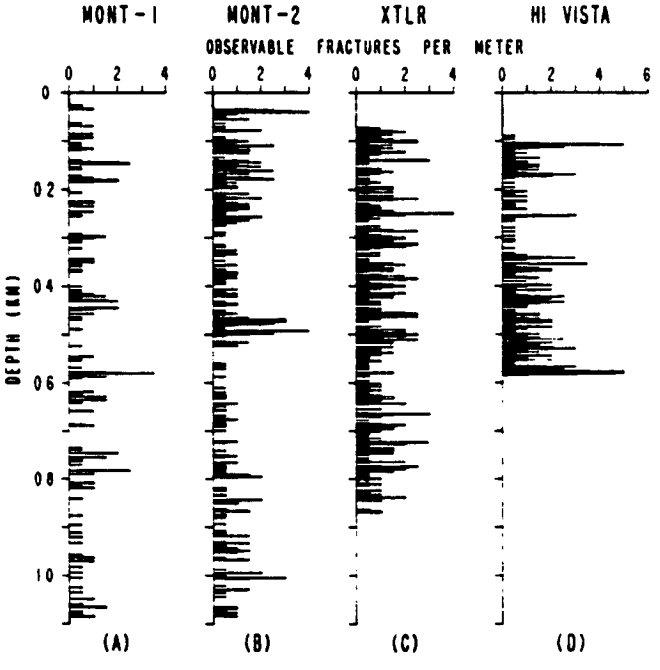

Fig. 1.3: The density of observable macroscopic fracturing as a function of depth for the four wells in this study. The fractures were picked from borehole televiewer records of the wells. The depth to which casing was set in each well is indicated by the upper shaded zone.

on fracture density is available for the cased sections. Fracturing in MONT-1 (Figure 1.3a) occurs in many small discrete zones distributed throughout the total depth of the well. In the lower 300-400 m of the well there are fewer fractures, and the fractures are more evenly distributed. The upper 280 m of MONT-2 is highly fractured (Figure 1.3b), and another dense fracture zone extends from 450 to 500 m. Several intense fracture zones are also seen in MONT-2 that span intervals of several tens of meters, and at nearly all depths the fracture density in MONT-2 is greater than that in MONT-1. In both Monticello wells the majority of the fractures are steeply dipping. In MONT-1 most of the horizontal fractures occur only in the upper 200 m; a few horizontal fractures are seen below 950 m. In MONT-2 the horizontal fractures are concentrated in the upper 250 m and within the fracture zone from 400 to 500 m.

The Crystallaire well (XTLR) and the Hi Vista well were drilled 4 and 34 km, respectively, from the San Andreas fault near Palmdale in the western Mojave Desert (Figure 1.2). The western Mojave Desert is underlain by pre-Tertiary crystalline rocks similar to those encountered in the XTLR and Hi Vista wells. This portion of the San Andreas fault last ruptured in the great 1857 Fort Tejon earthquake.

There is relatively little change in composition or mineralogy with depth in the XTLR and Hi Vista wells. The rock encountered in the XTLR well is a predominantly coarse grained biotitic quartz monzonite. Significant alteration was found in the cuttings from this well, and a core taken from the bottom of the well was pervasively altered. Small through-going veinlets of sheared calcite and quartz and microcracks within quartz grains suggest that the rock at this depth has been subjected to high shear stresses. The rock at Hi Vista is a medium to coarse grained quartz monzonite. There is relatively little alteration below 100 m in this well (D. Stierman, written comm), although some local zones of intense alteration were found. A sample from the bottom of the well contained several mineralized fractures with well developed slickensides, and was significantly less altered than the core from the XTLR well.

Many fractures intersect the XTLR well (Figure 1.3c) and the fracture density decreases slowly with increasing depth. Although localized fracture zones do occur in the XTLR well, numerous fractures are distributed throughout its entire depth, and the fracturing extends to the total depth of 869 m. The fracture distribution in the Hi Vista well (Figure 1.3d) is somewhat anomalous compared to the other wells. A dense near-surface fracture zone extends to about 180 m, the zone from 180 to 335 m

is relatively unfractured, and from 335 m to the total depth of 584 m the fracture density is again quite high and roughly similar to that observed in the XTLR well. There are several zones of intense fracturing throughout the Hi Vista well, but the most intense (with the possible exception of the near-surface fractures obscured by the casing) is near the bottom. The majority of the fractures in both XTLR and Hi Vista are steeply dipping; almost no horizontal fractures are present in these wells.

By considering these four wells we can examine sonic velocity under conditions of widely varying fracture distributions. MONT-1 is sparsely fractured and the fracture density decreases slightly with increasing depth; MONT-2 is more highly fractured than MONT-1, especially in the upper 280 m and from 450 to 500 m; the fracturing in the XTLR well is uniformly high and decreases slowly with increasing depth; the fracture density in the Hi Vista well is quite high at shallow depth and in the lower portion of the well.

RESULTS

P-Wave Sonic Velocity

Figures 1.4-1.7 show P wave velocity and observed fracture density as a function of depth in the four wells. Figures 1.4, 1.5, and 1.7 also show S wave velocity and V_p/V_S. The appendix contains a discussion of the method used in obtaining the sonic velocities shown in these figures. The sonic logs were run from the water table to the total depth in each well, except as noted below. In this section we present the results of the P wave velocity measurements. The S wave velocity data and V_p/V_S will be discussed below.

Figures 1.4-1.7 also show the P wave velocities in a representative sample from each well which was measured under confining pressure in the laboratory. The samples were evacuated and then saturated under 5 bars pore pressure. P wave velocities were measured at a frequency of about 2 MHz using a technique described by Peselnick and Stewart (1975). Travel time could be measured to within 10 ns, and the absolute accuracy of the measured velocities was about ± 0.5 %. Velocities were measured as a function of confining pressure with the pore pressure equal to atmospheric pressure. Pressure was converted to depth by assuming an *in situ* effective stress gradient of 16.7 MPa/km to correspond to the effective overburden stress. We think this conversion of pressure to depth is justified because (1) seismic

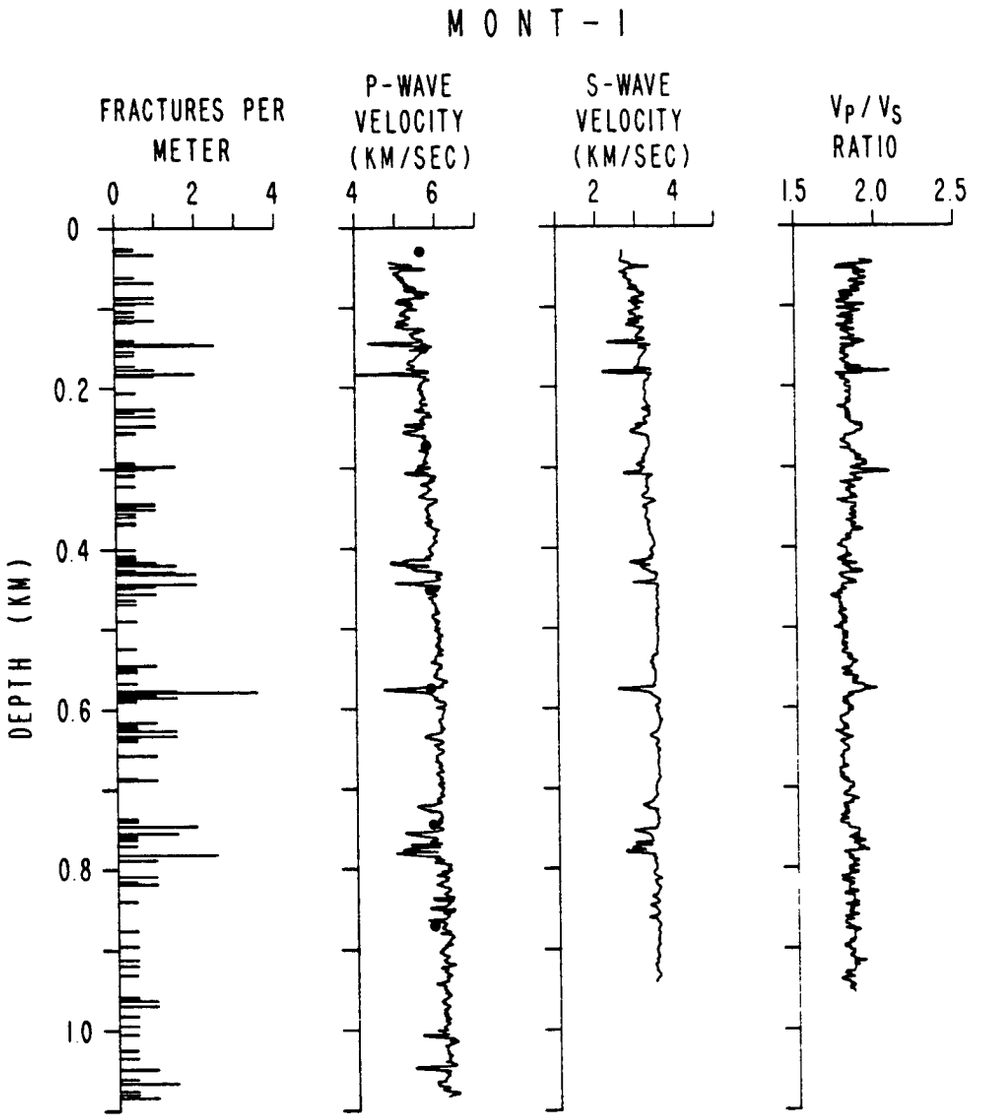

Fig. 1.4: Observable fracture density, P wave velocity, S wave velocity, and V_p/V_S as a function of depth for MONT-1. The solid circles show laboratory-determined P wave velocities for one sample from 545 m in the well plotted as a function of depth by assuming an effective stress gradient of 16.7 MPa/km.

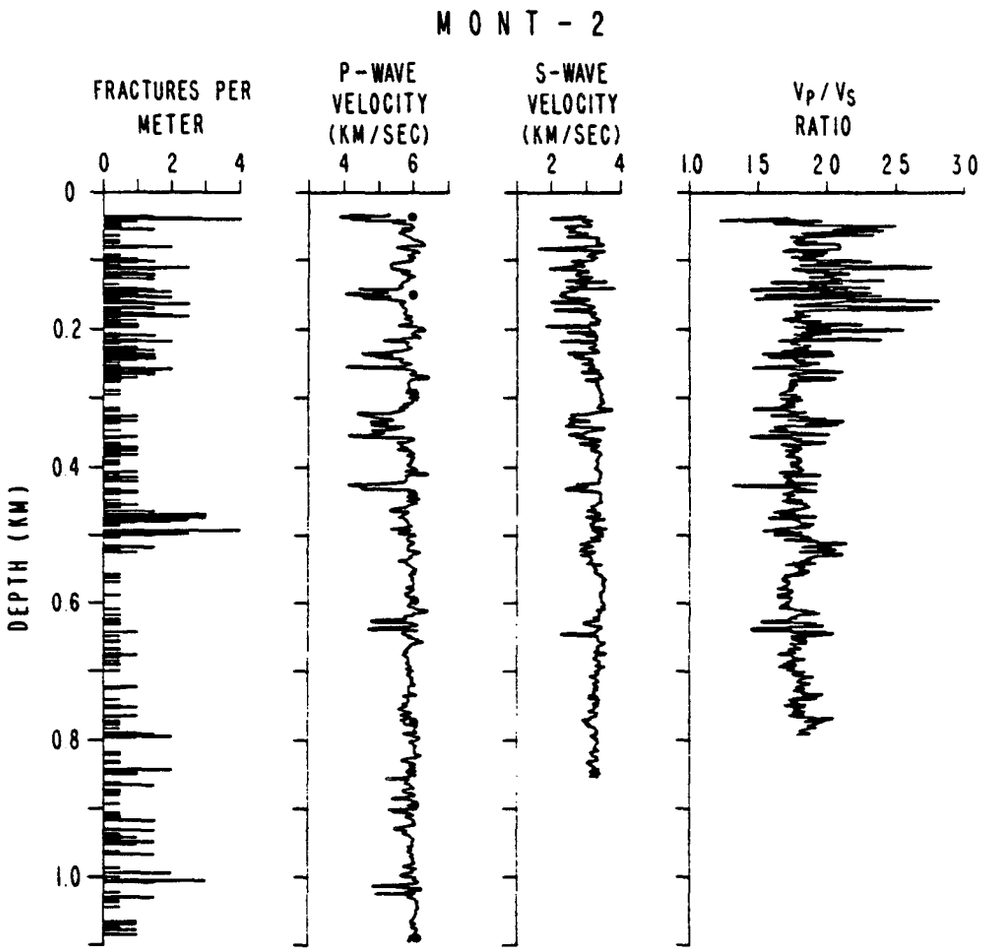

Fig. 1.5: Observable fracture density, P wave velocity, S wave velocity, and Vp/Vs ratio as a function of depth for MONT-2. The solid circles show laboratory-determined P wave velocities for one sample from 210 m in the well plotted as a function of depth by assuming an effective stress gradient of 16.7 MPa/km.

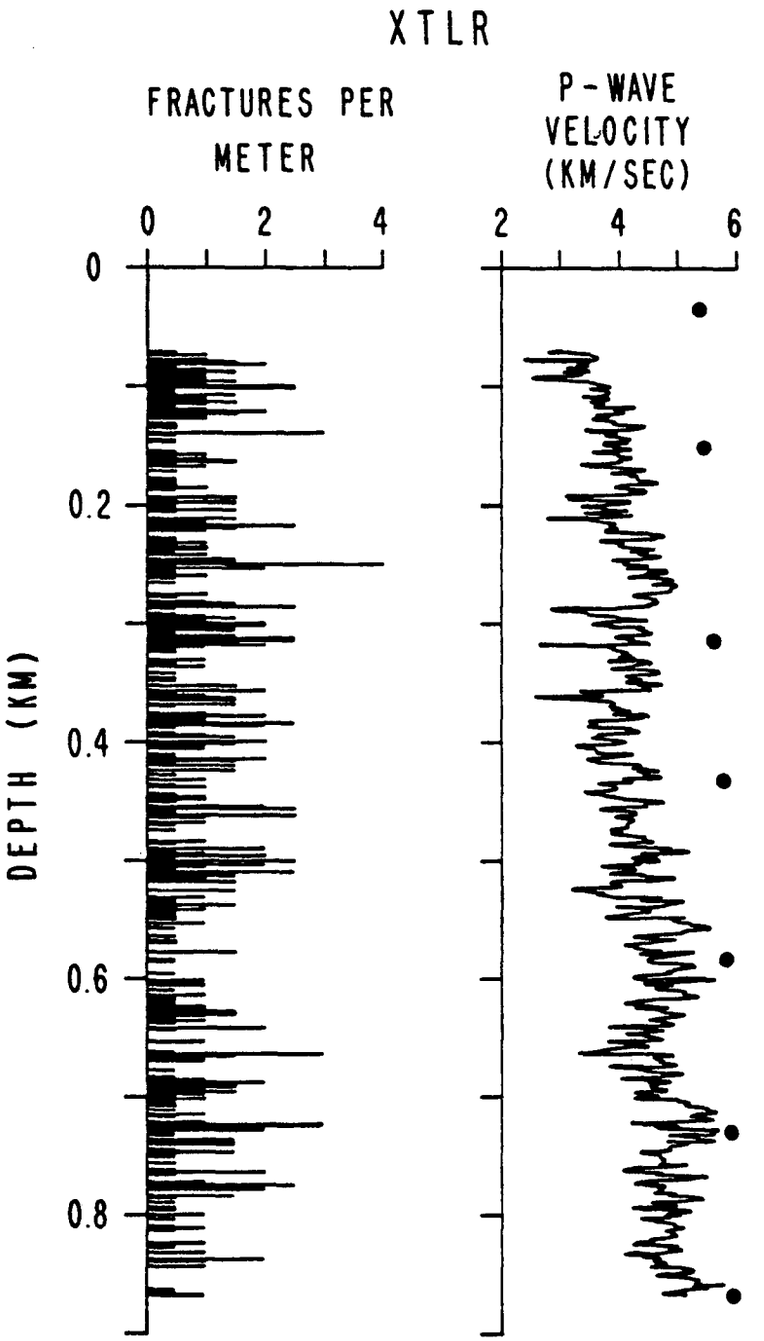

Fig. 1.6: Observable fracture density and P wave velocity as a function of depth for the XTLR well. The solid circles show laboratory-determined P wave velocities for one sample from the bottom of the well at 869 m plotted as a function of depth by assuming an effective stress gradient of 16.7 MPa/km. The high degree of fracturing in this well made measurements of S wave velocity unreliable.

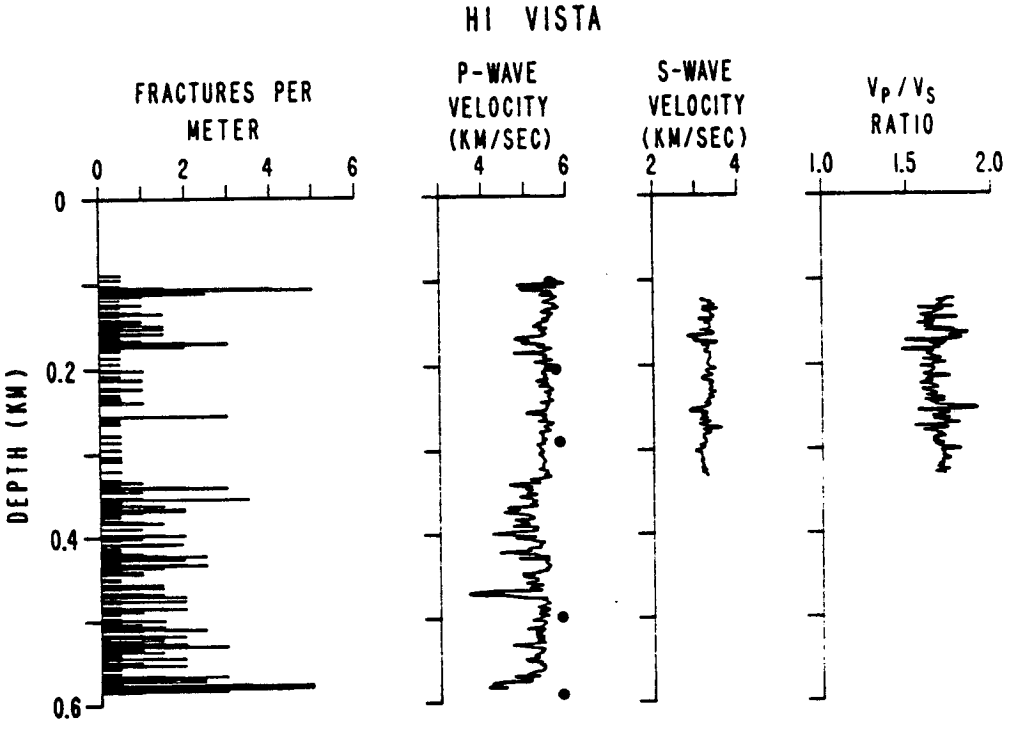

Fig. 1.7: Observable fracture density, P wave velocity, S wave velocity, and V_p/V_S as a function of depth for the Hi Vista well. The solid circles show laboratory-determined P wave velocities for one sample from the bottom of the well at 584 m plotted as a function of depth by assuming an effective stress gradient of 16.7 MPa/km. No S wave log was obtained for the lower portion of the Hi Vista well due to the high degree of fracturing.

velocity is essentially a function of the difference between confining pressure and pore pressure (Todd and Simmons, 1972), (2) the compressive stress in the direction of wave propagation (in this case the vertical stress) is most important in controlling P wave velocity, as suggested by the results of Bonner (1974) and Lockner *et al.* (1977), and (3) the mean stress in all of these wells is approximately equal to the overburden stress (Zoback *et al.*, 1980; Zoback and Hickman, 1982). Direct comparison to the field data at every depth may not be valid, as the laboratory data are obtained from only one sample in each well. However, qualitative comparison of the sonic and ultrasonic velocities and the changes of those velocities with depth and pressure provides additional information about the mechanisms controlling velocity.

The *in situ* P wave velocity in the MONT-1 well (Figure 1.4) increases from less than 5.4 km/s near the surface to about 6.1 km/s at 1100 m. The P wave velocity measured in a sample from a depth of 545 m increases from 5.7 to 6.0 km/s over the appropriate pressure interval. Except for the highly fractured low-velocity intervals, the velocity log and the laboratory measurements agree quite well, although the laboratory measurements are slightly slower at depths greater than 500 m. At the depth from which the sample was taken, the sonic and ultrasonic velocities are indistinguishable. There is a clear correlation between intervals of high fracture density and low sonic velocity. Almost every fracture zone is apparent as a low velocity zone on the sonic log.

The *in situ* P wave velocities in MONT-2 (Figure 1.5) are more variable than in MONT-1, possibly due to the more intense fracturing, and the results are quite dissimilar. The P wave velocity at shallow depth (about 5.9 km/s) is higher than in MONT-1, and the velocity increases only slightly with depth. Laboratory measurements on a sample from 210 m also show only a moderate increase of velocity with pressure (from 5.9 to 6.1 km/s). There is general agreement between the *in situ* and laboratory-determined velocities (with the exception of low-velocity intervals), although the laboratory-determined velocities are slightly higher than the *in situ* velocities at depths greater than 500 m. As in MONT-1, the sonic and ultrasonic velocities at the sample depth are the same. The striking correlation between intervals of high fracture density and low P wave velocity that was seen in MONT-1 is not obvious here, although relatively unfractured zones (e.g., 60-90 m, 270-300 m) have relatively higher velocity. The high uniform fracture density of the entire well appears to obscure the effect of local fracture zones on seismic velocity.

Figure 1.6 shows fracture density and P wave velocity in the XTLR well. The uniformly high degree of fracturing in this well causes large variations in velocity. The measured velocity in the near-surface region is extremely low (about 3.5 km/s), and the velocity increases to an average value of only about 5.2 km/s at 860 m. The *in situ* velocity in XTLR is significantly lower than it is in MONT-1 and MONT-2, apparently due to the greater number of fractures. As in MONT-2, the numerous fractures in this well obscure the correlation between highly fractured intervals and low velocity, but zones with fewer fractures (e.g., at 270, 560-610, and 720 m) have relatively high velocity. Laboratory measurements on a sample from the bottom of the well show an increase of velocity from 5.4 to 5.9 km/s over the appropriate pressure range. Thus the laboratory measurements are markedly higher than the *in situ* velocities. The discrepancy between the laboratory and *in situ* velocities seems to decrease with depth. However, the sample velocity is significantly higher than the *in situ* velocity even at 869 m, where the sample was taken.

Figure 1.7 shows the fracture density and P wave velocity in the Hi Vista well. The velocities are higher here than at XTLR, and there is no increase in velocity with increasing depth. In fact, the velocity at 100 m (about 5.6 km/s) is higher than the velocity at 580 m (about 5.4 km/s) due to the numerous fractures near the bottom of the well. The highest velocity in the well was measured in the interval from 180 to 335 m, where there are fewer fractures. Laboratory measurements on a sample from the bottom of the well show an increase of velocity from 5.6 to 5.9 km/s over a pressure range corresponding to depths from 118 m to 588 m. At the depth from which the sample was taken, the *in situ* velocity is markedly lower than the velocity measured in the sample.

A comparison between observed fracture density, *in situ* P wave velocity, and the velocity measured in the laboratory is summarized in Table 1. Several interesting trends emerge from these data. As might be expected, there is a correlation between the degree of fracturing in each well and the discrepancy between the laboratory and *in situ* values of the P wave velocity at the depths from which the samples were taken. For both MONT-1 and MONT-2 the velocity measured in the laboratory is nearly identical to the velocity measured in the field, but in the XTLR well and the Hi Vista well, where there are many fractures, the *in situ* P wave velocity is substantially lower than would be expected from laboratory measurements. However, the relative magnitudes of the ultrasonic velocities measured in samples from each well are the same as the relative magnitudes of the velocities measured *in situ*. The sample with

the largest ultrasonic velocity (MONT-2) comes from the well in which the highest sonic velocity was measured. The fact that the *in situ* velocity is higher at MONT-2 than at MONT-1, even though MONT-2 is highly fractured, suggests that, though macrofractures lower the velocity in a given well, the degree of *in situ* fracturing cannot be unambiguously estimated from *in situ* P wave velocity because of the importance of composition and microcracks.

The increase of velocity with pressure in the laboratory samples is related to the increase of velocity with depth in the field. The core from MONT-2 has the lowest increase in velocity with pressure and the smallest increase in velocity with depth *in situ*. The change in velocity with depth is greatest at XTLR; the core from XTLR also exhibited the largest increase in velocity with pressure. For these three wells the *in situ* velocity increase is equal to or greater than the increase measured in the laboratory, although at the Hi Vista well the anomalous fracture distribution masks the expected velocity increase.

TABLE 1: Laboratory-determined Vp, *in situ* Vp and macrofracturing for MONT-1, MONT-2, XTLR, and Hi Vista

	MONT-1	MONT-2	XTLR	Hi Vista
Fracture density	low	medium	high	high
In situ velocity	5.4-6.1 (14%)	5.9-6.1 (3%)	3.5-5.2 (49%)	5.6-5.4(-4%)
Laboratory velocity	5.7-6.0 (7%)	5.9-6.1 (3%)	5.4-5.9 (9%)	5.6-5.9 (6%)

Numbers in parentheses are the percent change of velocity with pressure or depth over the measured interval.

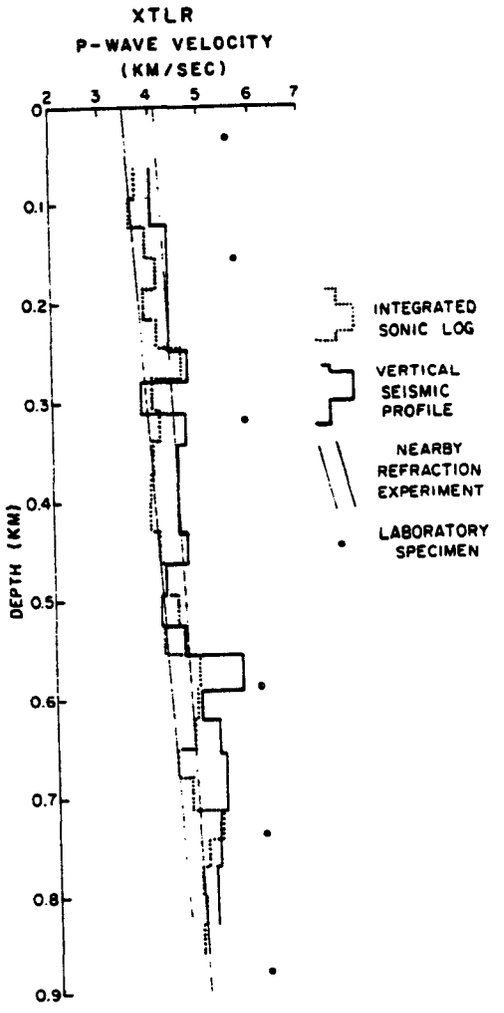

Fig. 1.8: Comparison of compressional velocity as a function of depth at the XTLR well for three different *in situ* measurements. Interval velocities from the downhole survey (fundamental frequency 75 Hz) are plotted as a solid line. The dotted line shows velocities measured by the sonic logging tool at 10-20 KHz averaged over the same intervals. The shaded area is bounded by two velocity-depth functions fitted to the data from a nearby refraction survey (fundamental frequency 10 Hz, G. Fuis, personal communication, 1982). Laboratory-determined P wave velocity of a core from the bottom of the well is also shown for comparison. Note that all three *in situ* measurements of velocity agree quite well and are markedly lower than the laboratory-determined velocity.

Vertical Seismic Profile

Because the wavelength of the energy from the sonic tool (20-60 cm) is similar to the spacing of many of the fractures, the frequency at which velocity is measured must be taken into account when sonic logs are analyzed. For example, field measurements of velocity using seismic refraction, reflection, or downhole surveys are made at frequencies that are several orders of magnitude lower than the frequencies of sonic logs. As the spacing of the macrofractures is similar to the sonic wavelength, but many orders of magnitude smaller than the wavelengths used in seismic experiments, the effect of the macrofractures on each measurement may be quite different.

Comparisons of seismic velocities over a wide frequency range are also complicated by the possible effects of dispersion. Recent laboratory measurements (Spencer, 1981; Murphy, 1982) have shown that there can be significant velocity dispersion in the frequency band from 10 Hz to 10 kHz in a wide variety of rocks. Although confining pressure moderates this effect, the change in Young's modulus (E) over this frequency range was about 22%for Oklahoma granite at room conditions (Spencer, 1981). Although Spencer suggests that this large effect on E was due primarily to stress relaxation in the shear modulus, this effect may still be large enough to affect measurements of P velocity.

In order to study the possible effects of frequency due to dispersion and of the finite size of the macrofracture in the rock volume sampled by the sonic wave, a vertical seismic profile (VSP) was run at XTLR using an air gun source. The air gun has a fundamental frequency of about 75 Hz. Interval velocities were calculated by differencing the arrival times to a geophone placed at 30-m intervals in the well (see appendix for further details). By summing the travel times measured by the sonic tool over these intervals, a comparison can be made between the velocity measured by the sonic tool over 30.5 cm intervals and the velocity calculated from the VSP (Figure 1.8). The interpretation of a nearby seismic refraction experiment with a fundamental frequency near 10 Hz (G. Fuis, personal communication, 1982) is plotted in Figure 1.8 for comparison. Overall, there is remarkable agreement between the sonic log (with 20- to 60-cm wavelengths), the vertical seismic profile (with wavelengths of about 60 m), and the refraction survey (at wavelengths of several hundred meters). However, the ultrasonic velocities (also shown in Figure 1.8) are significantly higher than the field measurements.

The field measurements of velocity shown in Figure 1.8 indicate that dispersion in the range of

frequencies from 10 Hz to 20 kHz is less than 10%, which is the combined accuracy of our measurements (see appendix). Interestingly, the velocity measured by the sonic log in XTLR is slightly lower than that measured by the VSP, and this difference cannot be explained by dispersion. One possible explanation for this effect is discussed in Chapter 3.

It is difficult to determine whether the discrepancy between the log velocities and the laboratory measurements is in part due to dispersion. However, in both MONT-1 and MONT-2 there is close agreement between log velocities and laboratory measurements. Therefore velocity dispersion over frequencies from 20 kHz to 2 MHz is probably small. However, the presence of many fractures in XTLR and Hi Vista causes large discrepancies between the P wave velocity measured in a 5-cm-long core and the log velocities. Thus it appears that the differences between the *in situ* data at the sample depth and the laboratory measurements result primarily from the presence of the macrofractures, and it appears that the effect of fractures on P wave velocities is roughly the same over the bandwidth from 10 Hz to 20 kHz.

S-Wave Sonic Velocities

Figures 1.4, 1.5, and 1.7 show S wave velocities and V_p/V_S measured at MONT-1, MONT-2, and in the upper portion of Hi Vista. Because of the high fracture density at XTLR and in the lower portion of Hi Vista it was not possible to record S wave logs. The method used to obtain these logs is described in the appendix.

Figure 1.4 shows S wave velocity and V_p/V_S ratio in MONT-1. The near-surface S wave velocity is about 2.8 km/s, and the velocity increases with depth to about 3.4 km/s in the lower portion of the well. The correlation between intervals of high fracture density and low velocities seen in the P wave log is also present in the S wave log. The V_p/V_S ratio in MONT-1 is about 1.9 in the near-surface region and decreases gradually with increasing depth to about 1.8 in the lower portion of the well. The V_p/V_S ratio also is strongly affected by the presence of fractures; the fracture zones at 180, 290-310, and 580 m have V_p/V_S ratios greater than 2.0.

Figure 1.5 shows S wave velocity and V_p/V_S ratio in MONT-2. The S wave velocity is quite low and highly variable in the highly fractured interval above 280 m. The average velocity for the zone below

280 m is 3.35 km/s and decreases slightly below 600 m. Zones where the P wave velocity is low are also zones of low S wave velocity (for example, at 300-330 m and 400-410 m). In general, unfractured zones have the highest S wave velocities (510-590 m), and in these zones the percentage increase in S wave velocity is more pronounced than for P wave velocity. There is more scatter in V_p/V_S because either spurious P or S wave velocities result in large variations of the ratio. In the densely fractured upper portion of MONT-2 the V_p/V_S ratio varies from 1.75 to more than 2.0. Below 280 m the V_p/V_S ratio varies between 1.65 and 1.95 (except in isolated sections) and seems to increase slightly with increasing depth. Several fractures seem to coincide with locally large V_p/V_S ratios (for example, for fractures in the zone from 193 to 270 m). However, from 320 to 370 m and from 510 to 560 m, high V_p/V_S ratios are seen in relatively unfractured rocks. In the interval from 320 to 370 m both P and S wave velocities are anomalously low, but in the interval from 510 to 560 m, only the S wave velocity is low. Furthermore, several fractured intervals are not clearly associated with higher V_p/V_S ratios.

S wave velocity and V_p/V_S ratio in the upper part of the Hi Vista well are shown in Figure 1.7. The S wave velocity in the upper 400 m is about 3.4 km/s and decreases slightly with increasing depth. There is no clear relationship between distinct fracture zones and S wave velocities. V_p/V_S is about 1.65 in the upper 200 m and increases slightly to 1.8 in the lower section. Densely fractured zones are again characterized by large variations in the calculated V_p/V_S ratio. The prominent fracture zone at 256 m has a V_p/V_S ratio of 1.9, much higher than that of the rest of the well. As in MONT-2, several fracture zones seem to have locally higher V_p/V_S ratios, although many do not.

Sonic Waveforms

In order to study in more detail the effect of *in situ* fractures on V_p and V_s, full waveforms were recorded at the Hi Vista well with the sonic tool stationary in the well. The first 10 ms of each waveform was digitized at 5 μs intervals. Waveforms were recorded every 30.5 cm over a 30-m interval that included both fractured and unfractured sections of the well.

Figures 1.9 and 1.10 show data from two intervals in the Hi Vista well. At the left side of each figure is the BHTV record of the interval. V_p and V_s calculated from the sonic logs at 30.5-cm intervals are shown in the center of each figure. The data points are plotted at the upper end of the interval over which differential travel time was measured. Where the travel times were picked incorrectly, velocities

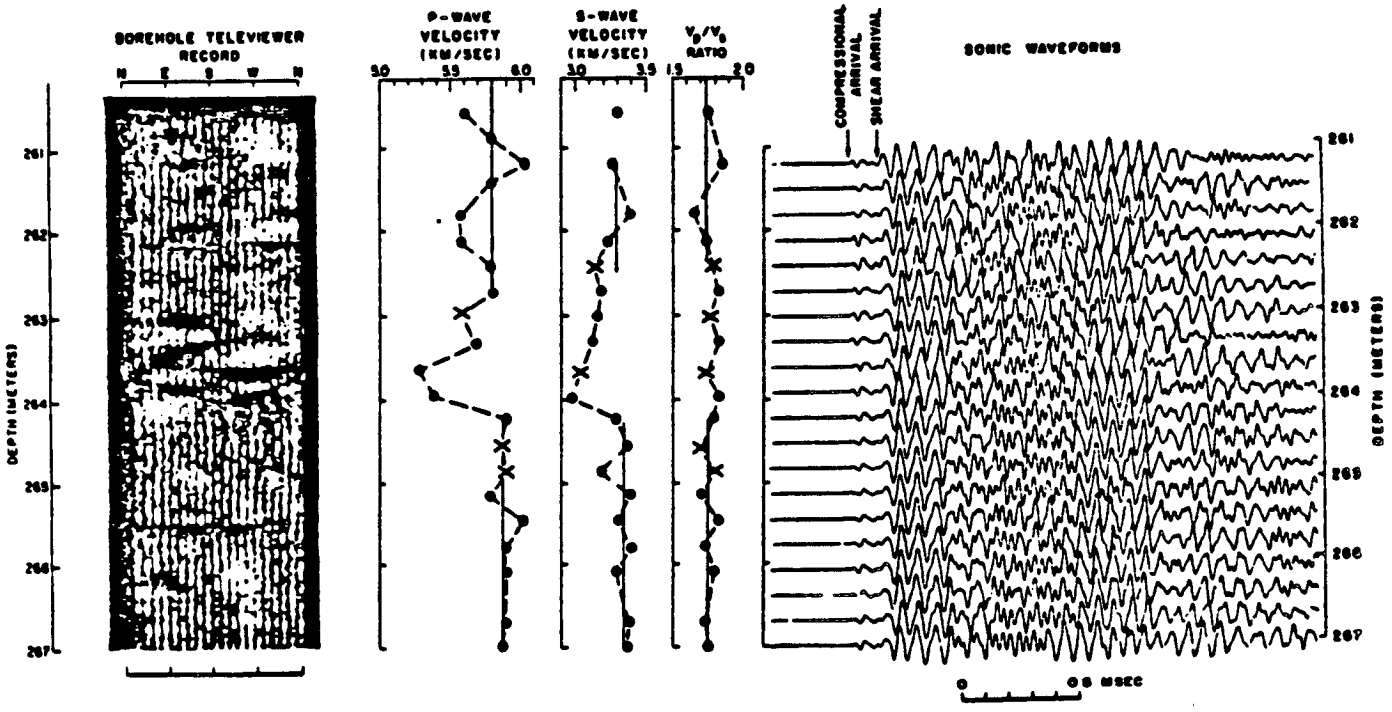

Fig. 1.9: Comparison of the borehole televiewer record to P wave velocity, S wave velocity, V_p/V_S, and sonic waveforms at the Hi Vista well in the depth interval from 260 to 267 m. The dark, sinusoidal line on the televiewer picture indicates a fracture at a depth of 263.6 m in the well. The velocities are plotted at the upper end of the 30.5-cm interval over which the measurements were made. Where the sonic tool picked the velocity incorrectly, the velocity was measured from the full waveforms and is plotted as a cross. The waveforms were recorded with the source 1.22 m below the receiver depth and displayed at the receiver depth.

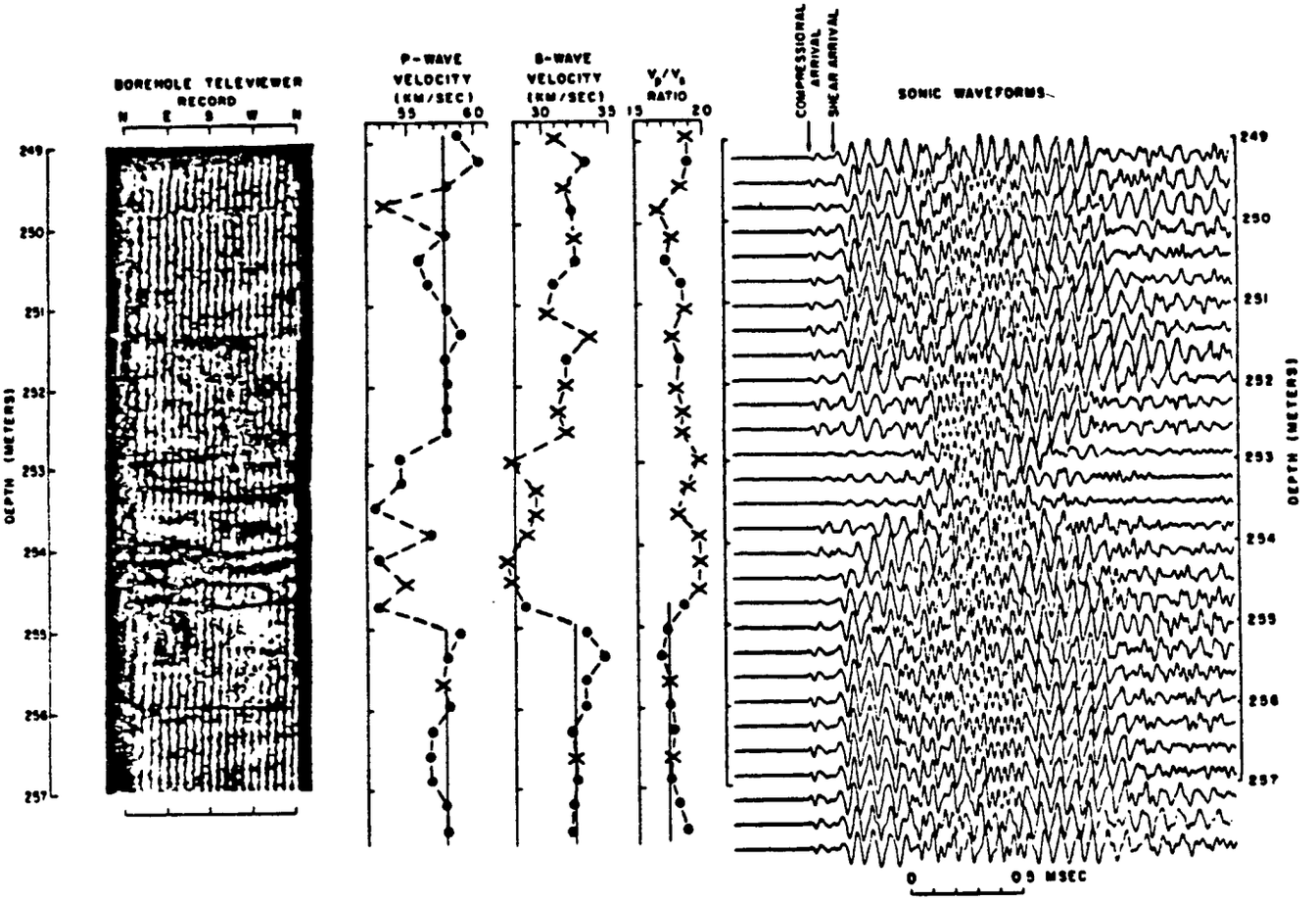

Fig. 1.10: Comparison of the borehole televiewer record to P wave velocity, S wave velocity, V_p/V_S, and sonic waveforms at the Hi Vista well from 249 to 258 m. The velocities are plotted at the upper end of the 30.5-cm interval over which the measurements were made. Where the sonic tool picked the velocity incorrectly, the velocity was measured from the full waveforms and is plotted as a cross. The waveforms were recorded with the source 1.22 m below the receiver depth and displayed at the receiver depth. There are a series of dipping fractures intersecting the well in the interval between 253.2 and 254.7 m.

were calculated from arrival times picked on the full waveforms and are denoted by crosses. Also plotted in these figures is the V_p/V_S calculated from the velocity data. Full waveforms from the receiver at a distance of 1.22 m from the source are displayed at the right side of each figure. The waveforms are plotted at the receiver depth. Since the source is below the receiver, the travel path extends over the 1.22-m interval below the plotted depth.

Figure 1.9 shows data from the depth interval between 260 and 267 m. A single macroscopic fracture intersects the borehole at 263.6 m, striking N45°W and dipping 40° to the southwest. The apparent aperture of the fracture is about 8 mm, although this could be misleading if drilling causes spalling of the rock near the fracture at the borehole. The average P wave velocity above the fracture is about 5.80 km/s, and the average velocity below the fracture is about 5.88 km/s. The average S wave velocity above the fracture is about 3.30 km/s and about 3.35 km/s below the fracture. This yields average V_p/V_S ratios of 1.73 and 1.76 above and below the fractured interval, respectively. The fracture clearly reduces both V_p and V_s; the principal reduction in velocity occurs over about a 1-m zone straddling the fracture. Importantly, the anomalously low velocity is not confined to travel paths intersecting the fracture plane. Also, the V_p/V_S ratio seems to be slightly increased in a broad zone surrounding the fracture.

The fracture at 263.6 m has little effect on the character of the waveforms displayed at the right. The arrivals below 264 m, which do not cross the fracture, are remarkably uniform. Both P and S amplitude are essentially unaffected by the fracture. Some subtle distortion, particularly in the S waveform, occurs in waveforms in the interval from 262 to 263.8 m, which cross the fracture, and the S arrival is slightly delayed. The compressional arrival time is quite variable near the fracture (262-263.8 m) and in general shows slightly more scatter than the shear arrival time over the entire interval. The fracture does not significantly affect the character of later arrivals.

Figure 1.10 shows a more intensely fractured zone at 254 m in the Hi Vista well. This fracture zone can also be seen in Figure 1.6; the sonic logs show sharply reduced V_p and V_s and sharply increased V_p/V_S. The average values of V_p, V_s, and V_p/V_S over the entire interval are identical to those obtained for the upper section of Figure 1.8. As in Figure 1.8, P wave velocity is reduced in both the fracture zone and the area adjacent to the fracture zone where the travel path does not intersect any apparent macrofractures. The S waves were so badly attenuated by the fractures that velocities could not be

determined by the sonic logging tool, although one markedly lower velocity was detected in the fracture zone. Velocities were calculated for intervals where the sonic log does not provide any data by picking arrival times from waveforms recorded at the two near receivers. The S wave velocity determined from the full waveforms is also measurably lower near the fracture zone, and V_p/V_S is higher. Although the largest velocity reduction occurs within the fracture zone, changes in V_p, V_s, and V_p/V_S extend at least 1 m above the fractures.

The fracture zone shown in Figure 1.10 causes significant distortion of the wave field. Compressional and shear energy is sharply reduced, and the arrivals are delayed significantly. The fracture zone also severely attenuates later arrivals, although the high-frequency direct fluid wave is unaffected.

DISCUSSION

It is well known that the presence of flat cracks or pores in an otherwise homogeneous material can substantially reduce its elastic moduli (and hence velocities). Microcracks in rock have been successfully invoked to explain laboratory velocity measurements as a function of confining pressure (Birch, 1961), pore pressure (Todd and Simmons, 1972), and saturation (Nur and Simmons, 1969). O'Connell and Budiansky (1974) theoretically deduced the effect that cracks should have on elastic moduli and seismic velocity, using a self-consistent model that is reasonable for a densely fractured medium where crack interaction is important. The model is formulated under the assumption that both matrix and crack distribution are isotropic and that the cracks are much smaller than the seismic wavelength. Qualitatively, the O'Connell and Budiansky (1974) model predicts that for saturated cracks an increase in spatial crack density increases V_p/V_S and decreases V_p and V_s.

In this discussion we concentrate on changes in the elastic moduli because density changes due to fracturing probably had a negligible effect on P and S wave velocity as (1) the presence of fractures would probably decrease the density of the aggregate, causing the velocity to increase, and (2) the functional dependence of velocity on density is the same for both P and S waves, so the ratio of the velocities will be independent of density.

The results presented here indicate that sonic velocities measured in boreholes are affected by macrofractures in a way similar to that predicted by O'Connell and Budiansky (1974) for the effect

of microcracks on velocity. That is, increased macrofracture density decreases V_p and V_s and increases V_p/V_S. However, the situation discussed here differs from that described by the O'Connell and Budiansky (1974) model in several fundamental ways. Because the macrofractures are large in comparison to the sonic wavelength, the aggregate including macrofractures cannot be considered as an ideal continuum. Also, as the macrofractures occur singly or in preferentially oriented clusters, they impart an anisotropy to the aggregate that is not adequately modeled by O'Connell and Budiansky (1974). Therefore it is unlikely that the model generally provides an adequate explanation for the effect of macrofractures on sonic velocity. It is interesting, however, that in one well (XTLR) the effect of the fractures on the sonic velocity is quite similar to the effect of the fractures on seismic velocity (see Figure 1.8). As the fractures in aggregate have a variety of orientations in this well (Seeburger and Zoback, 1982) and as the seismic wavelengths are several orders of magnitude larger than the fracture size, the O'Connell and Budiansky (1974) model probably can be used to describe the major features of the effect of the macrofractures on seismic velocity.

Let us now consider three conceptual models for macroscopic fractures, shown schematically in Figure 1.11. We assume, in all three cases, that granular debris, vein-forming minerals, or asperities are holding the fractures open under pressure and the fractures are observable only because the fracture faces are held apart. In the spring model a macroscopic fracture acts essentially like a compliant element in an elastic continuum. That is, there is no change in the elastic properties of the rock adjacent to the fracture. This macrofracture model can be simulated by the introduction of saw cuts in intact laboratory specimens. Stesky (1979) found that saw cuts in a low-porosity sample significantly lowered the velocity and increased the pressure dependence of velocity of the sample.

In the microfracture model the rock adjacent to the fracture is a zone of relatively intense microcracking, but otherwise little change has occurred in the rock. Thompson (1966) found zones of high fracture density adjacent to principal slip surfaces in granites. The increased crack density in these zones was believed to have developed during slip events. The presence of slickensides on fracture surfaces in samples taken at depth from both the XTLR well and Hi Vista is evidence that the fractures observed at depth have accommodated shear motion, and increased microcrack density may have resulted from that motion. Alternatively, the fracture we see may be the end product of an episode of crack growth that initially produces a large number of microcracks some of which then coalesce

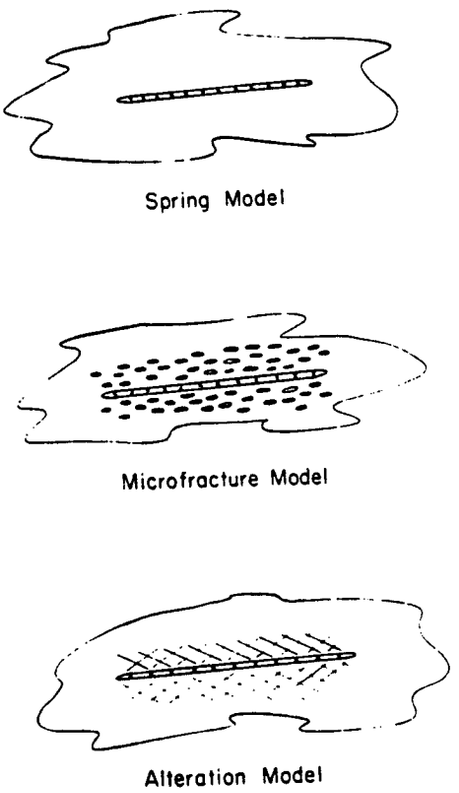

Fig. 1.11: Schematic representation of the three models of an *in situ* macrofracture. In the spring model the fracture is an elastic inclusion whose presence does not affect the properties of the surrounding matrix. In the microfracture model the fracture has accommodated shear motion resulting in additional microcracking of the matrix surrounding the fracture, and in the alteration model the matrix around the fracture is more highly altered than the host rock due to transmission of fluids through the fracture.

to produce the observed macrofracture.

In the alteration model the rock adjacent to the fracture has been mechanically and chemically altered so as to reduce the elastic moduli. Weathering can reduce the velocities of granites near the surface, and deep weathering is observed in granitic terranes where fractures provide conduits for surface water (Thomas, 1974). Analysis of cores from MONT-2 (D. Prowell, written communication, 1982) indicates that significant alteration is associated with the fractures in that well. Cuttings from the Hi Vista and XTLR wells also show the effects of weathering, particularly in the upper 100 m of the Hi Vista well (D. Stierman, written communication, 1982). A core from the bottom of the XTLR well, just below the fracture zone at 869 m, is highly altered, suggesting that weathering has extended to considerable depths.

Now let us consider the sonic log data in terms of the three conceptual models shown in Figure 1.11. The log data show that both compressional and shear wave velocities are reduced by macroscopic fractures *in situ*. In the case of relatively unfractured rock intervals the effect of localized fractures is to reduce the P and S wave velocities and increase V_p/V_S. In more highly fractured rock, *in situ* P wave velocities are lower than the ultrasonic velocities of intact samples in the laboratory (Figures 1.6 and 1.7). Both Figure 1.6 and Figure 1.7 suggest that the difference between the laboratory and *in situ* P wave velocities increases with fracture density. The difference in velocities gradually decreases as the macroscopic fracture density decreases with depth in Figure 1.6, and the difference increases with depth as the macrofracture density increases in Figure 1.7. Both of these cases suggest that in densely fractured rock the presence of macrofractures lowers the bulk elastic moduli of the rock. Importantly, anomalously low velocities are seen in Figures 1.4, 1.9, and 1.10 in the zones adjacent to the macroscopic fractures. Thus the macroscopic fracture has apparently affected the matrix properties of the rock surrounding it in a manner consistent with either the alteration model or the microcrack model.

Although the alteration and microcrack models are similar, the microcrack model predicts that there is a correlation between macrofracture and microcrack densities. If wells with the highest macrofracture density also had the greatest number of microcracks, one would therefore expect those wells to have the largest increase of velocity with depth. This is not the case, as comparison of the change of velocity with depth in MONT-1 and MONT-2 clearly shows. In fact, as shown in Table 1, laboratory velocities seem to be more pressure-dependent in samples from wells in which P wave velocity increases

significantly with depth (MONT-1 and XTLR). Therefore although microcracks affect velocities both *in situ* and in the laboratory, there does not seem to be a simple correlation between the degrees of macrofracture and microcrack density in these wells. Also, the effect of macrofractures on velocities should decrease with increasing depth, as the microcracks accompanying the fractures should be closed. Thus it is unlikely that enhanced microcracking near the macrofractures alone can adequately explain the observed data.

A surprising result of this study is that it is not possible to simply relate fracture density to P wave velocity or the change in P wave velocity with pressure in granitic rocks. As shown in Table 1, although MONT-2 is more fractured than MONT-1, it has a higher P wave velocity. The Hi Vista well is fractured similarly to the XTLR well at shallow depth but has a higher P wave velocity. Thus even though the presence of macrofractures has a marked effect on P wave velocity, the effects of composition and microfractures are also very important. This may explain why there are zones of anomalously low velocities in MONT-2 (Figure 1.5) which were not accompanied by obvious macrofracturing. It appears that at a given site one could probably not expect to predict approximate relative fracture densities from either P wave velocity or the change in velocity with depth.

Interestingly, fracture orientation does not appear to play a strong role in influencing the effect of fractures on sonic velocities in these wells. As the sonic travel path is vertical, one might expect that near-horizontal fractures would have a stronger effect on the velocities than would fractures with dips greater than 45°. In MONT-1, however, where no horizontal fractures occur between 200 and 950 m, the effect of the steeply dipping fractures within that interval was as strong as the effect of the more gently dipping fractures at shallower depths. In XTLR, where almost no horizontal fractures are seen, the *in situ* velocity was significantly reduced by the fractures even though most of the fractures had dips greater than 45°. Thus our data do not show any simple relationship between fracture dip and the degree to which the fracture affects sonic velocities.

The suspicion that fracture zones in the crust could be zones of low seismic velocities has led to the suggestion that fracture zones could be the cause of reflection events observed within otherwise homogeneous crystalline rocks. Mair and Green (1981) have identified a series of gently dipping fracture zones as the source of several strong events on a high-resolution seismic reflection profile in the Lac du Bonnet batholith of the Canadian Shield. Fracture zones have also been suggested as the source of

crustal reflections at much greater depths (Lynn, 1979; Schilt *et al.*, 1979). The Wind River Thrust Zone as observed on COCORP profiles (Smithson *et al.*, 1978) has been traced to more than 20 km depth. The fault zone is a strong reflector even where there is crystalline rock on both sides of the fault. Jones and Nur (1982) conclude that the mylonitization of the country rock, which may accompany large shear displacements at depth, cannot produce reflections of sufficient amplitude to explain the data. They suggest that high pore pressures in cracks along the fault zone may reduce the velocities and thus cause the reflections.

To examine this idea, synthetic reflection seismograms were calculated from the velocity logs. The reflection coefficient series was calculated from the velocity logs at 30.5-cm intervals using the formula $R = (\rho_1 V_1^2 - \rho_2 V_2^2)/(\rho_1 V_1^2 + \rho_2 V_2^2)$ assuming the density was constant. Two-way travel time was calculated by summing the slowness measured by the sonic log from the surface to the appropriate depth and multiplying by 2. A zero-phase source waveform with a 10- to 80-Hz bandwidth (which approximates the bandwidth of a Vibroseis source) was then convolved with the reflectivity log to produce the seismogram. The synthetic amplitudes are scaled by the maximum amplitude of the source waveform; thus the measured amplitudes correspond to the apparent reflection coefficients. Figure 1.12 shows the synthetic seismograms calculated for the MONT-1, MONT-2, XTLR, and Hi Vista wells. Also plotted in Figure 1.12 are the velocities and fracture densities as a function of two-way travel time, which allow direct comparison of the synthetic seismogram to the *in situ* data.

From the results in MONT-1 (Figure 1.12a) it is clear that although isolated fracture zones result in zones of distinctly lower velocity, the limited vertical extent of the zones compared to the seismic wavelength makes them difficult to detect. Although several fracture zones appear to produce low-amplitude reflections (e.g., at 245, 300, and 360 m), the reflections would probably be difficult to resolve at depth in a seismic section. At MONT-2 (Figure 1.12b), however, some of the low-velocity zones are of sufficient vertical extent that distinct reflections are seen, (e.g., at 100, 140, 240, and 330 m). In the XTLR well (Figure 1.12c), few distinct reflections are observed even though the well is quite fractured. The variations in velocity are too frequent to result in singular, distinguishable reflections; interference between the energy reflected at various depths produces a zone of apparent reflectors, perhaps similar to that observed in sections of the Wind River Thrust on COCORP profiles (Smithson *et al.*, 1978). The average amplitude of the reflected energy in the XTLR synthetic is comparable to that of the synthetic

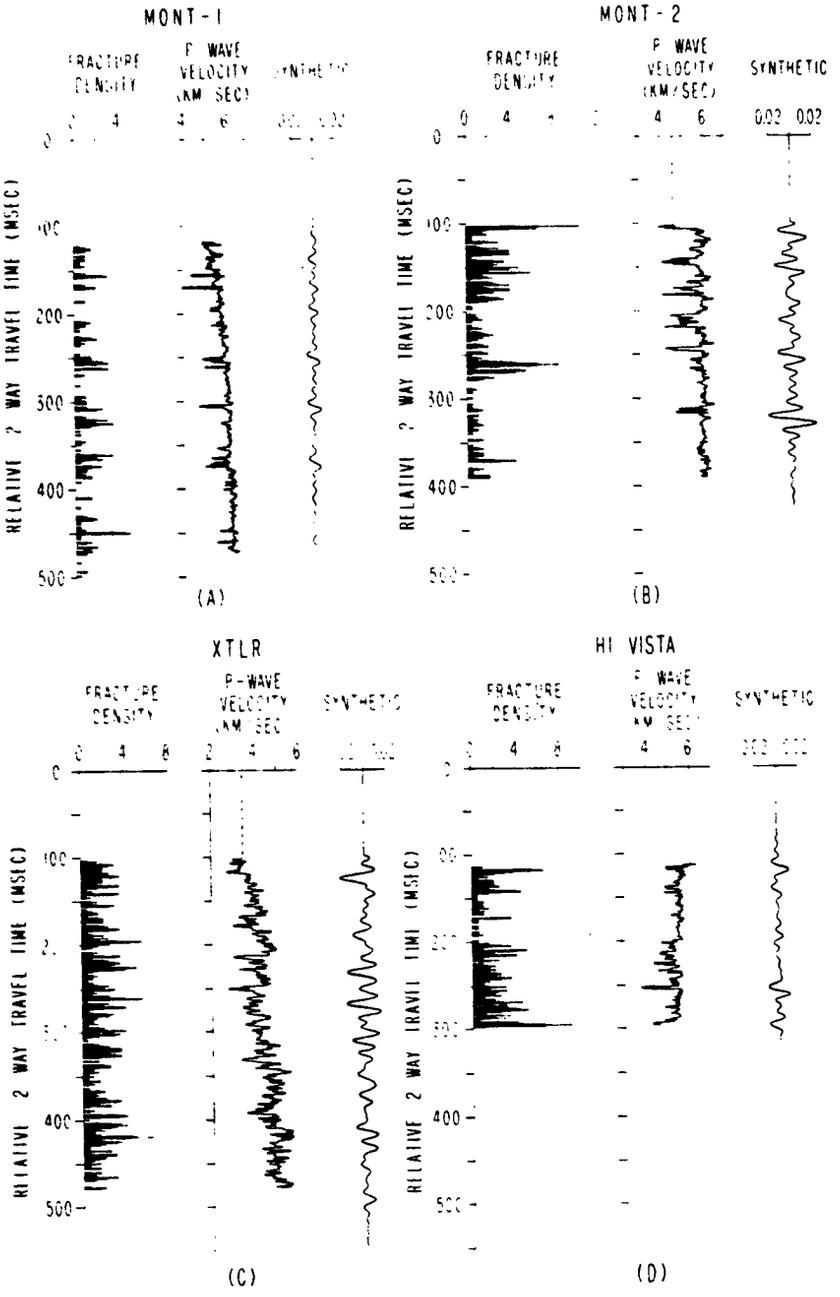

Fig. 1.12: Synthetic reflection seismograms for (a) MONT-1, (b) MONT-2, (c) XTLR, and (d) Hi Vista, plotted as a function of two-way travel time. The fracture density and seismic velocities are also plotted as a function of travel time. The synthetic amplitudes are scaled by the maximum amplitude of the source waveform.

from MONT-2. In the Hi Vista well (Figure 1.12d), several distinct reflections are seen that appear to correlate with changes in velocity due to fracturing. Also, a small reflection is observed at 200 m, corresponding to the top of the lower fracture zone. Reflections are also observed at 250 and 300 m due to the velocity increase at 480 m and the abrupt decrease at the bottom of the well. The amplitudes of the reflections in the Hi Vista synthetic are comparable to the amplitudes from XTLR and MONT-2. However, in Hi Vista the source of the reflection is clearly related to the observed fracture density. At Hi Vista the synthetic trace is relatively quiet between the reflections, which suggests that the reflected energy would be easily distinguishable.

These synthetic seismograms demonstrate qualitatively that velocity changes associated with fracture zones similar to those observed in these wells can produce reflections for energy in a suitable frequency band. Although it is difficult to relate any of the events observed in these synthetics directly to velocity anomalies, due to the problem of interference between adjacent reflections, it is significant that in several of the wells the velocity changes associated with fracture zones in crystalline rock appear to result in detectable reflections. If fracture zones like those found in these wells persist to great depth in the crust and if chemical alteration is as significant at great depth as it appears to be in the upper 1 km, then the presence of fracture zones of sufficient thickness at midcrustal depths could produce significant reflections.

CONCLUSIONS

The presence of macroscopic fractures *in situ* lowers both P and S wave velocities and increases V_P/V_S over a wide bandwidth. *In situ* macrofractures seem to affect velocity in a variety of ways: chemical alteration of the rock adjacent to macrofractures, increased microfracturing near the macrofractures, and the compliance of the macrofractures themselves all cause reductions in P and S wave velocity to some degree. The data suggest, however, that the effects of chemical and mechanical alteration may be very significant in lowering the elastic moduli and seismic velocity near macrofractures.

The magnitude of the velocity and its rate of change with depth of granitic rocks in the upper kilometer of the crust is largely controlled by the composition and microscopic properties of the rock. In general, the *in situ* velocity changes more rapidly with depth than laboratory data predict, which suggests that macrofractures are important in controlling the velocity- depth function.

Low-velocity zones produced by fracturing and its related effects appear to produce coherent reflections on synthetic seismograms, which suggests that crustal reflectors within crystalline rocks might result from fracture systems similar to those encountered in these wells, especially if chemical and mechanical alteration of the matrix is pervasive near macrofractures at depth.

CHAPTER 2

Pressure dependence of P- and S-wave velocities

The existence of precursory velocity anomalies prior to earthquakes has been widely discussed (see Ward, 1979). These include both changes in P– and S–wave velocities and in the ratio of the velocities (or t_s/t_p). Such variations presumably occur as a response to changing tectonic stresses. Relatively few studies have demonstrated convincingly the existance of such changes. It is well known, however, that large shear stresses can produce measureable velocity anisotropy in rocks with cracks (Nur and Simmons, 1969; Lockner *et al.*, 1977), and it has been suggested that *in situ* stresses could be inferred from velocity measurements (Nur, 1971). Knowledge of the degree of *in situ* pressure sensitivity of P– and S– wave velocities, and its variation with depth, is critically important in determining whether such effects are measureable.

Laboratory experiments indicate that elastic-wave velocities are strongly pressure dependent at low pressures (Birch 1960,1961; Nur and Simmons, 1969 among others). The pressure dependence of velocity decreases rapidly as microcracks close due to increasing effective pressure. Extrapolations of these results to the field suggest that the *in situ* pressure sensitivity of velocity decreases several orders of magnitude in the upper few kilometers of the earth's crust.

There have been few attempts to compare laboratory measurements of the fractional pressure dependence of velocity (here called α, where $\alpha = dV/VdP$) with field data. Stierman *et al.* (1979) compared ultrasonic compressional velocities measured in the laboratory to a sonic log run in a 600 m deep well in quartz diorite of the Gabilan Range in central California. In the near-surface (above 600 m) α_p was about .01 per bar. The inferred magnitude of α_p decreased rapidly below that depth to about 0.0001 per bar at 6 km. Saturated laboratory samples exhibited a smaller fractional pressure dependence whereas the fractional pressure dependence of velocity in dry samples was somewhat higher.

The pressure sensitivity of rocks in the near-surface has been inferred from tidal stress related velocity variations by a number of researchers. Reasenberg and Aki (1974) measured changes in the

surface-wave velocity of jointed granite in response to tidal stresses; the change in travel-time was about 0.5%, suggesting that the fractional pressure dependence of velocity at the site was about 0.2 per bar. They attributed this strong pressure dependence to the presence of the joints in the upper 15 meters of the rock mass. By extrapolating these results to depth, they deduced that the fractional pressure dependence of velocity is .001 per bar at 1.5 km. On the basis of airgun experiments conducted at Bouquet Reservoir, Malin and Leary (1981) developed a model for the near-surface behavior of the crust near the San Andreas fault that suggested that one bar changes in fluid pressure resulted in 0.1% changes in velocity for waves refracted at 0.5 km ($\alpha_p = 0.0002$ per bar), and inferred that for waves refracted at 2 km the fractional pressure dependence of compressional velocity would be about 0.0001 per bar. Thus the fractional pressure dependence of velocity predicted by Malin and Leary (1981) at depths greater than one km is an order of magnitude smaller than that predicted by Reasenberg and Aki (1974). These results indicate that although the fractional pressure dependence of velocity can be quite large in the near-surface, it decreases rapidly with increasing depth.

In this chapter, the sonic logs and ultrasonic velocity measurements discussed in Chapter 1 will be used to study the pressure sensitivity of velocity in fractured rocks. The absence of any major lithologic changes with depth in these wells suggests that any velocity changes are due to pressure effects. In addition, the relative magnitudes of the *in situ* stresses determined from hydrofracture stress measurements in the wells (Zoback *et al.*, 1980; Zoback and Hickman, 1982) will be compared to the *in situ* values of α. Thus comparisons can be made between the laboratory and *in situ* pressure sensitivity of velocity for a variety of stress regimes.

ANALYSIS

Comparisons of *in situ* velocity-depth functions to velocities determined in the laboratory as a function of pressure can be quite difficult because the *in situ* increase in velocity with depth is more variable than the increase of laboratory-determined velocities with pressure, due to the effects of local features such as fracture zones on the velocity. In order to facilitate comparisons of the *in situ* and laboratory measurements, both data sets were fitted to equations of the form:

$$V = a - be^{-cP} + kP \tag{2.1}$$

where a, b, c, and k are constants. Equations of this form were used by Stierman *et al.* (1979) to fit

velocity-pressure data in the fractured crystalline rock of the Gavilan Range. For the laboratory data P is the effective confining pressure. The *in situ* data were fitted after converting depth to pressure by assuming an effective pressure gradient of 167 bars/km. This is reasonable because the compressive stress in the direction of propagation (in this case, the overburden stress) is the most important in controlling the velocity, as suggested by the results of Bonner (1974) and Lockner *et al.* (1979). Here $V = a + kP$ describes the linear increase in velocity with pressure or depth at high pressures, and be^{-cP} describes the non-linear (crack-closing) behavior at low pressures, where b is chosen so that at the surface, or $P = 0$, $V = a - b$. The value of "b" determines the magnitude of the velocity increase due to crack closure, and "c" determines the pressure range over which crack closure is important. As "c" increases, this pressure range decreases. Using this equation, the change in velocity with pressure at a given effective pressure is then simply:

$$\frac{dV}{dP} = bce^{-cP} + k \tag{2.2}$$

A more meaningful measure of the ability to detect changes in velocity due to changes in pressure is the fractional pressure dependence of velocity, α, where $\alpha = dV/VdP$:

$$\alpha = \frac{dV}{VdP} = \frac{bce^{-cP} + k}{a - be^{-cP} + kP} \tag{2.3}$$

In order to compare the laboratory and field results using this equation, several assumptions must be made. First, it will be assumed that there is no systematic change in mineralogy with depth at the well which would cause a systematic change in the elastic properties or density of the rock that would mask the changes in velocity due to effective pressure. Second, the sample used to make the laboratory measurements must be typical of the *in situ* rock. Under these assumptions the linear portion of the laboratory velocity-pressure function can be used to describe the pressure dependence of velocity at depths below which microcracks and macroscopic fractures can be assumed to be closed.

The values of the parameters a, b, c, and k for the laboratory data were found using a multiple regression scheme. The field data were then fitted by choosing the laboratory values for a and k, which describe the high-pressure behavior of the rock in the absence of cracks, allowing b and c to vary until a best fit was achieved. The value of the parameter a was also allowed to vary. When fitting the field data the presence of discrete low velocity zones (e. g. at MONT-1) caused a small bias in the theoretical curve. To compensate for this we used the absolute error instead of the usual least squares criterion,

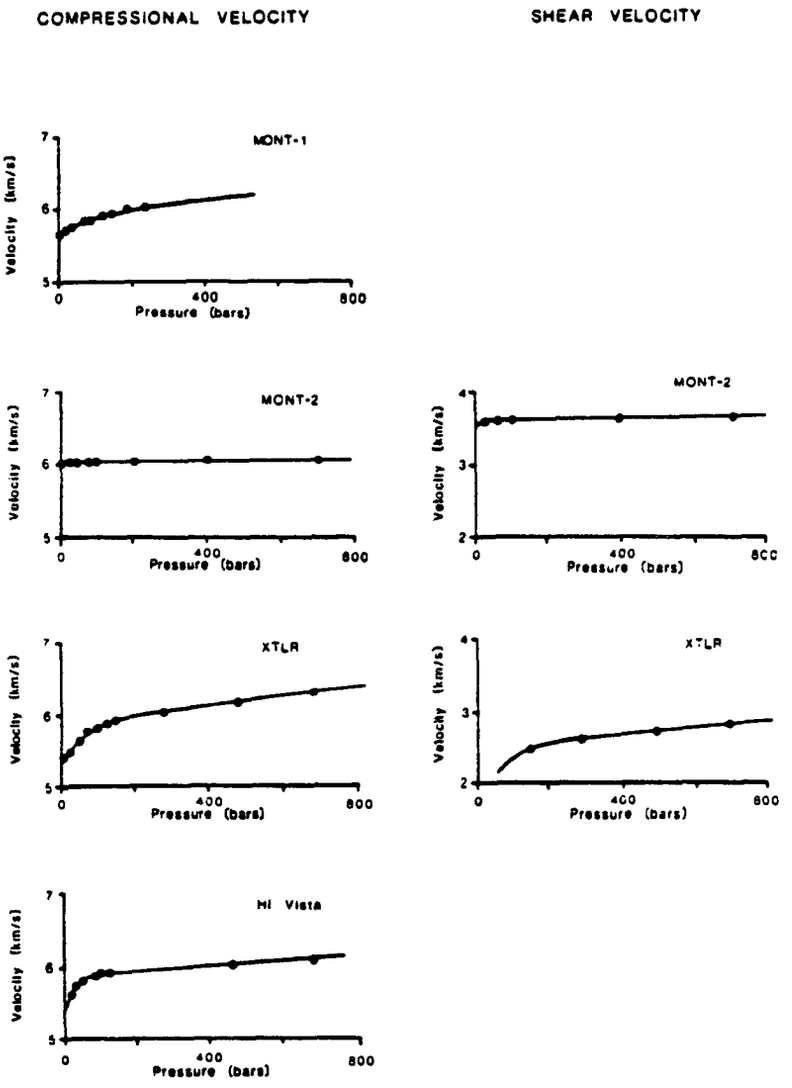

Figure 2.1: Laboratory measurements of compressional and shear velocity, and the fit of the theoretical curves to those measurements. The theoretical curves were computed from the values of the parameters shown in Table I.

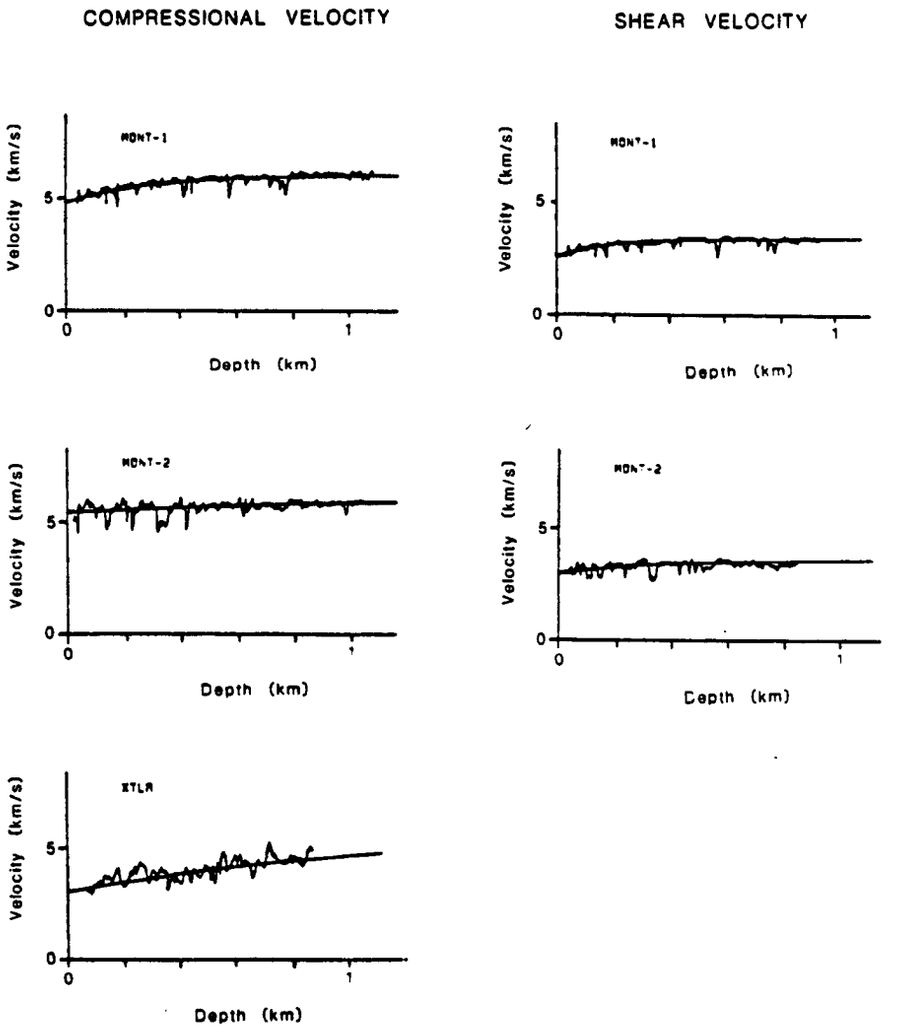

Figure 2.2: Fit of theoretical curves to the sonic velocity logs. The theoretical curves were computed from the average values of the parameters shown in Table I.

and also balanced the result so that the same number of data points lay above as below the theoretical curve. The values of the parameters obtained in this manner are shown in Table I. Data from the Hi Vista well could not be fitted to an equation of this type because of the anomalous fracture distribution. Only the laboratory data for saturated samples is presented in Table I, as the sonic logs were run below the water table where the rock is presumably fully saturated. The fit of the theoretical curves to laboratory data is quite good, as shown in Figure 2.1. Figure 2.2 shows the fit of curves (computed from the average value of the parameters in the table) to the *in situ* data. Although the velocities are not smooth functions of depth, the theoretical curves fit the *in situ* data quite well.

TABLE I: Values of a, b, c, and k in equation (2.1) for saturated samples from MONT-1, MONT-2, XTLR, and Hi Vista and for *in situ* data from MONT-1, MONT-2, and XTLR.

COMPRESSIONAL VELOCITY

	a km/sec	b km/sec	c 1/bar	k km/sec-bar
laboratory:				
MONT-1	5.914	0.275	10.36×10^{-3}	4.480×10^{-4}
MONT-2	6.025	0.039	72.90×10^{-3}	0.809×10^{-4}
XTLR	5.855	0.551	17.13×10^{-3}	6.625×10^{-4}
Hi Vista	5.896	0.591	36.94×10^{-3}	3.268×10^{-4}
in situ:				
MONT-1	5.914 ± 0.149*	$1.112 \pm .035$	$22.98 \pm 3.70 \times 10^{-3}$	4.480×10^{-4}**
MONT-2	6.025 ± 0.004*	$0.606 \pm .090$	$6.77 \pm 1.67 \times 10^{-3}$	0.809×10^{-4}**
XTLR	5.855 ± 0.023*	$2.852 \pm .407$	$4.57 \pm 1.00 \times 10^{-3}$	6.625×10^{-4}**

SHEAR VELOCITY

	a km/sec	b km/sec	c 1/bar	k km/sec-bar
laboratory:				
MONT-2	3.630	0.092	30.93×10^{-3}	0.559×10^{-4}
XTLR	2.515	0.998	16.63×10^{-3}	4.446×10^{-4}
in situ:				
MONT-1	3.401 ± 0.012	$0.816 \pm .057$	$34.07 \pm 5.01 \times 10^{-3}$	3.181×10^{-4}***
MONT-2	3.630 ± 0.015*	$0.632 \pm .060$	$10.51 \pm 2.33 \times 10^{-3}$	0.559×10^{-4}**

* Value assumed from laboratory data.
** Value assumed from laboratory P-wave data and the empirical relationship between laboratory shear and compressional pressure dependence.
Numbers in parentheses represent the range of values that provide a reasonable fit to the field data.

DISCUSSION

Some systematic variations can be seen in the values of the parameters "b" and "c" (which describe the effects of crack closure) shown in Table I. The *in situ* value of "b" is always greater than the laboratory value, suggesting that the influence of the crack closing term is more important in the field than in the laboratory. With the exception of MONT-1, the calculated value of "c" is always smaller in the field than in the laboratory. This implies that the effect of the crack closing term extends to greater

depths than would be predicted by the laboratory data. The P- and S-wave data yield similar values for "c", with the exception of those obtained from the laboratory sample from MONT-2. This is not unexpected, as theoretical results (e.g. O'Connell and Budiansky, 1974) suggest that for saturated rock changes in crack density due to crack closure affect V_p and V_s similarly. The apparent discrepency for the sample from MONT-2 may be due to slight undersaturation of the sample at low pressures, which resulted in a low measured P-wave velocity and a poor shear arrival which made the measurement of S-wave velocity unreliable.

The size of the velocity change due to crack closure in the laboratory is slightly larger for S-waves than for P-waves, presumably due to a larger change in shear modulus than bulk modulus as the cracks close. Interestingly, the field data does not show this relationship. In order to test this observation, the changes in K (the bulk modulus) and G (the shear modulus) as a function of pressure were calculated from the values of the parameters shown in Table I, using the relationships:

$$\begin{aligned} G &= \rho V_s^2; \\ K &= \rho(V_p^2 - \frac{4}{3}V_s^2) \end{aligned} \tag{2.4}$$

Figure 2.3 shows calculated dG/GdP and dK/KdP as a function of pressure for both laboratory and *in situ* data. For the laboratory data, as expected, dG/GdP is larger than dK/KdP at low pressures. As the pressure increases they become approximately equal. Although the *in situ* P-velocity increases more rapidly at shallow depth than the S-velocity, dG/GdP is greater than dK/KdP. Thus crack closure causes G to increase more rapidly than K both in the laboratory and in the field. As effective confining pressure increases and crack closure becomes less important, G and K increase at approximately the same rate.

There is also a systematic relationship between the value of "k" (which describes the high pressure behavior of the rock in the absence of cracks) for P- and S- waves. This relationship can also be seen in fits to data taken from the literature. Figure 2.4 shows the values of "k" obtained by fitting Eqn. (2.1) to laboratory velocity measurements made in saturated crystalline rock. The source of each data set is shown below the figure. In general, the relationship between k_p and k_s is:

$$k_s = 0.71 k_p \tag{2.5}$$

The *in situ* value of "k" for S-waves at MONT-1 was chosen by scaling the laboratory value of "k" for P-waves using this empirical relationship.

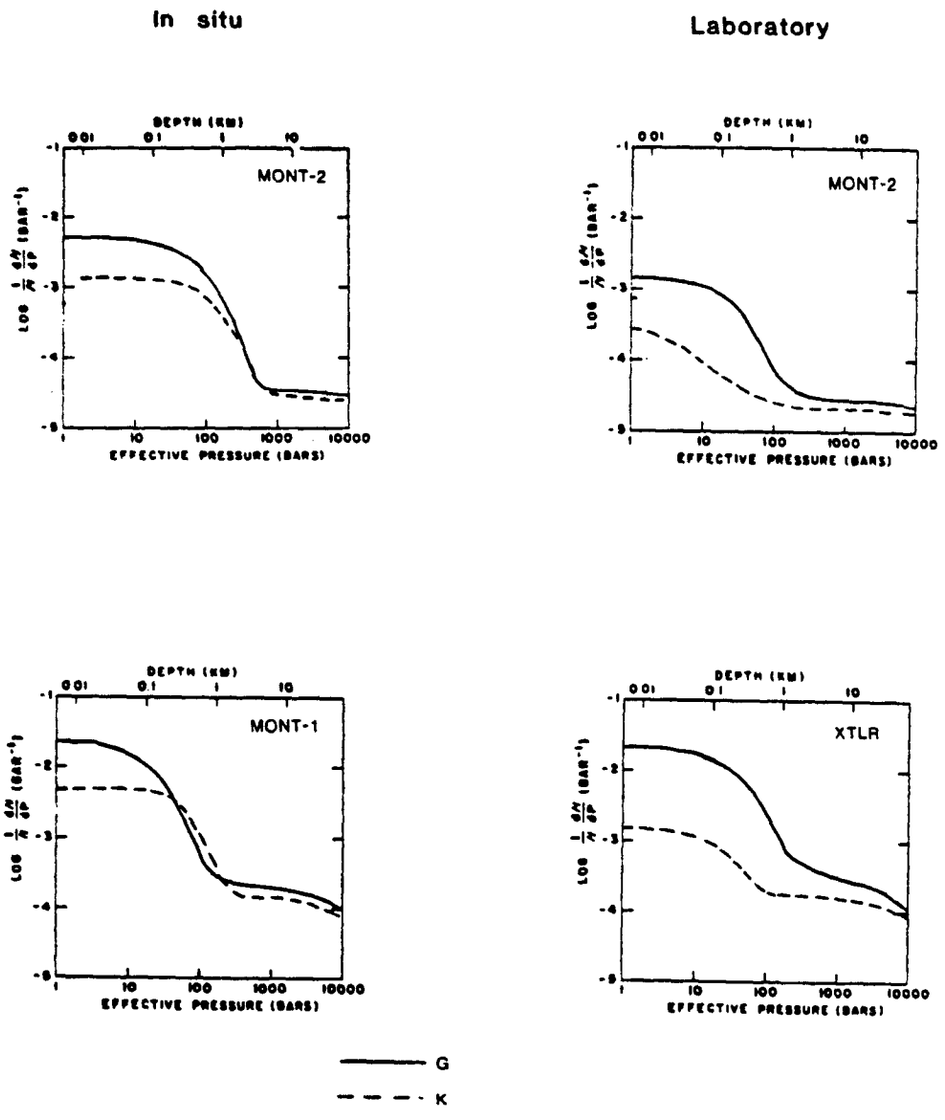

Figure 2.3: DG/GdP and dK/KdP calculated from Eqn. (2.4) using the values of the parameters in Table I.

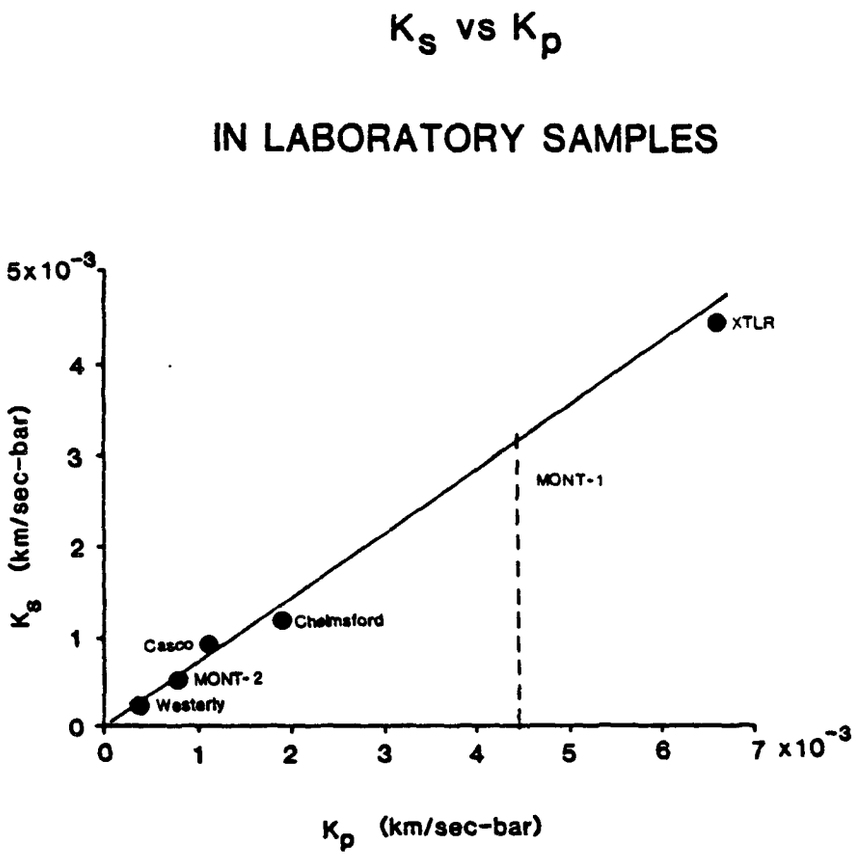

Figure 2.4: Comparison of k_p and k_e for laboratory data. Casco and Westerly data from Nur and Simmons (1969); Chelmsford data from Todd and Simmons (1972). The value of k_p for MONT-1 used to obtain k_e is shown.

At sufficiently high pressures (where $e^{-cP} \rightarrow 0$), α_p and α_s are controlled by the value of "k". Therefore, Eqn. (2.5) implies that there is a relationship between α_p and α_s. In the limit, as P$\rightarrow\infty$, Eqn. (2.3) becomes:

$$\lim_{P\rightarrow\infty} \alpha = \frac{1}{kP} \tag{2.6}$$

Thus the ratio $\alpha_p/\alpha_s = K_s/K_p = 0.71$. As V_p and V_s are algebraic combinations of the bulk and shear moduli, this implies that there is a relationship between the pressure sensitivities of K and G at high pressures which is invarient for the granitic rocks discussed here. This is not surprising, as the chemical composition of these samples is similar, and most of the difference in the pressure sensitivity of the velocities is due to differences in crack distribution and density.

Figure 2.5 shows α_p ($= dV_p/V_p dP$) and α_s ($= dV_s/V_s dP$) as a function of effective pressure or depth obtained by substituting the parameters presented in Table I into Eqn. (2.3). Several trends are immediately apparent. First, the discrepency between the *in situ* and laboratory pressure sensitivity of velocity is never more than about a factor of ten. Because of the method used to obtain the equations, the *in situ* curve asymptotically approaches the laboratory curve with increasing pressure. However, the rate at which the *in situ* pressure sensitivity approaches the laboratory curve is quite different for the different wells. At MONT-1 α_p is about 0.007 per bar in the near-surface (above 100 m) and decreases rapidly to less than 0.0001 per bar at depths greater than 1 km. At MONT-2 α_p is less than .001 per bar in the near-surface. However, α_p decreases more slowly with depth than at MONT-1, and at 1 km is still about 0.0005 per bar. Below 1 km α_p decreases rapidly to the high pressure laboratory value of 0.00002 per bar. At XTLR α_p is only slightly greater than the laboratory value at all pressures. The pressure sensitivity is similar to that at MONT-1 (about 0.007) in the near-surface, but decreases much more slowly with depth. At a depth of 1 km α_p is still 0.001, although it decreases rapidly below that depth to the laboratory value of 0.0001. In the Monticello wells α_s is slightly larger than α_p, but has approximately the same depth dependence. Thus, although the fractional pressure sensitivity of velocity can be as large as 0.01 per bar in the near-surface, it decreases rapidly with depth. Even though the pressure at which this rapid decrease occurs is greater *in situ* than in the laboratory, α is less than 0.0005 per bar at depths below 5 km (850 bars), and can be as low as 0.00002 per bar. This is approximately the same as that predicted by Malin and Leary (1981) and at least an order of magnitude smaller than that predicted by Reasenberg and Aki (1974).

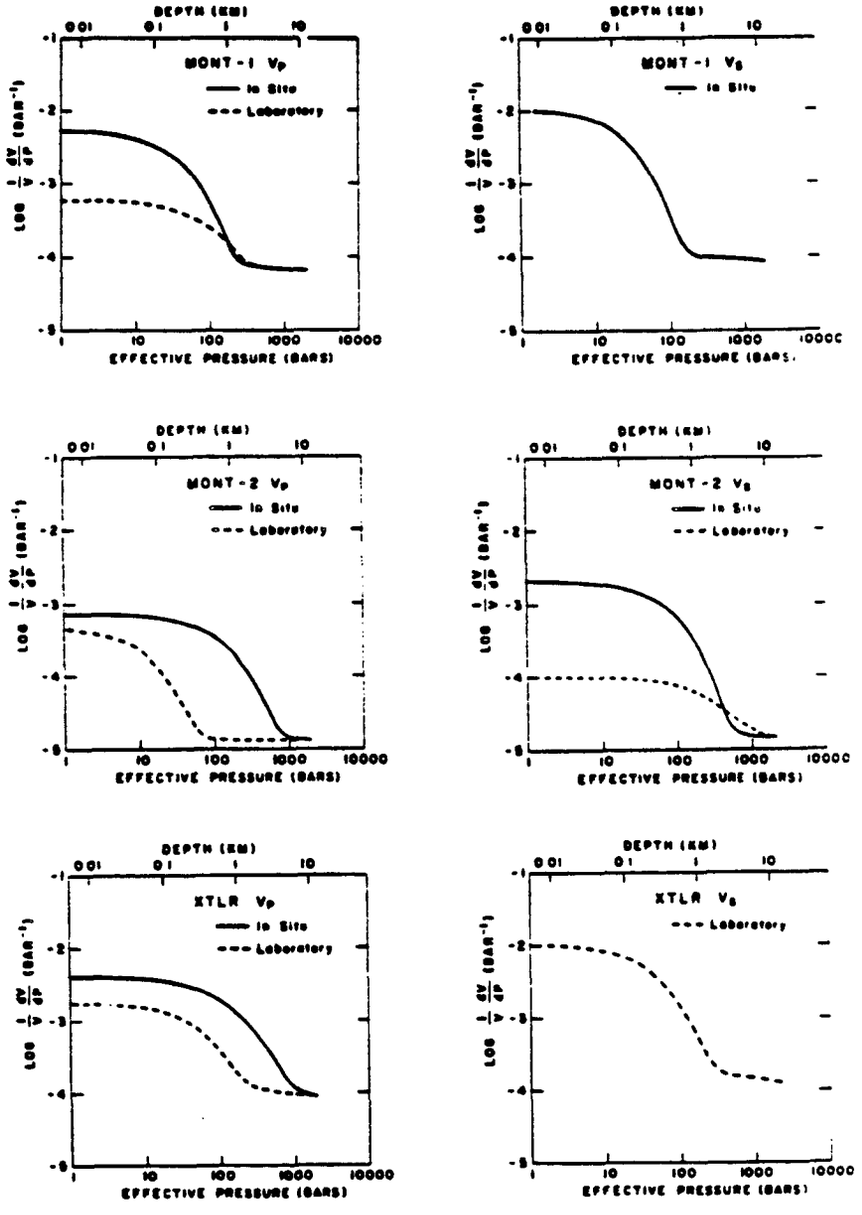

Figure 2.5: Fractional pressure dependence of the velocities as a function of pressure, calculated from Eqn. (2.3) and the values of the parameters shown in Table I. The *in situ* curves were calculated from the average values of the parameters.

The increase of velocity with pressure in laboratory samples has been explained by the presence of microcracks in the rock which close as the confining pressure is increased (Birch, 1961). The microcracks which are present in laboratory samples are not necessarily present *in situ*. Wang and Simmons (1978) showed that the removal of cores at depth from crystalline rock can result in the introduction of stress-relief microcracks, which close under pressures approximately equal to the vertical stress at the cored depth. The presence of these additional microcracks would cause the pressure sensitivity of the laboratory samples to be slightly higher than expected. Also, the depth to which the crack-closing term in Eqn. (2.1) is important may be affected by the presence of these cracks. There is, however, no systematic variation in the values of the parameters "b" and "c" for the laboratory data which is related to the depth from which the samples were taken. Therefore the presence of stress-relief microcracks does not significantly affect our results.

A more important consideration is the presence of macroscopic fractures. As Fig. 1.3 shows, there is a large difference in the degree of fracturing and in the change of fracture density with depth between these wells. There is no systematic increase in velocity with depth in the Hi Vista well, due to the anomalous fracture distribution.

Sonic velocity in the other wells is controlled primarily by the effective lithostatic stress, but differences in fracture density and distribution also influence the velocity-depth function. The MONT-1 well is relatively unfractured, and although the velocities are highly pressure dependent in the near surface the pressure dependence falls off rapidly with depth. There is, however, a relatively large discrepency between the *in situ* and laboratory pressure sensitivity of the P-wave velocity at shallow depths. The fracture density in the MONT-2 well is quite high in the upper 400-450 m. The laboratory pressure sensitivity of the P-wave velocity falls off rapidly with pressure, whereas the *in situ* pressure sensitivity decreases much more slowly. At intermediate pressures the *in situ* pressure sensitivity is much larger than the laboratory value. The S-wave data at the MONT-2 well show a very large discrepency between the laboratory and *in situ* pressure sensitivity, which similarly extends to about 100 bars. The high near-surface fracture density in the MONT-2 well (and its decrease with depth) may account for these features of the pressure sensitivity curves. The pressure sensitivity at depth in the XTLR well is much higher than in the Monticello wells. This may be partly due to the intrinsic pressure sensitivity of the rock which is evident from the laboratory measurements. However, the difference between the

laboratory and *in situ* pressure sensitivity extends to much greater depths in the XTLR well than in either of the Monticello wells. Fracturing also extends to much greater depths at XTLR. Therefore the fractures apparently increase the pressure sensitivity of the velocity.

DILATANCY

Up to this point I have discussed only changes in velocity due to changes in effective pressure. However, sufficiently large differential stresses can result in a decrease in velocity due to the opening of dilatant shear cracks (Nur, 1972; Hadley, 1975). If shear stresses are large enough, small changes in the applied stresses can cause relatively large changes in velocity, even at high confining pressures. This effect can be explained by the grain boundary sliding-axial crack model of Brace *et al.* (1966). The model suggests that dilatancy occurs in rocks when applied shear stresses are large enough to cause sliding along closed cracks or grain boundaries. However, this does not occur until the resolved shear stress along the crack is high enough to overcome the opposing frictional stress.

In the absence of cohesion, frictional failure will occur along a preexisting plane when the resolved shear stress exceeds the coefficient of friction times the effective normal stress. This occurs when the ratio of the maximum and minimum effective stresses is (Jaeger and Cook, 1969; p. 98):

$$\frac{S_1 - P}{S_3 - P} = (\sqrt{\mu^2 + 1} + \mu)^2 \tag{2.7}$$

where μ is the coefficient of friction. If dilatancy results essentially from sliding along closed cracks or grain boundaries, then its onset will be controlled by the coefficient of friction. Therefore, dilatancy will become important *in situ* only when the stress ratio exceeds the value defined by Eqn. (2.7).

The results of hydrofracture stress measurements made in these wells are summarized in Table II. The maximum and minimum horizontal stresses and the calculated lithostatic stress are presented for each of the hydrofracture stress measurements. The source of the data appears below the table. The calculated maximum shear stress is also shown. The maximum shear stress is simply one half the difference between the maximum and minimum compressive stresses. At shallow depth, where the minimum stress is vertical, the maximum shear stress is oriented along inclined planes and a thrust-type faulting regime is inferred. At some depth (different for each well) the minimum horizontal stress becomes the least principle stress, and a strike-slip regime develops.

TABLE II: Hydrofracture stress data in MONT-1, MONT-2, XTLR and Hi Vista. Source of dat: shown below the table.

Location	Depth (m)	P_p (bars)	S_h (bars±2)	S_H (bars±9)	S_v (bars)	τ_{max} (bars)
MONT-1**	165	17	79	135	44	45(t)
	486	49	119	135	129	37(ss)
	728	73	119	173	193	27(ss)
	961	97	186	317	255	65(ss)
MONT-2**	97	10	34	44	26	9(t)
	128	13	36	45	34	5(t)
	205	21	47	58	54	5(ss)
	298	30	56	75	79	10(n)
	312	31	64	95	83	27(ss)
	400	40	87	142	106	27(ss)
	646	64	166	305	171	70(ss)
MOJ-2*	149	15	50	88	40	24(t)
	167	17	51	89	45	22(t)
	230	23	83	140	62	39(t)
XTLR*	266	26	77	130	72	27(t)
	338	34	74	125	91	57(ss)
	561	56	150	264	152	57(ss)
	681	68	141	258	184	59(ss)
	751	75	188	356	203	84(ss)
	787	78	183	346	213	82(ss)
	849	85	193	352	230	80(ss)
Hi Vista***	180	8	74	137	48	45(t)
	227	12	71	121	60	30(t)
	273	17	58	87	72	15(t)
	325	22	94	136	86	25(t)
	493	39	124	250	131	63(ss)
	539	44	118	172	143	27(ss)
	546	45	105	172	145	34(ss)

*Zoback *et al.*, 1980
**Zoback and Hickman, 1982
***Hickman, written comm.
(MOJ-2 was drilled at the same site as XTLR)

Zoback and Hickman (1982) describe the results of stress measurements made using the hydraulic fracturing technique in the Monticello wells. The minimum horizontal principal stress in MONT-1 increases more slowly with increasing depth than the lithostat. At 165 m the least compressive stress is vertical, indicating a thrust faulting regime. Below that depth the least compressive stress is horizontal. The maximum shear stress is about 45 bars at 165 m, decreases at intermediate depths, and is about 65 bars at 961 m. In MONT-2 the horizontal principle stresses increase uniformly with depth (Zoback and Hickman, 1982). The transition from a thrust faulting environment to a strike-slip environment is more complex in this well, occuring over the interval between 128 and 312 m. The maximum stresses are quite low at shallow depth, but increase somewhat towards the bottom of the well.

A detailed analysis of the stress distribution as a function of depth in the XTLR well appears in Zoback *et al.* (1980). Both the horizontal principle stresses and the maximum shear stress increase with depth in a stepwise manner. The steps appear to be separated by zones of relatively intense fracturing. The transition from thrust to strike-slip faulting occurs at around 300 m. The shear stress in this well is higher than the shear stress in the Monticello wells at the same depth. The stress profile at Hi Vista was discussed by Hickman *et al.* (1981). The transition from a thrust to a strike-slip regime is poorly defined in this well. Although the principle stresses increase with increasing depth, the maximum shear stress is independent of depth. The shear stress is about 45 bars in the near-surface, decreases within the transition zone (except for the anomalously large value of 63 bars at 493 m) and is about 30 bars in the lower portion of the well.

Using the stress values in Table II, I have calculated the ratio of the maximum to minimum effective principal stresses. Where the minimum compressive stress is the lithostatic stress, I have used this value as S3. These values have been plotted in Fig. 2.6. The error bars are due to experimental uncertainties. The shaded area is the range within which the measured stresses are high enough to cause failure if μ (the coefficient of friction) is 0.6-0.85 and cohesion is assumed to be zero (after Byerlee, 1978). As we are interested here only in the magnitude of the stress ratio, the orientation of the theoretical plane for which the ratio is computed is not important. Although there is some variation in the value of the stress ratio at shallow depths, its magnitude is remarkably consistent below about 300 m in these wells. The difference between the principal stresses is close to that required for failure only at very shallow depths. Below 300 m the stress difference is too small to cause failure. As dilatancy will occur only when

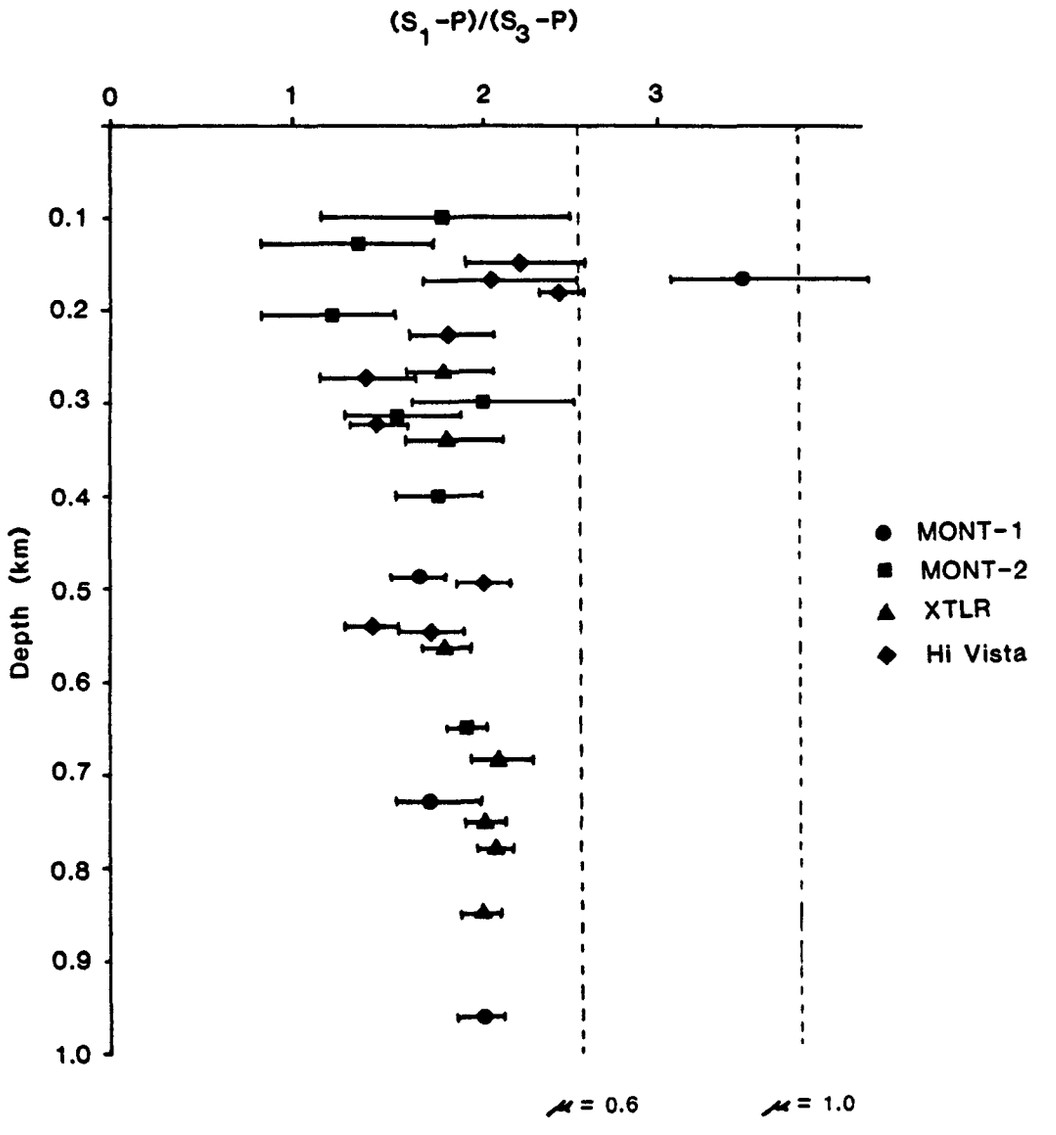

Figure 2.6: Stress ratios calculated from hydrofracture stress measurements. The ratios $(S_1-P)/(S_3-P)$ were calculated using the stress values shown in Table II. The error bars are due to experimental uncertainties. The vertical lines denote the stress ratio at failure for $\mu = 0.6$ and $\mu = 1.0$. With the exception of the measurements at very shallow depth, none of the measured stresses are near failure.

the stresses are large enough to overcome the opposing frictional forces on crack faces, it is unlikely that dilatant crack opening is a factor in controlling the pressure sensitivity of the velocities at depth in these wells.

STRESS INDUCED ANISOTROPY

Horizontal stress differences as large as those measured in these wells may, however, produce measureable velocity anisotropy. It has been shown that the application of uniaxial stress can cause significant elastic wave anisotropy in crystalline rock (Nur and Simmons, 1969). The increase in velocity parallel to the applied stress is much greater than the increase perpendicular to the stress direction. This can be explained by the generation of an anisotropic crack distribution due to the preferential closure of thin cracks (Nur, 1971). Thus confining pressure will decrease the induced anisotropy. For a more complicated stress field, velocity anisotropy is dependent on the symmetry of the applied stress if the initial crack distribution is random. The stress in the direction of particle motion has the greatest effect on velocity. For P-waves the velocity is most sensitive to the applied stress in the propagation direction.

Lockner *et al.* (1977) measured shear and compressional velocities in saturated samples at 500 bars confining pressure under applied axial compression. The velocity of shear waves polarized in the direction of applied stress increased at a rate of .003% per bar until the onset of dilatancy. There was no change in the velocity of shear waves polarized perpendicular to the applied stress, or in the velocity of compressional waves travelling perpendicular to the applied stress. If this is due to the effect of the stresses on thin cracks, then the anisotropy will be somewhat larger at lower confining pressures.

Healy and Kohler (1980) measured the compressional velocity of refracted arrivals from a series of 25 km long reversed profiles in the western Mojave desert near Palmdale and found that the velocity in the direction of maximum compression (5.57 km/s) was about 0.12 km/s greater than the velocity in the perpendicular direction. From the stress measurements tabulated above, the horizontal stress difference at XTLR is about 160 bars below 700 m. If the anisotropy is the result of the measured stresses, the velocity change is .012% per bar. This is only slightly lower than our *in situ* measurements of pressure sensitivity for the appropriate depth in the XTLR well, and is slightly larger than the laboratory measurements of shear- wave birefringence by Lockner *et al.* (1977).

CONCLUSIONS

Although the pressure sensitivity of velocity can be quite high in the near-surface, it decreases rapidly with increasing confining pressure. Measurements of the increase of sonic velocity with depth in relatively homogeneous crystalline rock indicate that the *in situ* pressure sensitivity decreases several orders of magnitude in the upper few hundred meters of the crust. Stress measurements in these wells indicate that differences in shear stress cannot explain the differences in the pressure sensitivity of velocity. However, pervasive *in situ* fracturing increases the pressure sensitivity, due to the effects of the stresses on the macroscopic fractures. Even in very highly fractured rock, however, the *in situ* pressure sensitivity below 1 km is less than an order of magnitude greater than laboratory-determined values. As expected, the shear modulus increases more rapidly at low pressures than the bulk modulus, due to the effect of crack closure. This results in a larger α_s than α_p in the laboratory. The *in situ* shear modulus also increases more rapidly than the bulk modulus at shallow depths, even though α_s is not always greater than α_p.

Differences in horizontal stresses as large as those measured in these wells can produce velocity anisotropy at shallow depths large enough to be detected by conventional seismic refraction profiling. The magnitude of the stress-induced velocity anisotropy at shallow depths is only slightly smaller than the calculated *in situ* pressure sensitivity would suggest. At greater depths, the stress-induced anisotropy will be much smaller.

These results have important consequences for trying to detect temporal stress induced velocity variations for the purpose of earthquake prediction. Both α_p and α_s are less than .0005 per bar at 5 km, and can be as low as .00002 per bar. Below 5 km α_p and α_s are essentially equal to the laboratory-determined values. At 10 km α_p and α_s will be less than .00001 per bar. Therefore travel-time changes for seismic energy travelling at depths greater than 5 km are expected to be from .05% to .001% per bar. Thus, unless stress changes are several tens of bars, stress induced velocity variations occurring below 5 km depth would seem to be extremely difficult to detect.

CHAPTER 3

Measurements of velocity and attenuation from vertical seismic profiles

The velocity data presented in the first two chapters was obtained primarily from borehole sonic logs at acoustic frequencies. Several potential problems arise when attempts are made to generalize these results to describe elastic properties at lower frequencies, or over larger volumes. One possibly severe problem is that the borehole sonic log samples a small region immediately surrounding the borehole. Within this region the concentration of horizontal stresses due to the presence of the borehole is particularly pronounced (see Jaeger and Cook, 1969 p 251), and may be large enough to cause failure (e.g. Gough and Bell, 1982; Zoback *et al.*, 1982). Furthermore, the rock near the well bore may have been damaged by the drilling process, and drilling fluids or the injection of cement may have altered the constituents and geometry within the pore space. These effects are particularly important in sedimentary rocks (Kokesh and Blizzard, 1959; Hicks, 1959; Tuman, 1961), or where the rock volume is highly fractured and thus relatively incompetent. Also, the elastic properties of the rock volume may be frequency dependent. This may be the result of anelasticity or of the presence of finite length inhomogeneities such as fractures or thin beds. The problem of the frequency dependence of the elastic properties in fractured rock was addressed briefly in the first chapter. It was shown that, when comparing the *in situ* velocities in fractured rock at sonic and seismic frequencies to the ultrasonic velocity measured in a laboratory sample, anelasticity and the scale dependence of rock properties are of secondary importance compared to the first order effects of the fractures themselves. The *in situ* compressional velocity measured in fractured rock is almost the same at sonic and seismic frequencies, and is considerably lower than the ultrasonic velocity in a saturated laboratory sample.

The relative contributions of scattering and of anelastic attenuation to *in situ* measurements of Q has been a hotly debated issue for many years. Schoenberger and Levin (1974,1978) demonstrated that 1/3 to 1/2 the intrinsic attenuation calculated from surface seismic surveys may in fact be due to the presence of "intrabed multiples". Ganley and Kanasewich (1980) calculated attenuation from VSP data

recorded in sediments, and after correcting for the effects of these multiples fitted both the amplitude and phase response of the material. They found that Q≈43 for the interval from 549–1193 m, and Q≈67 for the interval from 945–1311 m. Theoretical work by Kikuchi (1981a,b) has demonstrated that a non-attenuating scattering medium can mimic the amplitude response of a non-scattering attenuative medium, and thus demonstrated the difficulty of discriminating between the two. Richards and Mencke (in press, 1982) suggest methods for discriminating between scattering and intrinsic attenuation by examining the phase spectrum of the signal. Laboratory measurements by Brennan (1981) and Liu and Peselnick (written comm., 1983) suggest that most of what field researchers have long regarded as the result of intrinsic attenuation may in fact be due mostly to scattering.

In this chapter, I will compare in greater detail measurements of the sonic velocity from borehole logs and the seismic velocity from VSP's. This has been discussed previously by Gretener (1961) and is of continuing interest to exploration geophysicists. The relative importance of dispersion, mechanical damage at the well bore, and the effects of finite-length fractures will be discussed. Also, the value of the parameter Q will be calculated from the uncorrected VSP's using two different techniques (pulse rise time and spectral ratios). The effects of intrabed multiples will be calculated using a synthetic VSP program. By comparing the values measured from the VSP to the synthetic values, the relative contributions of anelastic attenuation and scattering to the *in situ* measurements can be estimated.

The measurements presented here were carried out in two quite different geologic settings. Although the same mechanical device was used as a source, the characteristics of the source and of the receivers were also different. The merits and limitations of the techniques used at the two sites will be compared to determine the most effective methods for obtaining VSP data.

SITE CHARACTERISTICS

The first VSP survey was run in the XTLR well. The geologic setting has been described in some detail in the first chapter. The well was drilled four km from the San Andreas fault in the western Mojave desert near Palmdale, California. The rock is a fairly homogeneous quartz monzonite, and fracturing as seen by the BHTV extends to the total depth of 859 m. Analysis of the cuttings and of a core removed from the bottom of the well suggest that the rock has undergone significant alteration throughout the entire depth of the well. Analysis of the fracture orientations (Seeburger and Zoback, 1982) shows that

most of the fractures are steeply dipping, and there is a pronounced maximum for fractures striking N5°-25° W and dipping about 60° SW. The VSP was run with the source 50 m NW of the well; the dominant fracture orientation was 30-45 degrees to the ray path. Seismic velocity measured from the VSP was compared to the sonic velocity log in Chapter 1. The two velocity measurements agree quite well, suggesting that, at least to first order, the effects of the fractures on sonic and seismic velocities is essentially the same.

The second survey was carried out in East Mesa well 5-1, drilled to a total depth of slightly less than 2000 m at the East Mesa known geothermal resource anomaly (KGRA) near El Centro in the Imperial Valley of southern California (Figure 3.1). Swanberg (1976) has discussed the results of a wide range of geophysical and geochemical surveys conducted at the anomaly, and I will draw largely from his paper to summarize the pertinent data.

The Mesa anomaly lies on the eastern flank of the Salton Trough, which forms the northern extension of the Gulf of California. The trough is filled largely by terrestrial sandstones, siltstones and clays of the Colorado River. Fuis *et al.* (1982) conclude, from seismic refraction experiments within the Imperial Valley, that the maximum depth of sedimentary and metasedimentary rocks is 10-16 km. Under the East Mesa KGRA the sediments extend to a depth of about 5-6 km. Sediment thickness is greatest in the center of the valley, which they believe corresponds to a zone of active rifting. Thermally metamorphosed sediments and possible igneous intrusions underlie the East Mesa and other geothermal anomalies within the valley.

East Mesa well 5-1 was completed in May 1974, and casing was set throughout its depth. Fifty-eight cm surface diameter casing was set from the surface to a depth of 6 m, thirty-four cm diameter casing was set from 6 m to 312 m, and from 312 to 1524 m the casing diameter was 19 cm. Slotted casing was emplaced in the lowest 305 m of the well to enable its use as a re-injection well for emplacement of waste fluids from experiments at the East Mesa site. The well has an excess fluid pressure of about 2 bars at the surface, which necessitated the use of a fluid containment device during our experiments.

Temperature logs run at the well shortly after its completion showed a temperature gradient of 150° C/km in the upper 600 m, several times larger than the typical value for sedimentary basins of approximately 30 to 40° C/km. Below 600 m the temperature gradient dropped to 29° C/km, due to

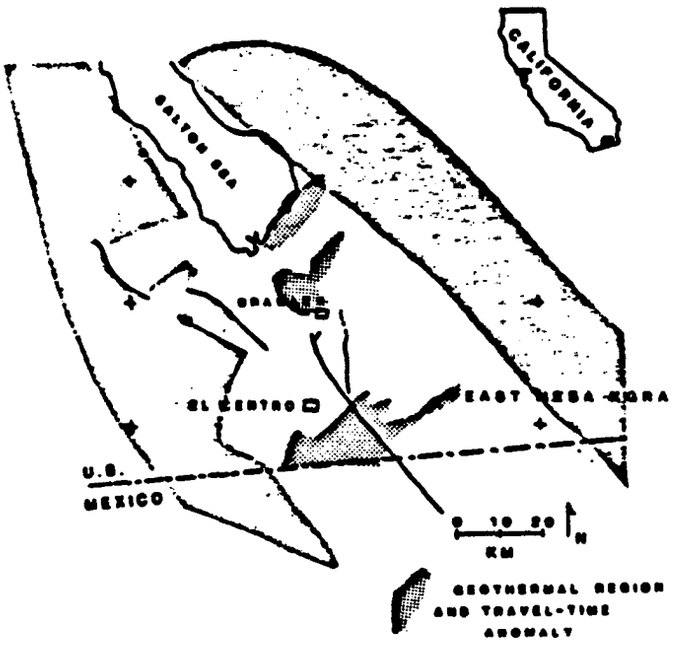

Figure 3.1: Location map of the East Mesa KGRA in the Imperial Valley of southern California. East Mesa well 5-1 was drilled to a depth of about 2 km at the East Mesa KGRA.

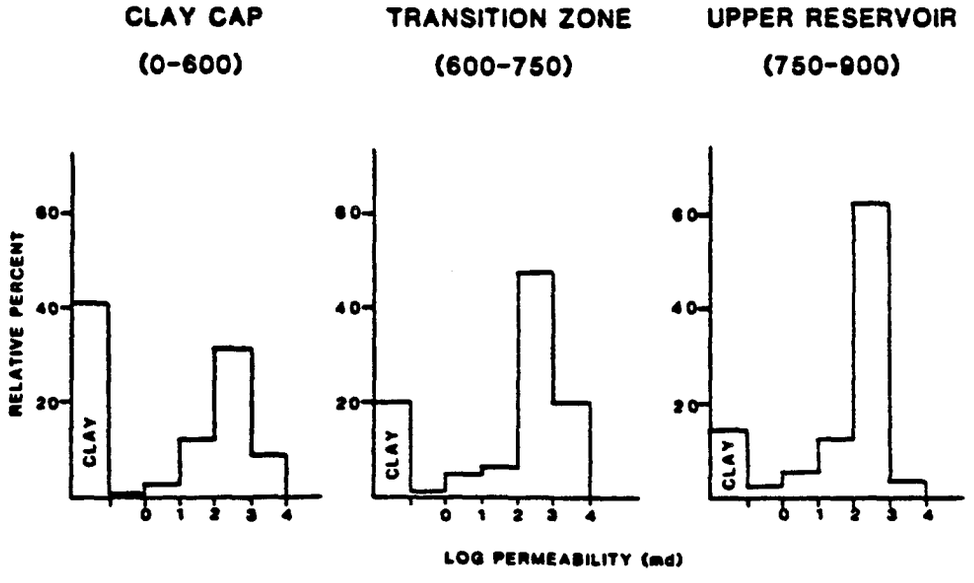

Figure 3.2: Composition as a function of depth for core samples removed from East Mes (after Swanberg, 1976). The relative percent clay and the results of a suite of p measurements made on the sand samples is presented for the uppermost three reg well. The regions were delineated by Swanberg (1976) on the basis of composition a properties.

a change in the primary heat transfer mode from conduction to convection below 600 m (Swanberg, 1976). Analysis of core properties from this well and others at the KGRA has resulted in the delineation of three distinct zones in these wells characterized by the relative percent of clays (Swanberg (1976). Although the permeability of sand samples is approximately the same within each well, the clay content decreases rapidly with depth. Figure 3.2 shows the composition as a function of depth for the upper 900 m of well 5-1. The clay content decreases markedly below 600 m, and although there is relatively little change in the modal permeability the effective permeability of the material increases due to the decrease in clay content. Aside from the change in clay content with depth, there is relatively little change in mineralogy in the well.

Prior to our arrival at the site well 5-1 was in constant use as a reinjection well. In order to study the effect of the reinjection of cold fluid, we ran two temperature surveys of the upper 900 m of the well (Figure 3.3). Although no fluid was injected above 1200 m, the survey run shortly after our arrival (about 10 hours after reinjection stopped) showed a gradient of about 40° C/km, much lower than that seen by Swanberg (1976). After the completion of our experiments, temperatures in the well had increased to within 20° of the earlier measured values. Therefore it appears that fluid injection in the well did not significantly affect temperatures in the surrounding rock volume away from the well. At 900 m, the maximum depth of the VSP survey, the temperature in the well was approximately 140°C.

A sonic velocity log was run in well 5-1 from 312 m to total depth, of which the upper 830 m are reproduced in Figure 3.4. Also shown in Fig. 3.4 are the interval velocities calculated from the VSP, which will be discussed below. The velocity increases gradually with depth, with a somewhat pronounced jump at about 400 m from 1.8 to 2.1 km/s. Below that depth the compressional velocity increases more slowly. At 800 m the compressional velocity is about 2.4 km/s. There are no obvious velocity changes corresponding to the compositional changes shown in Fig. 3.2. The velocity varies periodically with depth, which suggests that there is some periodic variation in rock properties below 400 m on a scale of 20-50 m. This variation will generate intrabed multiples of the type described by Schoenberger and Levin (1974, 1977). Thus, in the upper 900 m the material at East Mesa well 5-1 is characterized by high geothermal gradients, and decreased clay content and a slight increase in velocity with increasing depth.

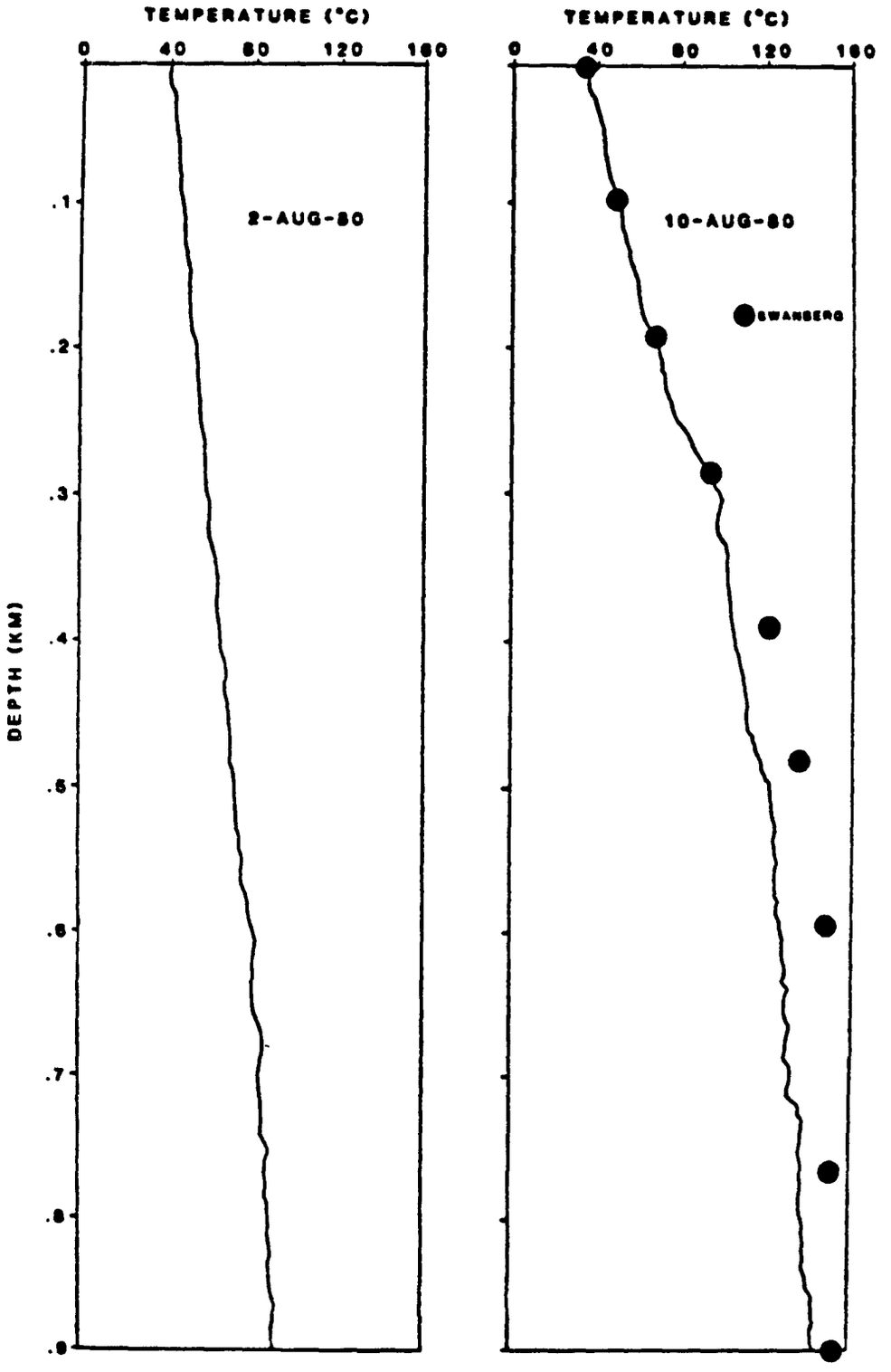

Figure 3.3: Temperature logs at East Mesa well 5–1 run shortly after our arrival at the site on August 2, and after the completion of our experiments on August 10. Also shown are the temperatures measured by Swanberg (1976) shortly after the well was drilled.

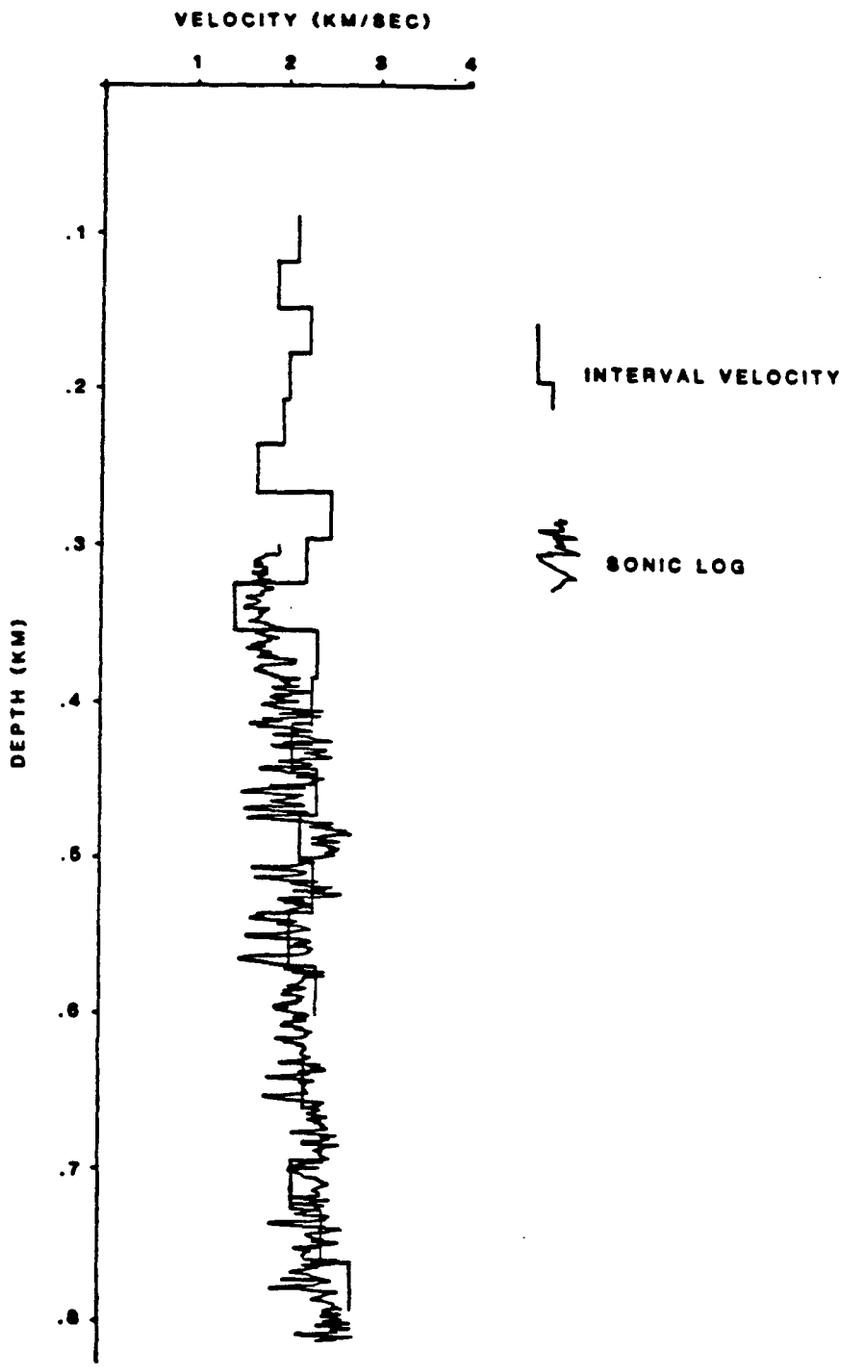

Figure 3.4: Results of a sonic velocity log run at East Mesa 5-1 from the bottom of the surface casing at 312 m. Also shown are the interval velocities calculated from the VSP run in the well.

TECHNIQUE

The airgun source used in these experiments was a Rix Industries 650 cu cm airgun operated at a pressure of approximately 270 b. The airgun was triggered from inside the logging truck, and source time was determined from the trigger pulse for the East Mesa experiment or from the arrival at a geophone suspended in the mud pit at XTLR. The measured arrival times of successive shots at a surface geophone was within .5 ms.

At XTLR the airgun source was placed in a 2 m diameter 2 m deep steel sided tank, which was emplaced in a pit dug 25 m from the wellhead. The pit was then filled with drilling mud to improve source coupling. Tests were made to determine the repeatability of the source waveform. Four shots recorded by a Mark Products L-10 4 Hz geophone placed in the mud pit are reproduced in Figure 3.5a. The first arrivals are identical, with a fundamental frequency of approximately 75 Hz, and the useable bandwidth is 25 to 250 Hz (Fig. 3.5b).

Depth to the water table at XTLR was more than 10 m. The airgun signal therefore traveled through an initial layer of highly attenuative low velocity material. This fact, combined with the relatively high noise at the site, resulted in the selection of the same 4 Hz geophone for use as a downhole receiver. The geophone was mounted vertically in a side-wall clamped case. At each depth, the geophone package was wedged into place and the cable was slackened to prevent the transmission of surface noise to the receiver. The waveforms were digitized on site by a Zonic DMS digitizing recorder at 200 μs intervals, (Nyquist frequency 2.5 KHz) and transfered to a Digital Equipment Corporation DECLAB 11/03 minicomputer for storage on floppy diskettes (see appendix).

Two surveys were run at the site over a period of three days. The raw data are reproduced in Figure 3.6. Each record is the result of a single shot recorded by the downhole geophone. The arrivals are quite impulsive, and there is little noise at all but the deepest geophone sites. There was considerable overlap in the coverage, which enabled an estimate of the stability of later measurements to be obtained.

At East Mesa well 5-1 the airgun was suspended at 24 m depth in the center of a 30 m deep 1 m diameter cased borehole 60 m from the wellhead. Depth to the water table was approximately 15 m during the course of the experiment. Thus the source was emplaced below the water table. Source time was determined from the trigger pulse generated by the airgun firing panel, as arrival times to a surface geophone were unuseable for source timing.

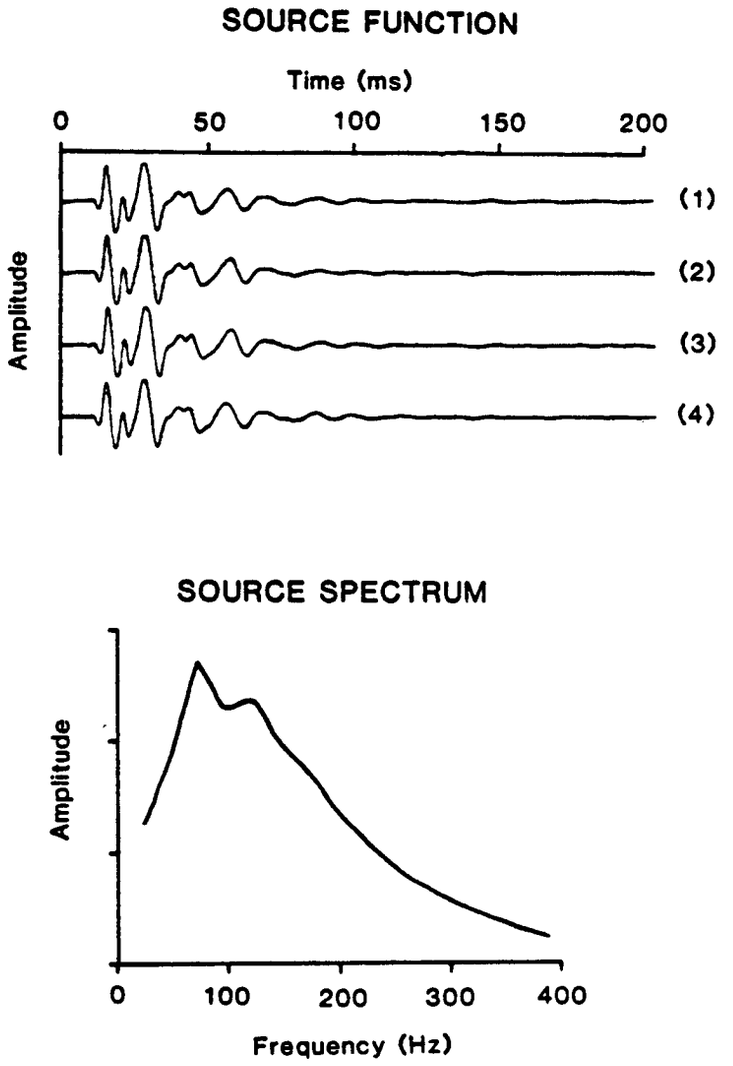

Figure 3.5: Arrivals recorded by a Mark Products L-10 4 Hz geophone placed in the mud pit next to the airgun source at XTLR; a) seismograms; b) amplitude spectra. The useable bandwidth of the source is 25-250 Hz.

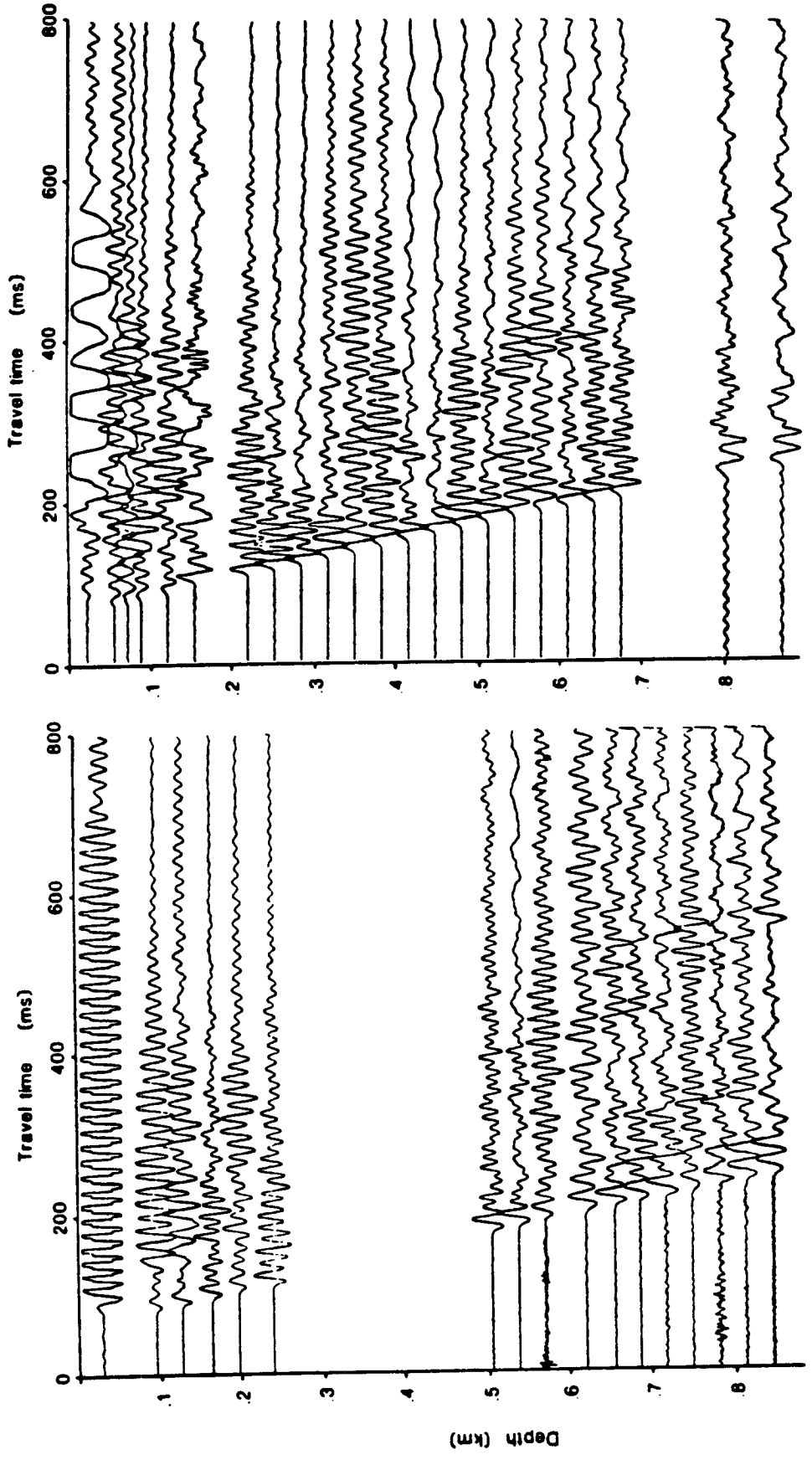

Figure 3.6: Vertical seismic profiles recorded at XTLR. The surveys were recorded on successive days, and the geophone polarity was reversed prior to the second survey.

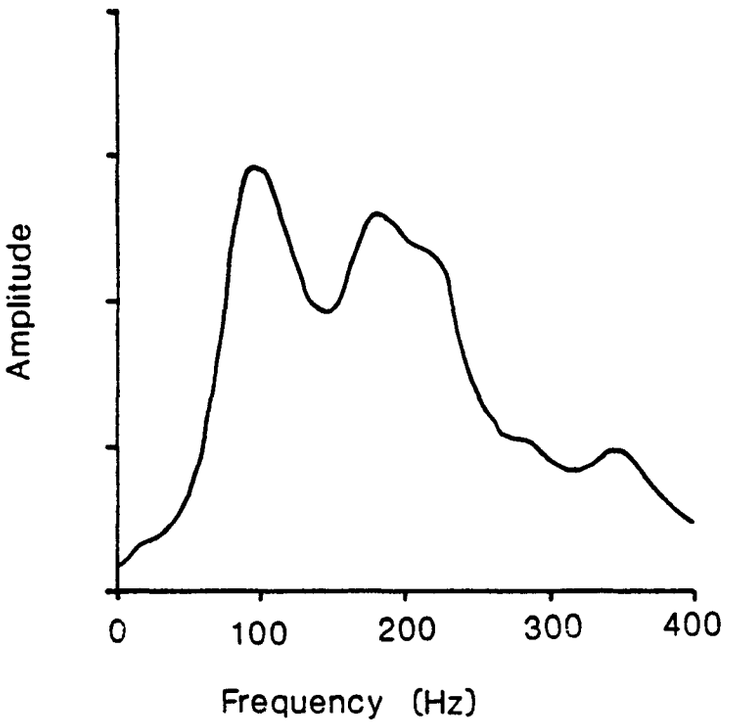

Figure 3.7: Frequency content of the signal recorded by the hydrophone at 274 m depth in East Mesa well 5-1.

The receiver used was a hydrophone manufactured by Simplec, specially modified for use in geothermal wells. The frequency response was flat to several KHz. The greater bandwidth of the hydrophone was useful, as the source was below the water table. The waveforms were sampled at 100 μs intervals using the system described above. Arrivals at 274 m in the well had a useable bandwidth from 75 to 300 Hz (Figure 3.7), and were remarkably reproduceable.

Figure 3.8a shows the results of the VSP in this well. The raw data are much noisier, and the fundamental frequency of the arrivals is considerably higher, than the data at XTLR. The data were low pass filtered using a 4 pole Butterworth filter with a high frequency cutoff at 200 Hz before later analysis was carried out. Figure 3.8b shows the data after filtering. Although the filtered data were used to calculate interval velocities, the analysis of the waveforms was carried out on the unfiltered records.

Comparison of the data from these two experiments reveals several of the most common features of VSP records. The East Mesa data were recorded with the source below the water table, and with broadband receivers. As a result the arrivals at East Mesa contained appreciably higher frequencies than those at XTLR. The source shown in Fig. 3.5 was recorded with the same instrument as the arrivals at depth, so the instrument response is probably not responsible for the loss of high frequencies, unless there is a coupling problem within the well-bore. Thus it appears that the loss of high frequencies at XTLR occurs at very shallow depth within the unsaturated zone.

The penalty for using a downhole hydrophone at East Mesa was much greater noise, and a poorer arrival at depth. The radiation pattern of a pressure source in a fluid-filled borehole was studied by Lee and Balch (1982). Relatively little energy is radiated at small angles to the borehole axis. By analogy, one would not expect a large pressure pulse within a borehole for a compressional arrival travelling along the borehole. The incident P-energy at East Mesa was travelling approximately along the axis of the borehole, and the incident angle decreased with depth. Therefore the effective transmission coefficient was small, and probably also decreased with increasing depth. This problem, coupled with the fact that the hydrophone was suspended on a taut cable (which is a very efficient transmitter of near-surface noise) resulted in the poor signal-to-noise ratio at East Mesa.

A very strong series of second arrivals was recorded at East Mesa. These arrivals, traveling at

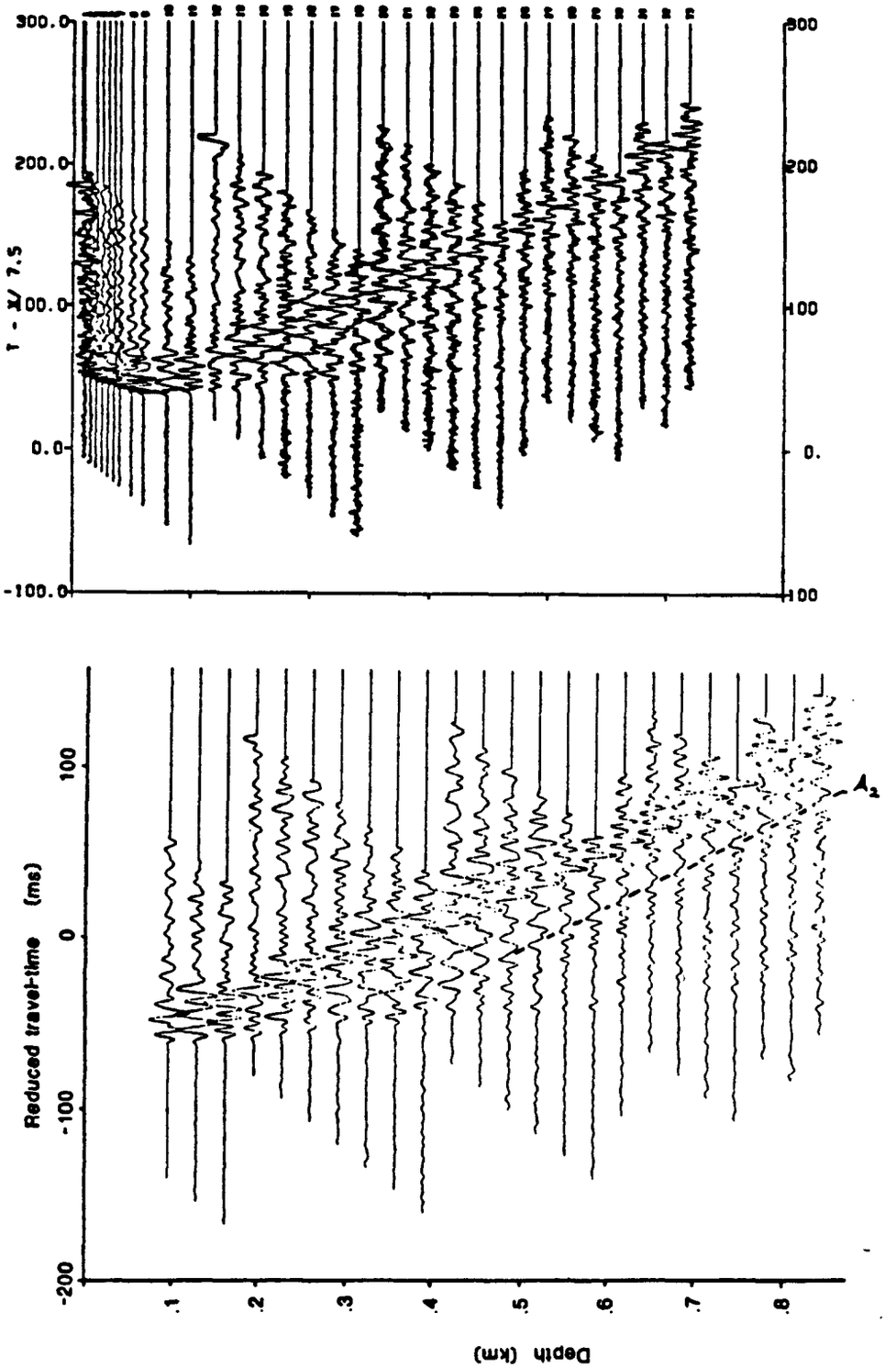

Figure 3.8: Vertical seismic profile recorded at East Mesa well 5-1; The uppermost figure is the unfiltered data, and the lower figure shows the data after it was filtered using a 4-pole Butterworth filter with a 200 Hz high frequency cutoff. The surveys are plotted on a reduced time axis, with a reduction velocity of 2.29 km/s, corresponding to the P-wave velocity for the lowermost hundred meters of the surveyed interval. The high amplitude second arrival is labeled A_2.

approximately 1.46 (±.05) km/s, are easily discernable on the VSP (Fig. 3.8). One particularly strong arrival (designated A-2 on the VSP) emerges from the P-wave arrival below about 100 m, and has a stable pulse shape throughout the depth of the survey. At greater depths, the incident P-wave excites smaller amplitude pulses which propagate at the same velocity. These phases are either tube waves, which are generated at impedence contrasts in the well-bore fluid column, or shear conversions generated at velocity contrasts within the sediments.

Tube waves are evanescent waves whose energy is concentrated mostly within the well-bore fluid (Biot, 1952). They travel at speeds which are slightly below the compressional velocity of the fluid. For water at normal temperatures and pressures, compressional velocities are greater than 1.55 km/s. However, at elevated temperatures the velocity decreases. The sound velocity in water above 100° C decreases smoothly from 1.55 km/s at 95°, to less than 1.47 km/s at 150° (Handbook of Chemistry and Physics, 52nd Edition, p. E-41). Tube-wave velocities are always less than the fluid velocity (Paillet and White, 1982). Therefore the second arrivals at East Mesa travel at approximately the tube wave velocity.

It is intriguing, however, to consider the possibility that these arrivals are converted shear energy. In this case the phase A-2 is the direct shear arrival from the source. The large amplitude of these arrivals is not surprising, as Lee and Balch (1982) found that the amplitude of shear waves generated by a compressional source in a fluid-filled borehole was greatest along the borehole axis. By analogy, the pressure pulse excited by a shear wave impinging on a fluid-filled borehole will be greatest for arrivals along the axis of the borehole.

To test the tentative conclusion that these arrivals are S-waves, V_p/V_S was calculated. Assuming an average compressional velocity of about 2.29 (±.05) km/s at 800 m, V_p/V_S is 1.48 to 1.66. This results in a Poisson's ratio of 0.08 to 0.21 for the sediments at 800 m in East Mesa 5-1. Laboratory measurements (Jones, 1978) suggest that these values are reasonable at room temperatures only if the material is partially saturated. Majer and McEvilly (1979) found Poisson's ratios of 0.15 to 0.24 for partially saturated rocks at the Geysers geothermal field. If these arrivals are in fact shear waves, this suggests an anomalously low value of Poisson's ratio, consisten, perhaps, with partial saturation at depth. The source of these strong second arrivals could not be identified solely on the basis of their velocity. Three-component data would be needed to determine unambiguously the cause of these

arrivals.

Interestingly, no corresponding arrivals were detected at the XTLR well. The absence of any converted shear phases is not surprising, as mode conversions due to reflections from finite length fractures will probably be somewhat incoherent. The absence of tube wave energy may be due to a combination of two factors. First, permeable fractures intersecting the well-bore will severely attenuate tube-wave energy. Second, as most of the energy is concentrated in the fluid, a side-wall clamped geophone would not be an efficient means of detecting tube waves. Large amplitude tube waves could be expected in the East Mesa survey, as cased boreholes are particularly efficient propagators of tube wave energy.

The presence of these second arrivals in the VSP data presents a difficult problem, as their frequency content is similar to that of the direct arrival. If the inter-receiver distance is sufficiently small, velocity filters can be applied to the data to remove most of these second arrivals, in a manner analogous to the techniques applied by Hardage (1982) and DiSienna *et al.* (1981) for removing tube waves from VSP data. Unfortunately, the data recorded here were not sampled densely enough, so the data analysis was carried out only where the later-arriving energy could be removed from the first arrival. These phases could not entirely be windowed out of the data before spectra were calculated, and are a major source of noise in the spectral ratio data disussed below.

CONPARISONS OF SONIC AND SEISMIC COMPRESSIONAL VELOCITIES

Compressional velocities were calculated from the VSP's over the intervals between the receivers by differencing the arrival times. Initially, the ray paths between source and receivers were assumed to be straight, and the interval velocities were calculated at successively greater depths after correction for the non-vertical ray path. These interval velocities were then entered as a first model to a synthetic program, and the velocities were slowly varied until a reasonable fit was obtained.

The results are presented in Figure 1.7 for XTLR and in Figure 3.4 for East Mesa. At East Mesa the sonic log velocities agree quite well with the seismic velocities from the VSP. Although there is some scatter in the data, there is no systematic difference in the velocities measured by the two methods. At XTLR, however, the sonic velocities are systematically lower than the seismic velocities. This difference

is second order, and was not discussed at length in Chapter 1 as the *in situ* velocities were much lower than the ultrasonic velocities determined in the laboratory, due to the presence of the macroscopic fractures. This difference is significant, however, and may be due to several factors. As the well was drilled through fairly competent (although weathered) granitic rock, it is unlikely that there was much drilling-induced damage that could have reduced the sonic log velocities. Also, the well was drilled with chemical foam (not drilling mud) so there was no mud-cake or fluid invasion of the formation during drilling. The lower velocity fractured zones seen in the sonic log at XTLR are local features. Seismic energy travelling within the rock away from the borehole would not necessarily travel through a plane-layered stack whose velocity-depth function is represented by the sonic log. First-arriving energy would travel along the path with the greatest average velocity. Therefore the material would exhibit a slightly higher velocity than expected from analysis of the sonic log, in which the energy is concentrated around the small-diameter cyllindrical borehole.

ANALYSIS OF P-WAVE ATTENUATION

Measurements of Q were obtained from the raw data using two methods. First, the rise time of the first arrival was measured at each receiver depth, using the definition of Gladwin and Stacey (1974), where the rise-time, τ, is simply defined as the maximum amplitude over the maximum slope of the first break. Using this definition for rise-time, Gladwin and Stacey (1974) found that the rise-time of an impulsive source was a linearly increasing function of traveltime:

$$\tau = \tau_0 + c \int \frac{dt}{Q(t)} \tag{3.1}$$

The value of the parameter c was determined to be 0.53 ± 0.04. For a mathematical model in which Q is independent of frequency, Kjartansson (1979) has shown that the rise time of a sufficiently impulsive signal increases linearly with frequency according to Eqn. (3.1). Interestingly, the theoretical value of c for an impulsive displacement source is 0.485 for Q greater than 10, when a displacement transducer is used as a receiver. Kjartansson (1979) has pointed out that the results are valid as long as the rise-time of the source function is small compared to the impulse response of the material being measured.

Figure 3.9a shows the rise-time as a function of arrival time for the VSP's at XTLR. The rise-times were measured from 122 m to total depth, as arrivals in the upper 100 m probably followed curved ray paths through the upper unsaturated zone. Although there is some scatter in the data, the rise-times

increase linearly with increasing travel-time. A least-square best fit equation was computed from the data having a slope of 0.0182, and is shown as a solid line. Using Eqn. (3.1), the apparent Q for these measurements is approximately 27, assuming that $c = 0.5$. I use the term "apparent Q" to indicate that no corrections have been applied to the raw data, and that the value of "c" used may not be valid for the airgun source.

Figure 3.9b shows the rise-times calculated from the VSP at East Mesa 5-1. Again, arrivals above 122 m were not used, as the ray paths were not congruent at shallow depths. Notice that the rise times at East Mesa are somewhat shorter than at XTLR. This is not surprising, as high frequencies were more abundant in the arrivals at East Mesa. Also, there is considerably more scatter in the data here. The data in the upper 330 m of the well can be fitted to a straight line with a slope of 0.00578, but below 330 m (the top of the second set of casing) there is too much scatter. This may be caused by variability in the coupling between the casing and rock due to poorly cemented casing. The apparent Q calculated from Eqn. (3.1), assuming again that $c = 0.5$, is 128 for depths from 122 – 330 m. This is considerably higher than the apparent Q calculated from the data at XTLR.

Spectral ratios of selected pairs of arrivals were calculated from the raw data, and a best-fit line was computed through the spectra where the amplitudes were above an appropriate threshold. The spectral ratio method is a commonly used technique for calculating attenuation. For Q independent of frequency within a given frequency band, the log of the ratio of the spectra is a linearly decreasing function of frequency:

$$\log \frac{A_1(f)}{A_0(f)} = \pi f \frac{z_0 - z_1}{vQ} + constant \tag{3.2}$$

The slope, m, of a best-fit line to the spectrum thus yields a value for Q:

$$Q = \pi f \frac{z_1 - z_0}{m} \tag{3.3}$$

Using this method, the uncorrected attenuation can be calculated from the raw waveforms. It turns out (Brennan and Smylie, 1981) that for Q greater than about 10, the exact mathematical dependence of Q on frequency for frequencies well outside the limits of the measurements does not affect this result.

Figure 3.10 is a plot of the attenuation factor (1000/Q) as a function of depth calculated from the uncorrected VSP's at XTLR (Fig. 3.10a) and at East Mesa (Fig. 3.10b). Each line is the calculated value from one pair of receivers. Only those receiver pairs for which the spectral ratio could be fitted

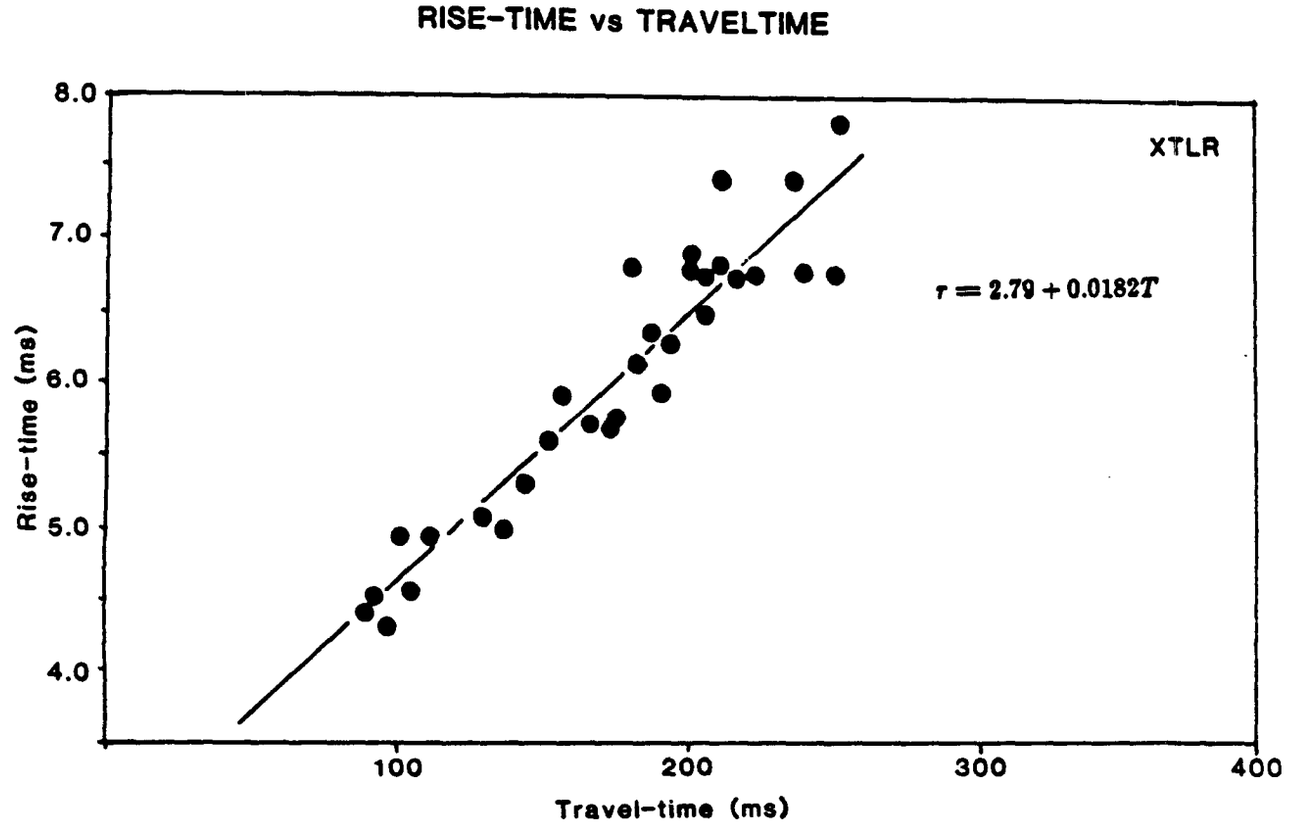

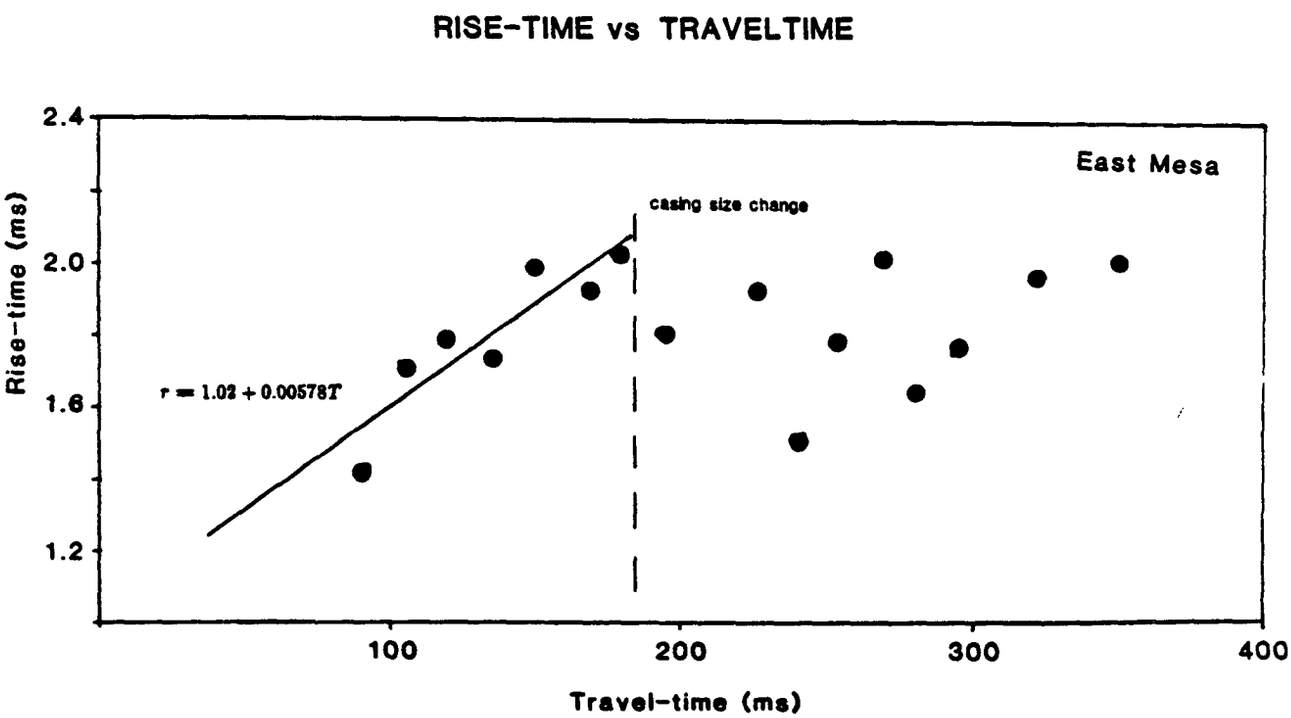

Figure 3.9: Rise-times as s function of travel-time calculated from the unfiltered data at a) XTLR and b) East Mesa well 5–1. The equation of a best-fit line through the entire XTLR data set, and of the data from the zone above the casing size change at East Mesa are shown. At East Mesa, the travel-time of about 180 ms corresponds to a depth of 312 m.

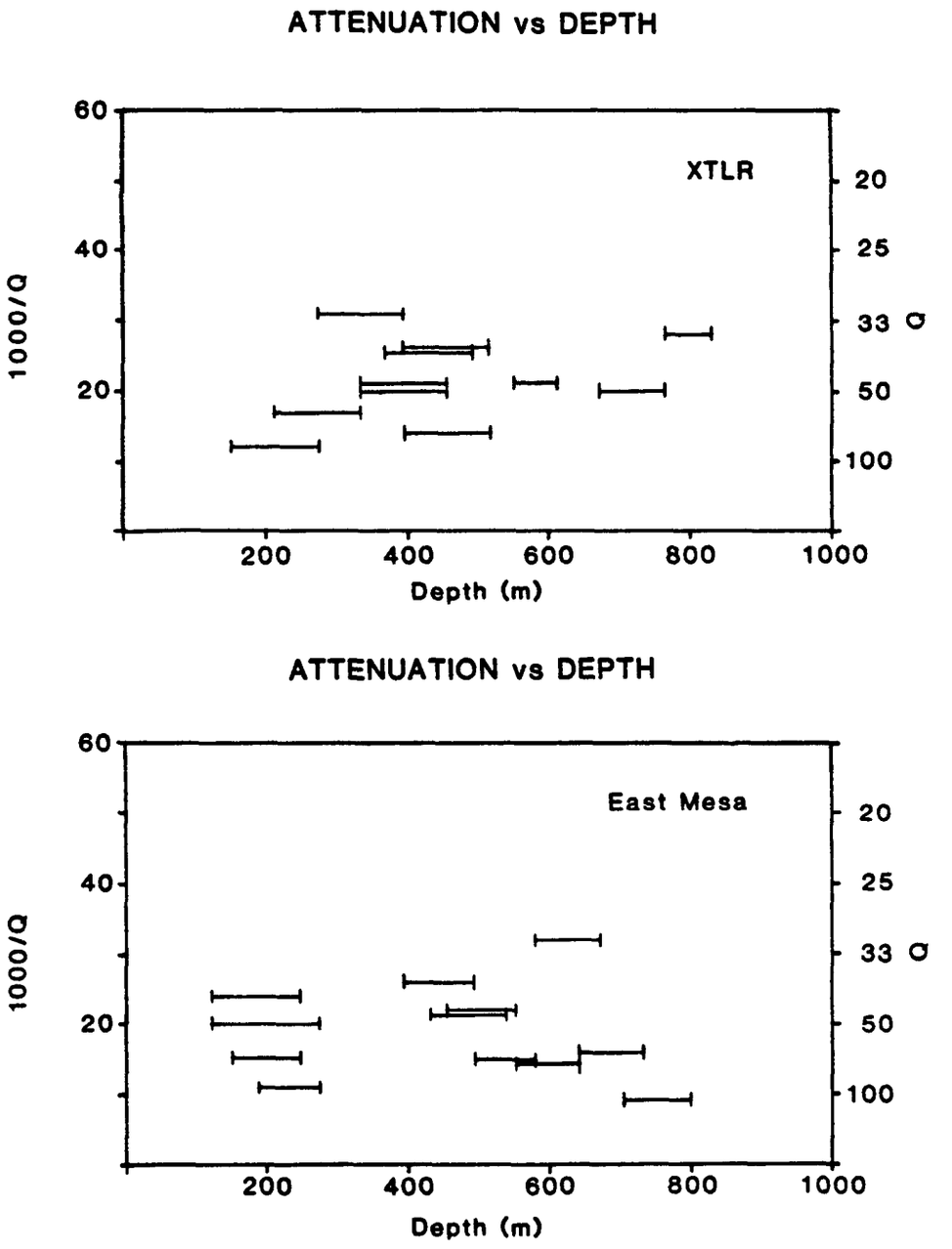

Figure 3.10: Plots of values of the attenuation factor (1000/Q) from spectral ratios calculated from the VSP data at a) XTLR, and b) East Mesa well 5–1. Only those receiver pairs whose spectral ratio could be fitted to an equation of the form (3.2) were used. The horizontal lines indicate the depth range over which the ratios were calculated.

by an equation of the form $A(f) = A_o - mf$ were included. The horizontal lines show the value of the attenuation factor for the depth range over which the spectral ratio was calculated. No attempt has been made to estimate the errors in the measurements, because the data were not corrected for intrabed multiples or other effects before the ratios were calculated. There is considerable scatter in both plots. From these plots there is no way to determine reliably the magnitude or the depth dependence of Q in these wells. At best, we can say only that the attenuation calculated from these data is independent of depth at East Mesa, and perhaps shows a moderate increase with depth at XTLR; at both wells the uncorrected attenuation factor is approximately 20. Therefore, the combination of intrinsic attenuation and other effects results in a $Q \approx 50$.

SYNTHETIC VSP's

In order to study the effect that multiple reflections from thin layers will have on the VSP waveforms, synthetic VSP's were generated from the sonic velocity logs of the two wells. The log data were obtained at 0.305 m intervals at each well from the water table (or the depth of surface casing) to the total depth (see the Appendix for an explanation of the method). The log velocities were averaged over 3 m intervals by summing the δt values, to generate velocity profiles which were then used as input to a synthetic program similar to that described by Ganley (1981). The program calculates synthetic amplitudes in the frequency domain. The source function is zero-phase, and its amplitude spectrum is the same as the amplitude spectrum of the airgun source at XTLR. First, a reflection coefficient series is generated at each frequency. The density is assumed to be constant, as no density logs were run in these wells. The synthetic amplitude of the up- and down-going wavefield is then obtained at each interface. As the synthetic is generated in the frequency domain, the effects of intrinsic attenuation can be included in the model. However, the method is one-dimensional and therefore does not include mode conversions or geometrical spreading.

Figures 3.11 and 3.12 show the results of the synthetic model at XTLR and East Mesa, respectively. Two synthetics were generated for each well. The first synthetic was generated with Q=1000 (Figs. 3.11a, 3.12a), and for the second synthetic Q=100 (Figs. 3.11b, 3.12b). A significant amount of internally reflected energy is present on all synthetics. At XTLR strong upgoing reflections are generated at several depths. At East Mesa, the reflected amplitudes are lower. The synthetic program used here could not be applied to the generation of converted phases, so Figs. 3.11 and 3.12 do not include mode conversions.

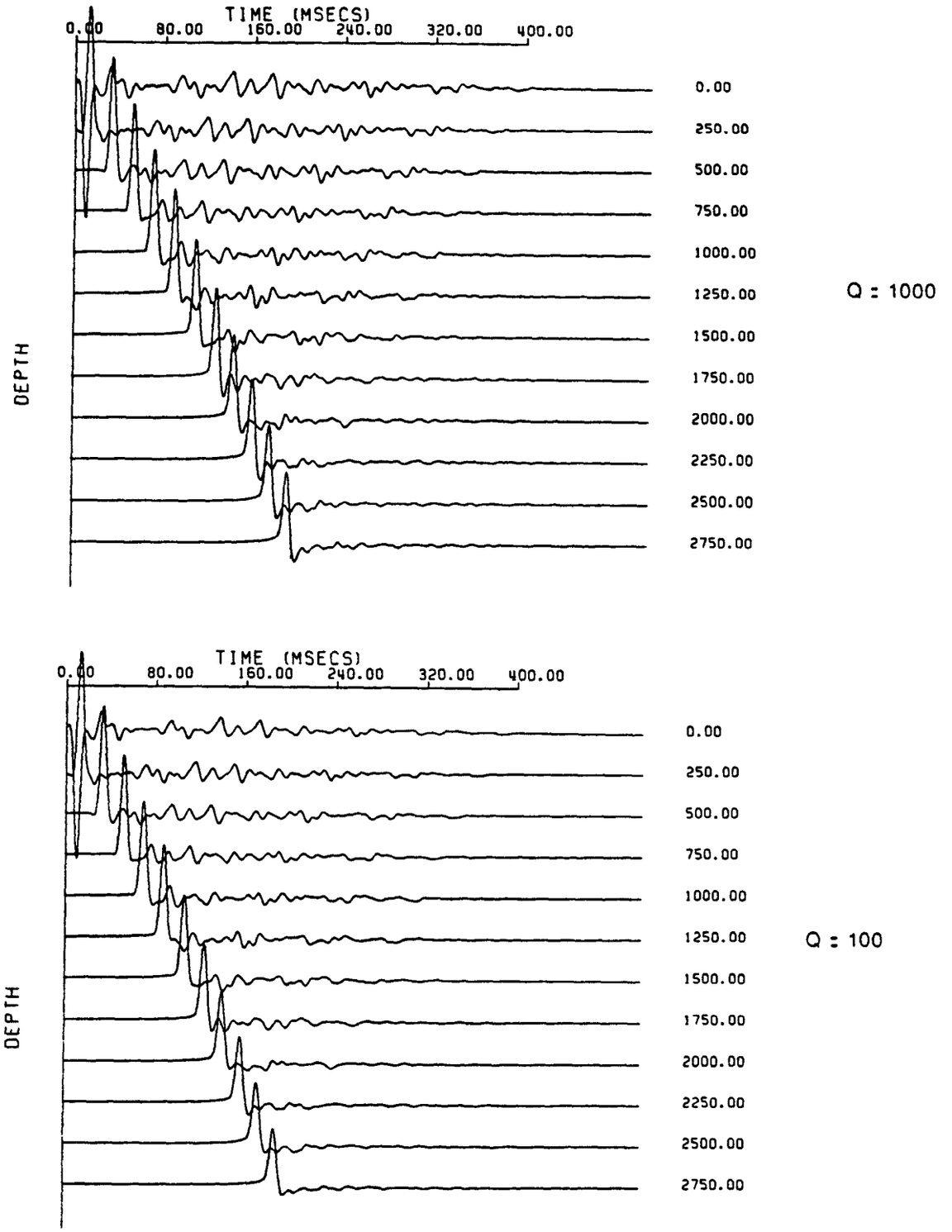

Figure 3.11: Synthetic vertical seismic profiles calculated by the method of Ganley (1981) for the XTLR well. The sonic log was used as a velocity model. The synthetics were calculated for Q=1000 (a) and for Q=100 (b). Note the presence of strong up- and down-going internal reflections.

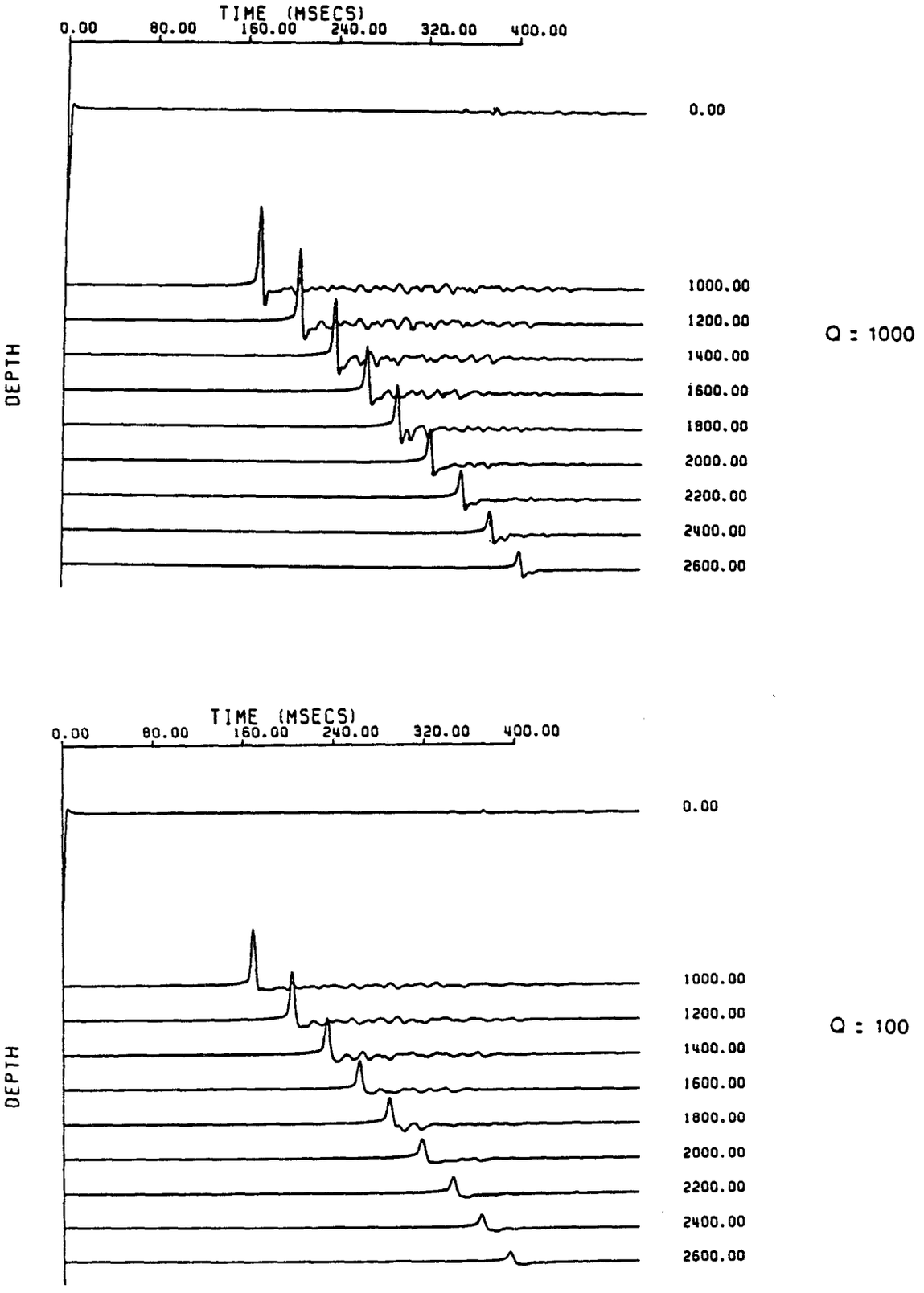

Figure 3.12: Synthetic vertical seismic profiles calculated by the method of Ganley (1981) for the East Mesa well. The sonic log shown in Fig. 3.5 was used as a velocity model. The synthetics were calculated for Q_c=1000 (a) and for Q_c=100 (b). Up- and down-going multiples are not as evident in this synthetic as in Fig. 3.11.

This is a serious problem with the data at East Mesa, as most of the intrabed multiples are probably not P-wave multiples. The addition of attenuation to the models clearly affects the resultant wavefield. At both wells the amplitudes decrease more rapidly with depth, and the high frequency content of the multiples is significantly reduced.

Figure 3.13 shows the rise-times calculated from the VSP's shown in Figs. 3.11 and 3.12. The equations of best-fit lines through the data are shown on the figures. Interestingly, the rise-time increases with travel-time in all four synthetics. At XTLR, the slope of the best-fit line is 0.0113 for Q=100, and 0.00995 for Q=1000. Therefore, the internal reflections generated within the fractured rock mass result in a measureable increase in the pulse rise-time as it travels, even when there is essentially no intrinsic attenuation. The synthetic data from East Mesa do not show this effect. The slope of the best-fit line for Q=100 is 0.00673, and for Q=1000 there is essentially no change in pulse-width with travel-time.

The synthetic data could not be used directly to correct the field data for the effects of intrabed multiples, for several reasons. First, the velocities calculated from the sonic logs were not the same as those measured from the VSP's. Second, the synthetics do not include geometrical spreading or the effects of non-vertical incidence. Also, the synthetics do not include converted phases, which are the major source of noise on the East Mesa survey. Direct deconvolution of the synthetic data would thus introduce considerable errors into the results. However, an estimate of the importance of scattering in the measurements can be made from comparisons of the synthetic and *in situ* measurements of Q.

DISCUSSION

It has been shown by a number of researchers that scattering can cause a significant loss of high frequencies for waves travelling through heterogeneous materials. The term "scattering" has been used to describe both the random scattering of energy from finite-length heterogeneities such as fractures or local weathered zones, as well as the loss of high frequency energy due to intrabed multiples discussed by Schoenberger and Levin (1974,1978). There is general agreement that loss of energy due to scattering cannot be distinguished from the effects of intrinsic attenuation from analysis of spectral amplitudes alone (Richards and Mencke, in press; Kikuchi, 1981a,b). However, it has been shown that scattering results in the concentration of high frequencies in the coda (Aki and Chouet, 1975), whereas in an attenuative material dispersion results in the concentration of high frequency energy at the front of the

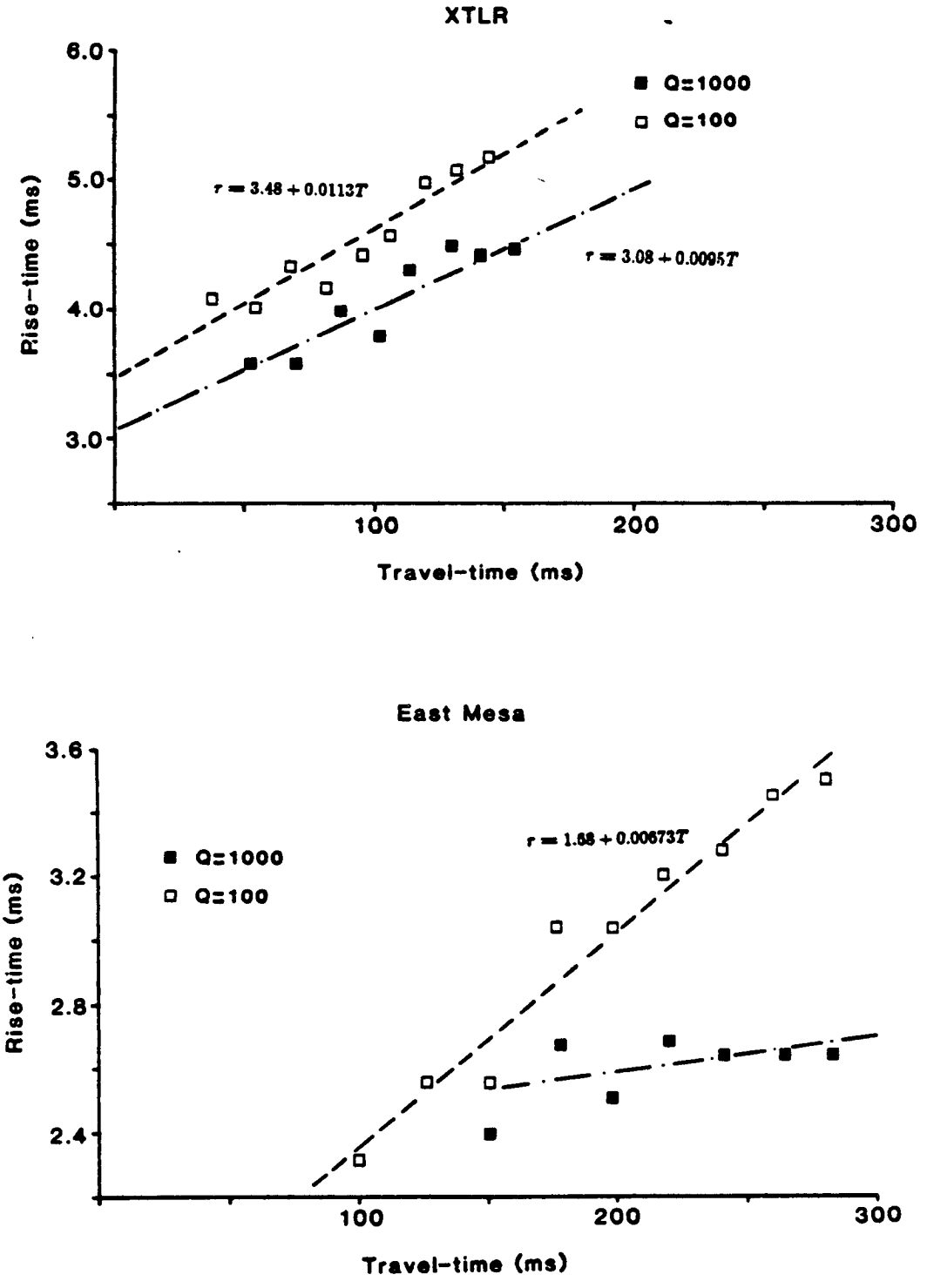

Figure 3.13: The rise-time of the first break as a function of travel-time calculated from the synthetic VSP data shown in Figs. 3.11 (a) and 3.12 (b). Each data set has been fitted to an equation of the form $r = r_o + mT$. The parameters of the curves are shown on the plots.

pulse.

Although the phase spectra of the VSP data at XTLR and East Mesa are not stable enough for an analysis of dispersion to be meaningful, such dispersion can be detected in the time domain by studying the pulse shapes of first arrivals. For a scattering material the pulse rise-time will increase more rapidly than expected for a given apparent Q calculated from spectral ratios. This discrepency is observed in the data from XTLR, where $Q_{rise-time}$ was approximately 27, and $Q_{spectral-ratio}$ was about 50. Results at East Mesa do not show this relationship, due to the probable inclusion of later arriving energy in most of the spectra.

Measurements of pulse rise-time from the synthetic VSP's also provide a means of discriminating between scattering and intrinsic attenuation. At East Mesa the rise-time changes very little for the non-attenuating case, which suggests that internally reflected P-waves do not affect Q measurements in this well. There is no way to estimate the effect that the second arrivals at this well have on the data. It is interesting, however, that the pulse rise-times increase much more slowly than expected from spectral ratio calculations of Q. This suggests that at East Mesa the more reliable Q values would be those obtained from rise-time measurements. The uncorrected pulse rise-time data gave Q=128 for the interval from 122 to 330 m at East Mesa 5–1, if "c" in Eqn. (3.1) is assumed to be 0.5. However, the synthetics suggest that, for the airgun source, $c \approx 0.00673$. Using this value for "c" yields $Q_{pulse-width} \approx 117$.

At XTLR, however, the rise-time increases significantly with travel-time in both the attenuating (Q=100) and non-attenuating (Q=1000) cases. Almost 90% of the measured change in pulse shape is due to scattering. In this case, the rise-times are clearly due both to scattering and to intrinsic attenuation. Both the spectral ratio and the rise-time techniques must be corrected for scattering.

By using the results of the synthetic analysis, the *in situ* rise-time measurements can be corrected for scattering. Richards and Mencke (in press) have shown that the contributions of intrinsic attenuation and scattering are approximately additive in the frequency domain. If this result can be applied in the time domain, then we may be able to determine the contribution of intrinsic attenuation after removing the changes in rise-time due to scattering. To test this assumption, synthetic VSP's were calculated from the sonic log at XTLR for Q=20 and Q=50. If the contributions of intrinsic attenuation and

scattering to the change in pulse shape are independent, then there should be a linear relationship between the slope of the rise-time vs. travel-time curve (after the removal of the rise-time change due to scattering) and the value of Q. That is:

$$corrected\ \frac{d\tau}{dT} = \left.\frac{d\tau}{dT}\right|_{Q} - \left.\frac{d\tau}{dT}\right|_{Q=\infty} = \alpha(1000/Q) + constant \tag{3.4}$$

The values of $d\tau/dT$ computed from the synthetic VSP's are shown in Table 3.1.

Table 3.1: Values of $d\tau/dT$ calculated from synthetic VSP data (using the sonic log at XTLR as an input model) for different values of Q.

Q	1000	100	50	20
$d\tau/dT$	.00995	.01130	.01450	.02420
1000/Q		10	20	50
Corrected $d\tau/dT$		.00135	.004455	.01425

Using the results shown in Table 3.1, Eqn. 3.4 becomes:

$$\left.\frac{d\tau}{dT}\right|_{Q} - \left.\frac{d\tau}{dT}\right|_{Q=\infty} = 0.0323(1000/Q) - 0.189 \tag{3.5}$$

After correcting the *in situ* rise-time measurements for the component of rise-time change due to scattering, the pulse rise-time increase due to intrinsic attenuation becomes 0.00825 ms per ms travel-time. Substituting this value into Eqn. (3.5) gives $1000/Q = 31$, or Q=32. Interestingly, this value is lower than the Q calculated from the uncorrected spectral ratios.

CONCLUSIONS

Vertical seismic profiles have been run in two wells. The first well (XTLR) was drilled through highly fractured granite, and the second well (East Mesa well 5-1) was drilled through a thick sequence of terrestrial sandstones, siltstones and clays. At XTLR a side-wall-clamped geophone was used as a reciever, and at East Mesa the arrivals were recorded by a down-hole hydrophone. Strong compressional arrivals were detected throughout the XTLR well. At East Mesa, however, compressional amplitudes were quite low. Very large direct and converted second arrivals were recorded at East Mesa, however. These arrivals could not be unambiguously identified as either shear or tube waves, due to the lack of three-component data at East Mesa.

Sonic velocity logs run in the wells were compared to the velocities measured from the VSP's. At East Mesa the two velocity measurements gave essentially the same results. At XTLR, however, the VSP data gave slightly higher velocities than expected from the results of the sonic log. This is probably due to the extremely heterogeneous nature of the fractured rock at XTLR. The details of the velocity-depth function calculated from the sonic log were probably due to laterally finite bodies. Thus the longer wavelength energy from the VSP "saw" an effectively faster medium than the sonic energy travelling along the borehole.

Measurements of Q from spectral ratios and the from rise-times of the first arrivals were compared at both wells. At East Mesa, the synthetic results suggest that P-wave scattering had almost no measureable effect on pulse rise-time. Therefore no correction for scattering was applied to the data. The large discrepency between measurements of attenuation from rise-time and spectral ratios was probably due to the presence of converted phases. At XTLR synthetic VSP's contained large amounts of intrabed multiples. Therefore the *in situ* Q measurements were probably contaminated by those multiples. Using the synthetic results, a corrected value of Q was obtained from the *in situ* rise-time measurements.

On the basis of these results, I feel that pulse rise-time is probably a more accurate method for obtaining measurements of Q than spectral ratios, where the data are contaminated by spurious arrivals. Where scattering is important, both spectral ratio and rise-time measurements must be corrected in order to get reliable estimates of intrinsic attenuation.

CONCLUSIONS

Although each chapter of this thesis includes a short section stating basic conclusions, it is useful at this time to discuss the larger implications of the work presented here. Therefore I will briefly summarize the results of the first three chapters, and then discuss some general insights into the importance of fractures on *in situ* measurements in light of those results.

In the first chapter, the relationship between sonic velocities and fracture density was investigated for crystalline rocks in the upper km of the earth's crust. Isolated fracture zones decreased both V_p and V_s, and increased V_p/V_s. For wells with a uniformly high fracture density, *in situ* velocities were measureably lower than laboratory determined ultrasonic velocities. The velocity of seismic waves in highly fractured rocks were also measureably lower than the ultrasonic velocity, although the log velocities were slightly lower than the seismic velocities. There was no measureable dispersion.

In the second chapter, measurements of sonic and ultrasonic velocities as a function of pressure or depth were fitted to smooth functions of pressure, in order to determine the relationship between the pressure dependence of velocity in the laboratory and in the field. At low pressures (<1 kb) the *in situ* pressure dependence was somewhat greater than the laboratory data would suggest. The presence of macroscopic fractures increased the *in situ* pressure dependence. At low pressures the shear modulus increased more rapidly than the bulk modulus both in the laboratory and *in situ*, due to the effects of crack closure. At higher pressures, when the majority of the cracks were closed, the moduli increased at approximately the same rate.

In the third chapter, velocity and attenuation were calculated from vertical seismic profiles run in two wells. At one well in sediments at the East Mesa KGRA, the velocity calculated from a sonic log of the well was essentially equal to the velocity measured from the VSP. Attenuation measurements were difficult to obtain due to interference from large amplitude second arrivals excited by the incident compressional arrival at impedence contrasts within the sedimentary section or within the well-bore. A synthetic VSP calculated using the sonic log as a velocity model revealed that, although intrabed compressional multiples were generated at velocity contrasts, their presence probably would have little

effect on the calculated attenuation. In a well drilled through fractured crystalline rock, both the attenuation measured from pulse rise-times and that measured from spectral ratios were contaminated by scattering from the fractures. By fitting the rise-times calculated from the *in situ* data to the synthetic rise-times, the measured value of Q was corrected to reflect only the contribution of intrinsic attenuation. After the correction, the *in situ* value of Q calculated from rise-times was lower than the Q calculated from uncorrected spectral ratios. This is consistent with theoretical results by Richards and Mencke (in press).

These results suggest that the presence of macroscopic fractures strongly affects almost every *in situ* measurement made using seismic techniques. The effect of finite-length fractures can be strongly dependent on the wavelength of the incident energy, which can result in a measureable discrepency between *in situ* measurements taken at different frequencies. Where fracturing is pervasive, *in situ* attenuation measurements must be corrected for scattering before reliable values of intrinsic attenuation can be obtained. The character of the energy scattered from finite-length fractures is different from the character of intrabed multiples generated by thinly bedded sediments.

Great care must be taken when laboratory measurements are extrapolated to the field. Where *in situ* fracture density is high, both the magnitude and the pressure sensitivity of the velocity is influenced by the fractures.

However, these results suggest that the presence of fractures, which may dominate the response of a rock body, is detectable from the surface using current technology. Thus the analysis of seismic data can be generalized to include the detection of fractures.

APPENDIX

With the advent of digital analysis and processing of data, and the increasing sophistication of such techniques, it has become apparent that early digitization of field data is of paramount importance. The earlier such data is digitized, the less deterioration occurs due to effects on the analog signal from distortion and noise in transmission, recording and reproduction. In general, this problem is less important for low frequency data, but where information is required at frequencies above several kilohertz the problem becomes increasingly difficult to overcome.

Large-scale computer-controlled digital access systems are commercially available and are widely used in seismic exploration. The advantages of these systems over the older analog type in terms of data acquisition, transport, storage and analysis are obvious. Such a system has immediate applications to on-site processing of a variety of logs and, in particular, to the analysis of velocity data and extraction of elastic parameters and Q.

In general, that system must meet several criteria:

1) Direct interfacing of downhole instruments with an onboard computer

2) Flexibility

3) Early digitization

4) Wide range of digitizing modes and speeds

5) Portability and reliability

6) Real-time display of data

7) Ease of operation

8) Compatibility with existing external computers.

In the early part of 1979 the U.S. Geological Survey in Menlo Park began developing such a system for use in logging operations and hydrofrac experiments. The decision to use the system in the study of attenuation and related rock properties was made in April of that year. At that time the equipment had already been selected and the system was in its final form except for software design and interfacing of the computer with the various borehole instruments. The overall system layout is shown in Figure A.1.

GEOPHYSICAL LOGGING SYSTEM

The heart of the geophysical logging system used in these experiments is a DECLAB 11/03 minicomputer. The computer is FORTRAN programmable and is easily interfaced to laboratory equipment as well as to standard data terminals, plotters and storage devices. The machine uses a 16-bit word and has direct access to 64 Kbytes of which about 28 K are useable by the programmer as memory and program storage. An RT-11 operating system was purchased from Digital Equipment Corporation and is fully supported by Digital and easy to use. Permanent data storage is on diskettes, each of which can hold 2 Mbytes. Plotting is done on a Houston Complot pen plotter, and a standard VT-55 terminal provides the programmer with video display and soft copy. Details of the operation of these devices may be found in the respective manuals. The limitations of the memory are minimal; the programmer can manipulate and analyze up to 10,000 real (16-bit) pieces of data without difficulty. Use of the diskettes as virtual memory is possible, but is slow and cumbersome in practice and should be avoided. For our purposes the memory size is not a limiting factor in either procurement or analysis of data.

The computer is interfaced to external equipment through a standard data bus. It is designed to accept data from three sources:
1) Analog data from standard logging tools, hydrofrac experiments, and low frequency ($<$ 10 kHz) sources.

2) High-speed digital data from an external A/D converter

3) Parallel BCD data, specifically from a depth counter.

Sources (1) and (3) are passive, requiring no interactive servicing by the computer. Source (2) is an active I-O line involving real-time user input and hardware interaction between the source and the computer. The next three sections will describe the operation of the system with each of these three inputs, taken in order.

1) Analog Inputs

The 11/03 computer was purchased with an auxiliary circuit board (ADV-11A) which is a 12-bit A-D converter capable of sampling at preprogrammed rates up to 6 kHz. This allows the acquisition of data from a single channel at a sampling interval of 160 μsec. For more than one channel, the speed is decreased by the number of channels sampled. The DEC object code library LSILIB contains

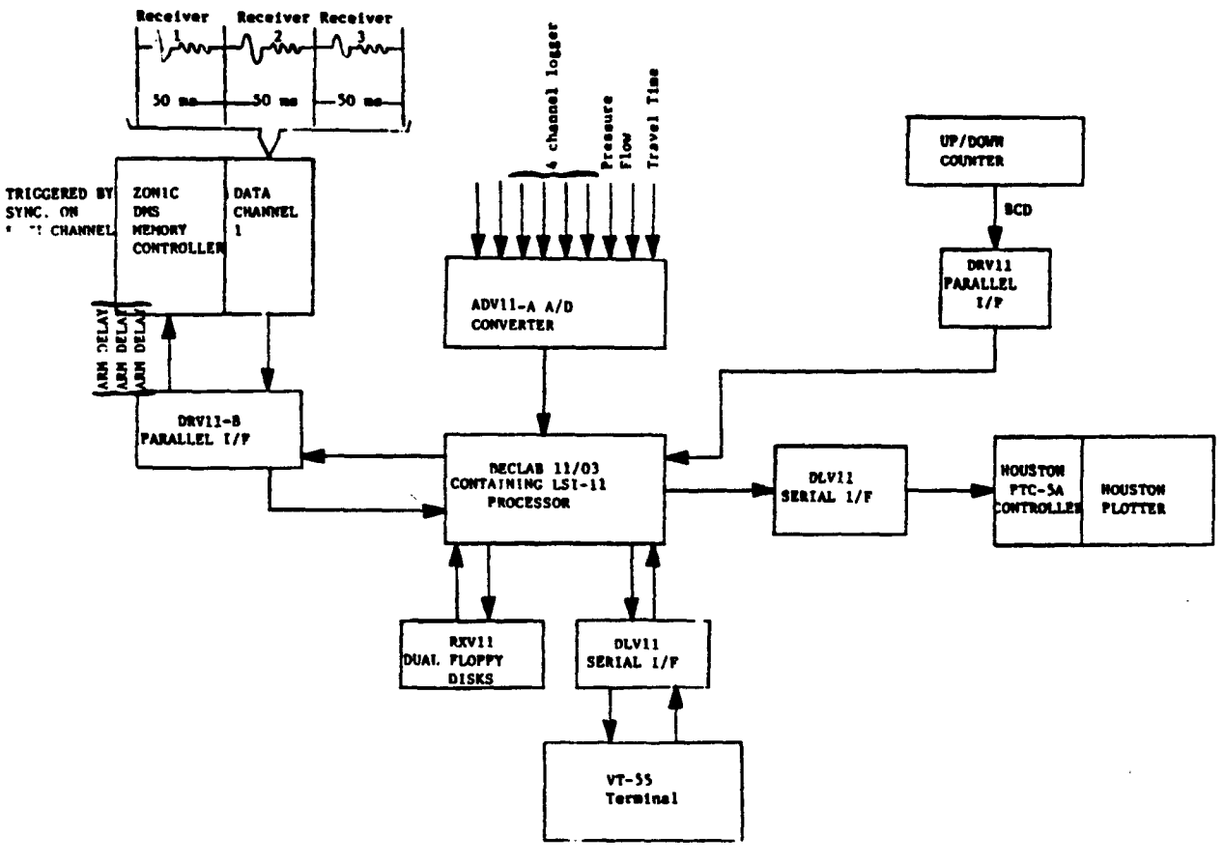

Figure A.1: Block diagram of data acquisition system used in these experiments. The system was developed at the U. S. Geological Survey in Menlo Park.

FORTRAN-callable subroutines enabling the programmer to control the operation of the A/D converter in software. The sample rate, number of channels, and number of samples are all software selectable. The ADV-11A accepts an analog signal of ±5.12 V full scale. Thus the system has a resolution of 2.5 mV. This necessitates amplification of the input data before digitization. Broadband amplifiers are used to minimize signal distortion.

The A/D converter is used for real-time digitization of sonic and other logs. Data is stored on diskettes as the experiment proceeds. The recorded data can be plotted immediately at any desired scale, to determine the reliability of the raw data. It can then be rerecorded if necessary.

2) High-Speed Digital Input

The upper limit of the ADV-11A is 6 kHz, several orders of magnitude too slow to adequately sample full-waveform sonic data. This necessitated the purchase of a high-speed digitizer capable of sample rates up to 200 kHz (f_N = 100 kHz). The ZONIC (Data Memory System) has the required speed but provides only 10-bit resolution, or about 48 dB dynamic range. However, its flexibility makes up for the loss of dynamic range to some extent.

The ZONIC has a temporary buffer of variable length and sampled data are stored there for output to a digital device. A DMA (Direct Memory Access) allows rapid transfer of data from the ZONIC to the 11/03. This system is used to digitize and store waveforms from a variety of devices including the SIMPLEC model CGY Velocity Logging System described below. During operation the computer acts both as a data storage device and as a control device, allowing the operator to control all phases of the experiment from the VT55 keyboard.

3) Parallel BCD Input

A depth counter maintains a digital record of the depth to the nearest foot of the tools in the well. This is interfaced directly to the computer via a DRV-11 parallel interface. A FORTRAN-callable subroutine allows the computer to access this information as desired. By continually monitoring the depth in this manner, logging data can be sampled at fixed depth intervals, which facilitates reproduction and processing.

Recording Full Sonic Waveforms

Recording high frequency waveforms requires the use of digitizing speeds which exceed the capabilities of the ADV-11A. For these purposes the waveforms are digitized by the ZONIC DMS. This device can accept data from a variety of tools, including the SIMPLEC Velocity Logging System, downhole hydrophones, and surface instruments. Transfer of data from the ZONIC to the 11/03 is done interactively. Therefore, the operator monitors the experiment from the VT55 keyboard. As an example of this type of operation, the procedure for recording one suite of three waveforms from the sonic tool is described below.

The velocity tool is lowered to a fixed depth in the borehole. Pertinent data, including well number and depth in the well, are entered by the operator. When the equipment is ready the operator initiates the recording sequence and control is transferred to the computer. The ZONIC is armed to receive the signal from the first receiver, and is triggered by the source firing pulse. Ten milliseconds of data are sampled and stored in a temporary buffer by the ZONIC. In the remaining 40 milliseconds before the tool fires again, this data is transferred to the 11/03 which then clears the ZONIC memory, rearms the ZONIC, and waits for the next arrival. This sequence is repeated for the third receiver. At that point the waveforms are displayed on the VT55 terminal and the operator has the option of storing the data and repeating the experiment at the same or a different depth. Waveforms from other sources are recorded in a similar manner. Successive waveforms can be summed if desired before the data are stored.

Sonic logs

We logged MONT-2, XTLR, and Hi Vista using a Simplec model CGY sonic velocity logging tool. The Simplec velocity tool consists of a downhole magnetostrictive pressure source and three receivers spaced 1.22, 1.53, and 2.14 m uphole from the source. An automatic picking device at the surface determines the arrival time of a selected waveform at each receiver. The voltage threshold of the picking device is adjustable to compensate for changes in the received signal, and the waveforms are continually checked to ensure that the correct arrival is picked.

The sonic velocity is calculated by dividing the distance between two receivers by the travel time

difference. The logs discussed here were obtained by differencing the arrival times to the receivers at 1.22 and 1.53 m. Thus the sonic velocity was measured over a 30.5-cm interval in the well about 1.22-1.53 m above the source depth. The frequency band of the received signal is 10-20 kHz.

P and S wave sonic velocities in MONT-1 were obtained from a Birdwell three-dimensional velocity log with a 1.8-m transmitter-receiver spacing. The logs we ran were recorded digitally by a Declab 11/03 minicomputer, and for direct comparison to the Birdwell logs in MONT-1, the figures displayed in the paper are a six-point running mean of the field data. Before the mean is taken, spurious δt values caused by cycle skipping are removed.

S wave logs in the MONT-2 and Hi Vista wells were obtained with the P wave logging tool by raising the voltage threshold of the picking device. As wave propagation in boreholes is extremely complicated, it is necessary to ensure that this method accurately measures S wave velocity and not the velocity of some other mode. Several authors have discussed the characteristics of waveforms in cylindrical boreholes (see White and Zechman, 1968; Tsang and Rader, 1979; Cheng and Toksöz, 1981; Paillet, 1981). Although such factors as borehole and tool radius and the acoustic properties of the surrounding rock and of the fluid in the borehole affect wave propagation, several features of the arrivals recorded by a sonic logging tool are common to all such measurements. In the case examined here (a water-filled borehole drilled through relatively fine-grained crystalline rock), both the shear and the compressional wave velocities of the rock are higher than the compressional velocity of the fluid. For this case both Cheng and Toksoz (1981) and Paillet (1981) found that the first arriving energy is a P wave refracted along the borehole wall. The second arrival is a refracted S wave. All of the other borehole modes, including the direct fluid wave and variously named normal modes (pseudo-Raleigh waves, Stonely waves, etc.), travel at velocities below that of the refracted shear wave. The experimental conditions in this study are similar to those described by Paillet and White (1982) as case 3. For this case the shear arrival is much larger than the compressional arrival and is easily separated from the pseudo-Rayleigh wave. This relationship is apparent in most of the waveforms recorded during our study. The method used should yield a reliable measurement of shear velocity as long as this relationship holds. Around fractures the relative amplitudes of the shear and compressional arrivals were more variable, and much greater care was required to ensure that the measurements were reliable. As the values of Poisson's ratio we obtained are reasonable for saturated granitic rock, we feel that the logs shown in Figures 1.3 and 1.5 do in fact

accurately measure the *in situ* shear velocity.

MEASUREMENT ERRORS

VSP

The shot time was recorded by a geophone placed inside the pit dug for the air gun. Tests were run to determine timing accuracy at various depths in the well. For a surface geophone the measured arrival time of successive shots was repeatable to within 0.2 ms. The worst case timing error was about 0.5 ms. As the accuracy of the depth measurements was 0.5 m, the calculated maximum error in interval velocity was about 8%, or $\pm$0.4 km/s for a velocity of 5 km/s. This is somewhat larger than the error in picking the arrival times from the waveforms, which was about 0.1–0.2 ms.

Sonic Logs

Because of the nature of the picking device incorporated in the sonic logging tool, changes in the amplitude of the received signal will produce small changes in the observed travel time. The largest this source of error can be is about 1/2 period for each waveform; in general, however, when the amplitude varies enough to cause mispicking by about 1/4 period, the picker will skip one or more cycles, and the resulting value of δt is removed before the analysis is carried out. Also, as the amplitudes of arrivals at the two receivers generally vary in the same manner, the arrival time errors will cancel when the interval travel time is calculated. Assuming that the signal has a fundamental frequency of 15 kHz and that the largest error in arrival time is 1/4 period, the largest error in the δt should be 8 μs.

In order to study this effect, the amplitude of one of the two signals used to compute δt was varied while the threshold of the picking device was held constant. This resulted in a change in the calculated travel time of only 3μs, or $\pm$3% of a 50μs travel time. This results in an error of $\pm$3% in the calculated velocities. Thus, in practice, the errors in the travel time measurements introduced by variation in the amplitude of the arriving signal are less than half the maximum theoretical error. Therefore we believe the measurements of sonic velocity reported here are accurate to within $\pm$3% of the maximum velocity; lower velocities that result in longer travel times can be measured with correspondingly less error.

BIBLIOGRAPHY

Aki, K., and B. Chouet, Origin of coda waves, source attenuation, and scattering effects, *Bull. Seis. Soc. Am.*, 71, 1687-1700, 1981.

Biot, M. A., Propagation of elastic waves in a cyllindrical bore containing a fluid, *J. Appl. Phys.*, 23, 997–1009, 1952.

Birch, F., The velocity of compressional waves in rocks to 10 kbars, Part I, *J. Geophys. Res.*, 65, 1083–1102, 1960.

Birch, F., The velocity of compressional waves in rocks to 10 kbars, Part II, *J. Geophys. Res.*, 66, 2199–2228, 1961.

Bonner, B. P., Shear wave birefringence in dilating granite, *Geophys. Res. Lett.*, 1, 217–220, 1974.

Bouchon, M., A simple method to calculate Green's functions for elastic layered media, *Bull. Seis. Soc. Am.*, 71(4), 959–971, 1981.

Brace, W.F., B. W. Pauling, Jr., and C. H. Scholtz, Dilatency in the fracture of crystalline rocks, *J. Geophys. Res.*, 71, 3939–3953, 1966.

Brennan, B. J., Linear viscoelastic behavior in rocks, in *Anelasticity in the Earth*, F. D. Stacey, M. S. Paterson, A. Nicolas, eds., Am. Geophys. U., Washington, DC., 13–21, 1981.

Brennan, B. J. and D. E. Smylie, Linear viscoelasticity and dispersion in seismic wave propagation, *Rev. of Geophys. and Space Phys.*, 19, 233–246, 1981.

Byerlee, J. D., Brittle-ductile transition in rocks, *J. Geophys. Res.*, 73, 4741–4750, 1968.

Byerlee, J. D., Friction of rocks, *Pure Appl. Geophys.*, 116, 615–626, 1978.

Cheng, C. H., and M. N. Toksoz, Elastic wave propagation in a fluid-filled borehole and synthetic acoustic logs, *Geophys.*, 46, 1042-1053, 1981.

DiSiena, J. P., B. S. Byun, and J. E. Fix, Vertical seismic profiling — a processing and case study, presented at 51st annual meeting SEG, paper R-19, 2085–2105, 1981.

Dix, C. H., The interpretation of well-shot data, *Geophys.*, 10(2), 160–170, 1945.

Fuis, G. S., W. D. Mooney, J. H. Healey, G. A. McMechan, and W. J. Lutter, Crustal structure of the Imperial Valley Region, *USGS Prof. Paper 1254*, 25-49, 1982.

Ganley, D. C. and E. R. Kanasewich, Measurement of absorption and dispersion from check-shot surveys, *J. Geophys. Res.*, 85, 5219–5226, 1980

Gladwin, M. T. and F. D. Stacey, Anelastic degradation of acoustic pulses in rock, *Phys. Earth and Planet. Inter.*, 8, 332–336, 1974.

Gough, D. I., and J. S. Bell, Stress orientaions from borehole wall fractures with examples from Colorado, east Texas, and northern Canada, *Can. Jour. Earth Sci.*, 19, 1358–1370, 1982.

Gretener, P. E. F., An analysis of the observed time discrepencies between continuous and conventional well velocity surveys, *Geophys.*, 26(1), 1–11, 1961.

Hadley, K., Vp/Vs anomalies in dilatent rock samples, *Pure Appl. Geophys.*, 113, 1–23, 1975.

Hardage, B. A., An examination of tube wave noise in vertical seismic profiling data, *Geophys.*, 46(6), 892–903, 1981.

Healy, J. and W. Kohler, Anisotropy of upper crustal rocks (abs.), *EOS, Trans. AGU*, 61(46), 1024, 1980.

Hickman S., J. Healy, M. D. Zoback, and J. Svitek, Recent *in situ* stress measurements at depth in the western Mojave Desert (abs.), *EOS, Trans. AGU*, 62(45), 1048, 1981.

Hicks, W. G., Lateral velocity variations near boreholes, *Geophys.*, 24(3), 451–464, 1959.

Hron, F. and B.G. Mikhailenko, Numerical modeling of nongeometrical effects by the Alekseyev-Mikhailenko method, *Bull. Seis. Soc. Am.*, 71(4), 1011–1029, 1981.

Jaeger, J. C. and N. G. W. Cook, *Fundamentals of Rock Mechanics*, 513 pp, Methuen, London, 1969.

Jones, T. D., The problem of Poisson's ratio in sandstone, *Stanford Rock Physics vol. 5*, Stanford University, 1978.

Jones, T. D., and A. Nur, Seismic velocity and anisotropy in mylonites and the reflectivity of deep crustal fault zones, *Geology*, 10, 260-263, 1982.

Kan, T. K., D. Corrigan, and P. D. Huddleston, Attenuation measurement from vertical seismic profiles, presented at 51st annual meeting SEG, 1981.

Kennett, B.L.N., On coupled seismic waves, *Geophys. Jour. Royal Astron. Soc.*, 64, 91–114, 1981.

Keys, W. S., Preliminary interpretation of borehole geophysical data- Whiteshell Nuclear Research Establishment, Manitoba, Canada, Tech. Memo. 53, U.S. Geol. Surv., Denver, Colo., 1979.

Kikuchi, M., Dispersion and attenuation of elastic waves due to multiple scattering from inclusions, *Phys. Earth and Planet. Inter.*, 25, 159-162, 1981a.

Kikuchi, M., Dispersion and attenuation of elastic waves due to multiple scattering from cracks, *Phys. Earth and Planet. Inter.*, 27, 100-105, 1981b.

Kokesh, F. P., The long interval method of measuring seismic velocity, *Geophys.*, 21(3), 724–738, 1956.

Kokesh, F. P. and R. B. Blizard, Geometrical factors in sonic logging, *Geophys.*, 24(1), 64–76, 1959.

Lee, M. W. and A. H. Balch, Theoretical seismic wave radiation from a fluid-filled borehole, *Geophys.*, 47(9), 1308-1314, 1982.

Levin, F. K. and R. D. Lynn, Deep-hole geophone studies, *Geophys.*, 23(4), 639–664, 1958.

Lockner, D. A., J. B. Walsh and J. D. Byerlee, Changes in seismic velocity and attenuation during deformation of granite, *J. Geophys. Res.*, 82, 5374–5378, 1977.

Lynn, H. B., Migration and interpretation of deep crustal seismic reflection data, Ph.D. thesis, 158 pp., Stanford Univ., Stanford, Calif., 1979.

Mair, J. A., and A. G. Green, High resolution seismic reflection profiles reveal fracture zones within a "homogeneous" granite batholith, *Nature*, 294(5840), 439-442, 1981.

Majer, E. L. and T. V. McEvilly, Seismological investigations at The Geysers geothermal field, *Geophys.*, 44(2), 246–269, 1979.

Malin, P. E. and P. C. Leary, The seismic velocity stress sensitivity of the crust near Palmdale, California (abs.), *EOS, Trans. AGU*, 62(45), 967, 1981.

Manchee, E. B., Direct integration of continuous velocity logs, *Geophys.*, 24(2), 335–343, 1959.

Murphy, W. F., Effects of partial water saturation on attenuation in Massilon sandstone and Vycor porous glass, *J. Acoust. Soc. Am.*, 71(6), 1458-1468, 1982.

Moos, D. and M. D. Zoback, *In situ* studies of velocity in fractured crystalline rocks, *J. Geophys. Res.*, (in press), 1983.

Nur, A. and G. Simmons, The effect of saturation on velocity in low porosity rocks, *Earth Planet. Sci. Lett.*, 7, 183–193, 1969.

Nur, A., Effects of stress on velocity anisotropy in rocks with cracks, *J. Geophys. Res.*, 76, 2022–2034, 1971.

Nur, A., Dilatency, pore fluids, and premonitory variations is t_s/t_p travel times, *Bull. Seis. Soc. Am.*, 62, 1217–, 1972.

O'Connell, R. J., and B. Budiansky, Seismic velocities in dry and saturated cracked solids, *J. Geophys. Res.*, 79, 5412-5426, 1974.

Paillet, F. L., Predicting the frequency content of acoustic waveforms obtained in boreholes, *Society of Professional Well Log Analysts 22nd Annual Logging Symposium, Transactions*, 1, 1-29, 1981.

Paillet, F. L., and J. E. White, Acoustic modes of propagation in the borehole and their relationship to rock properties, *Geophys.*, 47(8), 1215-1228, 1982.

Peselnick, L. and R. Stewart, A sample assembly for velocity measurements of rocks at elevated temperatures and pressures, *J. Geophys. Res.*, 80, 3765–3768, 1975.

Reasenberg, P. and K. Aki, A precise, continuous measurement of seismic velocity for monitoring *in situ* stress, *J. Geophys. Res.*, 79, 399–406, 1974.

Rice, B.R., S.J. Allen, O.J. Gant, Jr.,R.N. Hodgson, D.E. Larson, J.P. Lindsey, J.R. Patch, T. R. LaFehr, G.R. Picket, W.A. Scneider, J. E. White, J. C. Roberts, Developments in exploration geophysics, *Geophys.*, 46(8), 1088–1099, 1981.

Richards, P. G. and W. Mencke, The apparent attenuation of a scattering medium, submitted to *Bull. Seis. Soc. Am.*.

Riggs, E. D., Seismic wave types in a borehole, *Geophys.*, 20(1), 53–67, 1955.

Schilt, S., J. Oliver, L. Brown, S. Kaufman, D. Albaugh, J. Brewer, F. Cook, L. Jensen, P. Krumhansl, G. Long, and D. Steiner, The heterogeneity of the continental crust: Results from deep crustal seismic reflection profiling using Vibroseis technique, *Rev. of Geophys. and Space Phys.*, 17, 354-368, 1979.

Schoenberger, M. and F. K. Levin, Apparent attenuation due to intrabed multiples, I, *Geophys.*, 39, 278-291, 1974.

Schoenberger, M. and F. K. Levin, Apparent attenuation due to intrabed multiples, II, *Geophys.*, 43(?), 730–737, 1978.

Secor, D. T., Jr., L. S. Peck, D. M. Pitcher, D. C. Prowell, D. H. Simpson, W. A. Smith, and A. W. Snoke, Geology of an area of induced seismic activity at Monticello Reservoir, South Carolina, *J. Geophys. Res.*(in press).

Seeburger, D. and M. D. Zoback, The distribution of natural fractures and joints at depth in crystalline rock, *J. Geophys. Res.*, 87, 5517–5534, 1982.

Simmons, G., and A. Nur, Granites: Relation of properties *in situ* to laboratory measurements, *Science*, 162, 789-791, 1968.

Sjogren, B., A. Ofsthus, and J. Sandberg, Seismic classification of rock mass qualities, *Geophys. Prospect.*, 27, 409-442, 1979.

Smithson, S. B., J. Brewer, S. Kaufman, J. Oliver, and C. Hunch, Nature of the Wind River Thrust, Wyoming, from COCORP deep-reflection data and from gravity data, *Geology*, 6, 648-652, 1978.

Spencer, J. W., Jr., Stress relaxations at low frequencies in fluid saturated rocks: Attenuation and modulus dispersion, *J. Geophys. Res.*, 86, 1803-1812, 1981.

Stesky, R. M., Compressional wave velocity of jointed rock: A laboratory simulation (abstact), *EOS, Trans. AGU*, 60, 939, 1979.

Stierman, D. J., and R. L. Kovach, An *in situ* velocity study: The Stone Canyon well, *J. Geophys. Res.*, 84, 672-678, 1979.

Stierman, D. J., J. H. Healy, and R. L. Kovach, Pressure-induced velocity gradient: an alternative to a Pg refractor in the Gabilan Range, central California, *Bull. Seis. Soc. Am.*, 69(2), 397–415, 1979.

Swanberg, C. A., The Mesa geothermal anomaly, Imperial Valley, California: A comparison and evaluation of results obtained from surface geophysics and deep drilling: *Second UN Symposium on the Development and Use of Geothermal Resources, San Francisco, Proceedings*, Lawrence Berkeley Lab., Univ. of California, 1217–1228, 1976.

Talwani, P., D. Stevenson, J. Sanber, B. K. Rastogi, A. Drew, J. Chiang, and D. Amick, Seventh

technical report, contract 14–08–0001–14553, U. S. Geol. Surv., Reston, Va., 1978.

Talwani, P. D., B. K. Rastogi, and D. Stevenson, Induced seismicity and earthquake prediction studies in South Carolina, Tenth tech. rep., contract 14-08-0001-17670, U.S. Geol. Surv., Reston, Virg., 1980.

Thomas, M. F., Granite landforms: A review of some recurrent problems of interpretation, in *Progress in Geomorphology–Papers in Honor of D. L. Linton, Inst. Br. Geogr. Spec. Publ. 7*, edited by E. H. Brown and R. S. Waters, 13-38, Alden and Mowbray, London, 1974.

Thompson, T. F., San Jacinto tunnel, in *Engineering Geology in Southern California*, edited by R. Lund and R. Proctor, pp. 105-107, Association of Engineering Geologists, Los Angeles, Calif., 1966.

Todd, T. and G. Simmons, Effect of pore pressure on the velocity of compressional waves in low-porosity rocks, *J. Geophys. Res.*, 77, 3731–3743.

Toksöz, M. N., R. M. Turpening, and R. R. Stewart, Final report — Assessment of the Antrim Oil Shale fracture zone by vertical seismic profiling, FE–2346–91, contract EX76–C–01–2346, MIT, 1980.

Tsang, L., and D. Rader, Numerical evaluation of transient acoustic waveforms due to a point source in a fluid-filled borehole, *Geophys.*, 44, 1706-1719, 1979.

van Sandt, D. R. and F. K. Levin, A study of cased and open holes for deep-hole siesmic detection, *Geophys.*, 28, 8–13, 1963.

Wang, H. F. and G. Simmons, Microcracks in crystalline rock from 5.3 km depth in the Michigan Basin, *J. Geophys. Res..*, 83, 5849–5856, 1978.

Ward, P. L., Earthquake prediction, *Rev. of Geophys. and Space Phys.*, 17(2), 343–353, 1979.

White, J. E., and R. E. Zechman, Computed response of an acoustic logging tool, *Geophys.*, 33, 302-310, 1968.

Zemanek, J., E. E. Glenn, Jr., L. J. Norton, and R. L. Caldwell, Formation evaluation by inspection

with the borehole televiewer, *Geophys.*, 35, 254–269, 1970.

Zoback, M. D., H. Tsukahara, and S. Hickman, Stress measurements at depth in the vicinity of the San Andreas fault: implications for the magnitude of shear stress at depth, *J. Geophys. Res.*, 85, 6157–6173, 1980.

Zoback, M. D. and S. Hickman, *In situ* study of the physical mechanisms controlling induced seismicity at Monticello Reservoir, South Carolina, *J. Geophys. Res.*, 87, 6959–6974, 1982.

Zoback, M. D., D. Moos, and R. N. Anderson, Determination of the horizontal principle stresses from well-bore breakouts (abs), *EOS, Trans. AGU*, 63, 1183, 1982.